UNIVERSITY OF CALGARY

Asphaltene Precipitation from Crude Oil Blends, Conventional Oils, and Oils with Emulsified Water

by

Asok Kumar Tharanivasan

A THESIS
SUBMITTED TO THE FACULTY OF GRADUATE STUDIES IN
PARTIAL FULFILMENT OF THE REQUIREMENTS FOR THE
DEGREE OF DOCTOR OF PHILOSOPHY

DEPARTMENT OF CHEMICAL AND PETROLEUM ENGINEERING

CALGARY, ALBERTA
JANUARY, 2012

UNIVERSITY OF CALGARY

FACULTY OF GRADUATE STUDIES

The undersigned certify that they have read, and recommended to the Faculty of Graduate Studies for acceptance, a thesis entitled "Asphaltene Precipitation from Crude Oil Blends, Conventional Oils, and Oils with Emulsified Water" submitted by Asok Kumar Tharanivasan in partial fulfilment of the requirements for the degree of Doctor of Philosophy.

Supervisor, Dr. Harvey W. Yarranton
Department of Chemical and Petroleum Engineering

Co-supervisor, Dr. Shawn D. Taylor
DBR Technology Center, Schlumberger, Edmonton, AB, Canada

Supervisory Committee, Dr. William Y. Svrcek
Department of Chemical and Petroleum Engineering

Supervisory Committee, Dr. Michael W. Foley
Department of Chemical and Petroleum Engineering

Internal Examiner, Dr. Laurence R. Lines
Department of Geology and Geophysics

External Examiner, Dr. Norman Freitag
Saskatchewan Research Council, Regina, SK, Canada

Date

Abstract

Asphaltene precipitation from crude oils is one of the flow assurance issues for the oil industry. Precipitation can be significantly affected by the changes in composition and pressure of the crude oil. For example, asphaltenes precipitate upon mixing of incompatible oils or solvents to crude oils, and pressure depletion in conventional oils containing solution gas. The focus of this thesis was to develop a phase behavior model for predicting the onset and the amount of precipitation from solvent-diluted crude oil blends and oils undergoing depressurization. Furthermore, crude oils with no or very little water are always considered for asphaltene precipitation measurements and modeling. In reality, the crude oils are often co-produced or extracted with water. Hence, the thesis also investigates the effect of water on asphaltene precipitation.

Previously, a regular solution approach was successfully used to model the precipitation from heavy oils diluted with pure *n*-alkanes. The model inputs are the mole fraction, molar volume, and solubility parameter of each component in the *n*-alkane-heavy oil mixture. Heavy oil was characterized into saturates, aromatics, resins, and asphaltenes (SARA) fractions. Asphaltenes were sub-divided into fractions based on the gamma function to account for the distribution of aggregates resulting from self-association. Precipitation was modeled assuming liquid-liquid equilibrium between an asphaltenic and a non-asphaltenic phase. The only unknown parameter in the model was the average molar mass of the asphaltenes. The average molar mass was determined by fitting the model to precipitation yield data for *n*-heptane diluted heavy oil. In this thesis, the regular solution model was first extended for crude oil blends and then modified to handle conventional oils.

Blends were prepared from oils from ten different sources. A methodology was proposed to estimate the composition of the blends and to calculate the molar mass distribution of the asphaltenes in the blends. The mass fraction of each SARA fraction in the blends was

experimentally confirmed as a weight average of the respective fraction in the constituent oils. The asphaltene distribution in the blends was calculated assuming either an interaction between the asphaltene distributions from each constituent oils or no interaction. The model methodology was then tested on blends where only one of the constituent oils contained asphaltenes and also on blends where both oils contained asphaltenes. It was found that the model could predict onsets and amounts of precipitation for all the blends when no interaction between the asphaltene distributions was assumed.

For conventional oils, a compositional characterization methodology was developed for a recombined oil based on gas chromatography analysis and SARA fractionation. The characterization included the determination of effective molar volumes and solubility parameters for light hydrocarbons. Both the characterization and the model were then tested against measured precipitation data from the dead and live oils. The common oil characterization methodology captured the behavior for both solvent- and pressure-induced asphaltene precipitation. However, the yield predictions were very sensitive to the fitted average molar mass of asphaltenes, limiting the predictive capability of the model. As part of the modeling methodology, the densities of the recombined oil were remarkably well predicted above the bubble point.

To investigate the effect of water, precipitation yields were measured and compared for oils with and without emulsified water at different dilution ratios of *n*-heptane. At dilution ratios above the onset of precipitation for water-free oils, asphaltene yields were observed to be the same for both water-free oils and oils with emulsified water. For dilution ratios below the onset for water-free oils, there was no detectable precipitation but asphaltenes adsorbed on the water-oil interface appeared as yield. Hence, the solubility of asphaltenes was not affected in the presence of water.

Acknowledgements

First of all, I would like to express my deep and profound gratitude to my supervisor, Dr. Harvey W. Yarranton, for his continuous support, timely encouragement and excellent guidance throughout my graduate studies. I benefited a lot from him through thought-provoking technical discussions. His inputs on the modeling work were highly valuable. I sincerely appreciate his supervision, patience and trust during my doctoral program.

I would like to extend my sincere gratitude to my co-supervisor, Dr. Shawn D. Taylor, for his constant support, patience and assistance in various aspects. I highly appreciate his guidance in developing experimental methods and data interpretation. Technical interactions with him allowed me to develop practical knowledge and to learn the industry trends. His suggestions were very helpful for making progress and in the preparation of thesis.

I am grateful to the Department of Chemical and Petroleum Engineering at the University of Calgary and the Natural Sciences and Engineering Research Council (NSERC) of Canada for the financial support as a post-graduate scholarship. I thank the Consortium of Asphaltenes and Emulsions Research (C-AER) sponsors, Shell, Schlumberger, Petrobras, Total and Syncrude Canada Ltd., for supporting the thesis project.

I would like to thank Dr. Parviz Rahimi from National Center for Upgrading Technology (NCUT), Devon, Alberta, Canada and Dr. Daniel Merino-Garcia from Repsol, Spain, for providing additional experimental data for the crude oil blend modeling work. I also acknowledge Husky Oil Ltd., Syncrude Canada Ltd., Shell Canada Ltd., and British Petroleum for supplying the oil samples.

I am thankful to all members of Asphaltene and Emulsion Research group during my graduate studies for their co-operation and useful discussions. I especially thank Shinil

George, Diana Ortiz and the summer student, Masoud Abdolmohammadi, for their help in performing some experiments. I extend my thanks to Elaine Baydak as well. I also appreciate Dr. Kamran Akbarzadeh for transferring the knowledge on the previously developed modeling work.

I would like to acknowledge Schlumberger's DBR Technology Center in Edmonton for providing me a valuable opportunity to spend about eight months in their facility to carry out the live oil experiments. I thank Ryan Jacobsen, Josh Genereux, John Duchesne, Mila Goretic and Sajjad Hussein at DBR for performing live oil experiments and asphaltene analysis. I also appreciate Dr. Abdel Kharrat, Dr. Huang Zeng, Afzal Memon and Jose Zacharia for helping me with experimental procedures.

I extend my thanks to Dr. Dan Zhang, Dr. Julian Zuo, and Dr. Vladimir Tertychnyi for their trust, patience and support to complete the thesis after starting to work at Schlumberger.

Finally, I would like to express my sincere thanks to my parents and my wife, Advaitha, for their patience, encouragement and understanding.

Dedication

Dedicated to my Parents

Table of Contents

List of Tables

List of Figures

Nomenclature

Symbols

A	heat of vaporization of asphaltene (kJ/g)
A	surface area of emulsion (m^2)
a	fitting parameter (m^3/kPa^2)
a_0	fitting parameter (kg/m^3)
a_1	fitting parameter (kPa^{-1})
a_2	fitting parameter (-)
b	fitting parameter (m^3/kPa)
b_0	fitting parameter (kg/m^3K)
b_1	fitting parameter (1/kPaK)
b_2	fitting parameter (K^{-1})
c	fitting parameter (m^3)
c_0	fitting parameter (kg/m^3K^2)
c_2	fitting parameter (K^{-2})
d	diameter (m)
d_{32}	Sauter mean diameter (m)
E	cohesive energy (J)
f	probability of the molar mass distribution function (-)
f_i	frequency (-)
H	enthalpy (J/mol)
h	height (cm)
I	intercept of the linear fit of Eq. (3.1) (m^3/kg)
K	equilibrium ratio (-)

M	molar mass (g/mol)
$\overline{M}$	average molar mass of self-associated asphaltenes (g/mol)
m	mass (kg or g)
n	fitting parameter (-)
P	pressure (MPa or kPa or atm)
q	number of measurements
R	universal gas constant (8.314 J/molK)
r	aggregation number (-)
$\bar{r}$	average aggregation number (-)
S	slope of the linear fit of Eq. (3.1) (m^3/kg)
T	temperature (°C or K)
V	volume (m^3)
v	molar volume (cm^3/mol)
w	mass fraction (-)
x	mole fraction (-)
Y	Y-function as defined in Eq. (3.5)

Greek Letters

α_1	compressibility at high pressure (kPa^{-1})
α_2	fitted or calculated temperature-dependent parameter (-)
β	decay rate from the low to high pressure compressibility (kPa^{-1})
β	shape factor (-)
Δ	difference (-)
δ	solubility parameter ($MPa^{0.5}$)

ϕ	volume fraction (-)
Γ	asphaltene surface coverage (mg/m²)
Γ	gamma function (-)
υ	fitted/predicted/experimental measurement
ρ	density (kg/m³)

Superscripts

h	heavy liquid phase
l	light liquid phase
*vap**	vaporization

Subscripts

0	condition at 101 kPa
1	crude oil 1
2	crude oil 2
A	asphaltenes or resin
a	asphaltene sub-fraction
aro	aromatics
asph/bit	asphaltenes or bitumen
e	effective value
fp	fluid + piston
I	water-oil interface
i	i^{th} component, i^{th} droplet
liq	liquid
m	asphaltene monomer

m	light or heavy liquid phase
mix	mixture
oil	live or dead oil
p	piston
sat	saturates
*sat**	saturation condition
tol	toluene
tot	total
w	emulsified water

Abbreviations

AAD	average absolute deviation
API	American Petroleum Institute
ASTM	American Society of Testing and Materials
CPA	cubic plus association
DBR	DBR Technology Center, Schlumberger, Edmonton, AB, Canada
EoS	equation of state
FID	flame ionization detector
GC	gas chromatography
GOR	gas-oil ratio
HBT	Hankinson-Brobst-Thomson
HPM	high pressure microscope
IP	Institute of Petroleum
LGO	light gas oil
LLE	liquid-liquid equilibrium

NCUT	National Center for Upgrading Technology, Devon, AB, Canada
NIST	National Institute of Standards and Technology
PC	perturbed chain
PR	Peng-Robinson
PVT	pressure, volume, temperature
Repsol	Centro Tecnológico Repsol, Móstoles, Spain
SAFT	statistical associating fluid theory
SARA	saturates, aromatics, resins, and asphaltenes
SIMDIST	simulated distillation
TCD	thermal conductivity detector
UofC	University of Calgary, Calgary, AB, Canada
VLE	vapor-liquid equilibrium

CHAPTER 1

Introduction

1.1 Overview

With the depletion of conventional on-shore crude oil resources, oil production has been shifting to offshore fields and towards unconventional resources like heavy oils and bitumen, an area of hydrocarbon production where Alberta plays a leading role. An important aspect of both offshore and heavy oil production is flow assurance. Flow assurance is the general term used to describe a variety of fluid property related issues that impact the flow of oil, gas and water through production or transportation systems. The goal of a flow assurance engineer is to assure that fluids flow through the systems as designed.

One of the major issues in flow assurance is the formation or precipitation of organic and inorganic solids from crude oil. Solids can be precipitated when the oil undergoes phase transitions due to changes in pressure, temperature and composition. Precipitation can lead to solid particle build-up and deposition that restrict fluid flow. The presence of precipitated solids in the oil can also change the fluid properties, such as viscosity. Particle build-up is usually significant at low fluid flow rate and depends on the geometry of the flowline; for example, build-up can occur in situations where there are constrictions and expansions in the flowline. Deposition is generally affected by fluid flow rate, fluid properties (such as density, viscosity), type of solid precipitated, and adsorption of precipitated particles on to the metal surface or already deposited layer. Overall, precipitation is the first step leading to solids build-up and deposition.

Solids precipitation, build-up and deposition can be found in reservoir, wellbore, production tubing, transportation pipeline and downstream process equipment. In the

reservoir, solids can precipitate due to mixing of injection fluids for oil recovery with the reservoir fluid and when reservoir fluids from different formations are commingled. Precipitated solids can build-up and deposit in the reservoir thereby blocking the pore space over time and reducing permeability. Solid precipitation and deposition in the wellbore, production tubing, and pipeline can be caused by pressure changes, gas-lift operations, and large temperature variations. At the surface, mixing of incompatible streams produced from different fields and dilution of heavy oils or bitumen can cause solids precipitation. Precipitated solids can also deposit on process equipment in heavy oil upgraders and refineries and can lead to fouling problems. Consequently, there is a strong incentive for petroleum producers to better understand the flow assurance issues related to solids formation and to develop the capability for identifying potential problem fluids.

Typical solids formed as a result of phase transitions of reservoir fluids include gas hydrates, waxes, inorganic scales and asphaltenes. Some less common solids formed due to phase transitions include diamondoids, elemental sulphur and naphthenates. Other inorganic solids such as sand, clay and corrosion products may also be present in the produced oil or extracted bitumen and these solids can contribute to flow assurance issues. A brief description of more common solids formed due to phase transition is given below.

Gas hydrates are formed when the water is in contact with light hydrocarbon fluid (composition with carbon numbers less than or equal to 6) under high pressure and low temperature conditions. At these conditions, small hydrocarbon compounds (*e.g.* methane, ethane) can occupy the spaces within the geometric lattices formed by water molecules. This may result in the formation of a semi-stable solid similar to ice at temperatures as high as 20°C. Gas hydrates formation, plugging, and deposition are the most common flow assurance problem in the upstream petroleum operations.

Waxes are heavy paraffinic hydrocarbons (typically *n*-alkanes with carbon numbers greater than 18) that may form or precipitate as a solid or solid-like gel material when the reservoir fluid is cooled down to and below a certain temperature, known as the wax appearance temperature. The most common field condition for wax formation and deposition is the transportation of highly paraffinic off-shore reservoir fluid in subsea pipelines. In subsea conditions, the temperature of the pipeline soon reaches the temperature of the surrounding seawater and therefore cools down the reservoir fluid that is being transported. If the temperature of the reservoir fluid within the pipeline falls below the wax appearance temperature, wax precipitates and deposit as a solid layer inside the pipeline. Precipitated wax may also be transported in suspended form and lead to an increased apparent viscosity of oil and associated pressure drops. Another major issue with the wax precipitation is the formation of wax-gel during shut-down period of well or pipeline. The wax-gel formed will lead to difficulties during start-up requiring greater pumping power or possible well/pipeline abandonment in extreme cases.

Inorganic scales are formed from inorganic ions in the formation water that precipitate if their solubility limits are exceeded when, for example, cooled in the well bore. Major ions present in the formation water that contribute to scale formation are Na^{+}, K^{+}, Ca^{2+}, Mg^{2+}, Ba^{2+} Sr^{2+}, Cl^{-}, HCO_3^{-} and SO_4^{2-}. The two most common types of inorganic scales are calcite ($CaCO_3$) and barite ($BaSO_4$). Scale deposition causes formation damage, enhances corrosion problems in production tubing and transportation pipelines, damages down-hole control or logging devices and may cause fluid flow restrictions.

Asphaltenes, the heaviest hydrocarbon fraction in the petroleum or crude oil, are the focus of this study. They are usually defined as a fraction of crude oil soluble in aromatic solvents such as toluene or benzene and insoluble in paraffinic solvents such as *n*-pentane or *n*-heptane. During field operations, asphaltenes can precipitate upon changes in pressure, temperature and composition of the crude oil. Asphaltenes also contribute significantly to the high viscosity and the coking tendency of heavy oils and bitumen.

1.2 Asphaltene Related Issues

Asphaltene precipitation and deposition can occur during production of reservoir fluid, transportation of produced fluid and processing the fluid in downstream operations. Conditions where asphaltene precipitation can occur during conventional crude oil production include normal pressure depletion, acid stimulation, gas-lift operations and miscible flooding for enhanced oil recovery. In some field cases, asphaltenes and waxes co-precipitate. During heavy oil operations, the dilution of heavy oil with paraffinic solvent or lighter oils to reduce its viscosity can cause asphaltene precipitation in pipelines, tubulars and surface facilities. Asphaltenes also precipitate during paraffinic froth treatment in oil sands processing and vapor extraction process for heavy oil recovery.

Precipitation of dispersed asphaltene particles is a precondition for deposition in process equipment. Deposition of asphaltenes in oil wells, pumps, flowlines, pipelines and production facilities can reduce well productivity, damage pumps, restrict or plug flowline and pipelines and foul production handling facilities (Cimino et al., 1995; Saniere et al., 2004). Precipitated asphaltenes may also build-up in the near wellbore, reservoir rock and clog the porous matrix of the reservoir during drilling and chemical treatment (Leontaritis et al., 1994; Luo et al., 2008). Apart from causing the reservoir formation damage, asphaltene deposits could also result in reversal of the rock wettability to oil-wet, which leads to a lower recovery factor (Yan and Plancher, 1997).

Field problems from plugging of wellbore, tubing and surface facilities due to asphaltenes have been reported for a large number of production fields with both light and heavy oil production. Some examples of these cases are in the Algeria (Haskett and Tartera, 1965), USA (Leontaritis and Mansoori, 1988), North Sea (Thawer et al., 1990), Venezuela (Cassani et al., 1992), and Kuwait (Alkafeef et al., 2005). The current remediation methods for asphaltene deposition problems include injecting aromatic solvents or dispersants to dissolve the deposit by soaking, mechanically cutting or

pigging the pipe section of the deposit, or hydraulically fracturing to overcome the damaged formation near the wellbore. In a few cases, coiled tubing has been used with a jet attachment to remove deposits in the wellbore (Afghoul et al., 2004; Kumar et al., 2008; Frenier et al., 2010).

In addition to the problems related to flow assurance and reservoir impairment, asphaltenes are also known to contribute to the formation of stable emulsions in process facilities (Lindemuth et al., 2001) and act as coke precursors and catalyst poisons (Gray, 1994). Although operators try to avoid the conditions where asphaltene precipitation occurs, in some cases, precipitation and the potential accumulation of asphaltene deposits is inevitable. Therefore, operators must rely on chemical and mechanical remediation methods (Chang and Fogler, 1996; Al-Sahhaf et al., 2002) to mitigate deposition. These methods are expensive and are often only partially effective. Consequently, understanding the mechanisms of asphaltene precipitation and deposition is vital to the application of these remedial mitigation methods.

1.3 Scope and Objectives

Asphaltene precipitation is arguably the first and most important step in the processes that lead to plugging of formation pores and deposition. Therefore, asphaltene precipitation phase behavior modeling is the focus of this thesis. Several modeling approaches have been adapted in the literature to model asphaltene precipitation from crude oils. The main approaches are based on colloidal and thermodynamic models. Thermodynamic models are by far the most widely used. Thermodynamic models applied to asphaltene precipitation include regular solution theory, cubic equations of state, and association equations of state. Equations of state (EoS) based models are well suited for vapor-liquid equilibrium calculations and are generally used for oils at high pressure and temperature and with solution or injected gas. They have not yet been successfully applied to asphaltene precipitation due to blending of oils probably because

the standard mixing rules are inadequate for these asymmetric mixtures (Castellanos Díaz et al., 2011). The regular solution approach is the simplest and is easily adapted to model precipitation as a result of dilution with incompatible solvents. In this thesis, the regular solution approach is adapted to model asphaltene precipitation from crude oil blends and oils undergoing depressurization.

Most of the available regular solution based models focus on predicting precipitation from individual crude oils diluted with pure solvents. In reality, crude oils are often blended with another crude oil or a multi-component solvent (Hong and Watkinson, 2004). For instance, mixtures of produced heavy oils or bitumen are often diluted with a distillation cut (naphtha) or a condensate to reduce the viscosity for transportation through pipelines. Upgraded or produced crude oils from different sources are usually mixed before refining. If the fluids are not compatible with each other, blending can cause asphaltene precipitation. Precipitation onset tests on constituent oils are usually conducted to assess the stability of such crude oil blends (Wiehe and Kennedy, 2000; Schermer et al., 2004). Here, stability refers to amount of asphaltenes precipitate in the fluid. These onset tests are not always sufficient because the solubility of asphaltenes in the blend could be affected by the amount and/or composition of the non-asphaltenic fraction of constituent oils (Wiehe et al., 2001). In some cases, crude oil blends are less stable than the constituent oils. Interaction between the asphaltenes from source oils may also affect phase behavior. These issues must be considered in extending the existing asphaltene precipitation models to crude oil blends.

The existing regular solution based models were also mainly tested on diluted dead oils, which are depressurized oils from which all of the solution or dissolved gas has evolved. Asphaltene precipitation from dead oils is caused by the addition of a solvent, which alters the properties (density and solubility parameter) of the mixture to the point where asphaltenes are no longer soluble. Hence, these models can describe asphaltenes when there is a change in the composition from the addition of any paraffinic diluent. On the

other hand, precipitation in live oils (which are oils containing solution or dissolved gas under high pressure) is caused primarily by depressurization. As pressure decreases, the density and solubility parameter of the live oil decreases to the point where asphaltenes are no longer soluble in the oil. Although the pathway to precipitation is not the same for diluted dead oils, it is expected that, in both cases, asphaltenes phase behavior can be predicted from the properties of the solution.

Another issue with the asphaltene phase behavior modeling is to consider the presence of emulsified water in crude oils. Usually, the reservoir fluid samples with no or very little water are used for asphaltenes phase behavior modeling or assessing the precipitation risks in the laboratory. However, reservoir fluids are often co-produced with formation water and/or injected water during secondary or enhanced oil recovery processes. In the case of bitumen extraction processes, a large amount of water is used for froth treatment and therefore water-in-oil emulsion formation is unavoidable. The effect of the presence of water on asphaltene precipitation is not understood in terms of the measured onset and yield of precipitated asphaltenes. Hence, the effect of emulsified water on asphaltenes precipitation from crude oils should be investigated as well. If there is an effect, the phase behavior modeling for asphaltenes precipitation must be modified accordingly.

The objectives of this thesis are to:

1. develop a predictive model for the stability of crude oil blends. A generalized model previously developed for precipitation from *n*-alkane diluted heavy oils (Akbarzadeh et al., 2005) is adapted for blends. Crude oil blends are prepared from oils from different sources. A methodology is proposed to estimate the composition of crude oil blend and to predict the onsets and/or amounts of precipitation from oil blends diluted with *n*-alkanes or a mixture of toluene and *n*-heptane. The model methodology and underlying assumptions are tested on blends where only one of the constituent oils contains asphaltenes and also on blends where both oils contain asphaltenes.

2. develop and test a characterization methodology that is applicable to both solvent-induced and pressure-induced asphaltene precipitation. The Akbarzadeh et al. (2005) model is extended to live oils, including the determination of effective molar volumes for light hydrocarbons. A compositional characterization methodology is presented that is based on analysis by gas chromatography and saturates, aromatics, resins and asphaltenes (SARA) fractionation. The characterization and model are tested on measured precipitation data from a dead and live crude oil sample.

3. investigate the effect of emulsified water on the asphaltenes precipitation from crude oils. Asphaltene precipitation yields are measured and compared for oils with and without emulsified water at various dilution ratios. The study is extended to analyze the composition of the precipitated asphaltenes from water-free oils and oils with emulsified water. Elemental and heavy metal analysis are used for asphaltene composition analysis. The data generated in this study will also determine if the presence of emulsified water needs to be accounted for when modeling phase behavior for the design and optimization of oilfield production and processing facilities.

1.4 Outline of the Thesis

The thesis is composed of eight chapters. The current chapter presented an introduction to the thesis research topic together with the scope and objectives of this study. Chapter 2 reviews the literature on characterization of crude oils related to asphaltene precipitation modeling, asphaltene characteristics and behavior, and modeling approaches available for asphaltene precipitation. Chapter 3 describes the experimental apparatus and procedures used in this thesis study including the characterization of crude oil blends and live oils, bubble point measurements, precipitation onsets and yields. Chapter 4 covers

the modified regular solution model that is adapted for modeling the specific application in the subsequent chapters.

Objectives 1, 2 and 3 are addressed in Chapters 5, 6 and 7, respectively. Chapter 5 presents the developed asphaltene precipitation modeling methodology and the data collected for the crude oil blends. Chapter 6 provides the detailed characterization and modeling methodology for asphaltenes precipitation from conventional oils due to depressurization. This chapter also presents the experimental data collected for conventional oils. Chapter 7 investigates the effect of emulsified water on asphaltenes precipitation from crude oils. This chapter details all asphaltene precipitation yield measurements and the compositional analysis of asphaltenes samples. Finally, Chapter 8 is a summary of major conclusions, recommendations for future research, and contributions of this thesis.

CHAPTER 2

Literature Review

This chapter presents a review of the literature on crude oil characterization, asphaltene characteristics and properties, asphaltene precipitation test methods and available asphaltenes precipitation models. A review of the effect of water on asphaltene precipitation is also presented.

2.1 Crude Oil Characterization

2.1.1 General Chemistry

Crude oil (or petroleum) is a multicomponent mixture consisting of naturally occurring hydrocarbons, together with organic compounds of sulphur, nitrogen and oxygen, as well as trace amounts of metallic constituents, such as vanadium, nickel and iron. The origin of crude oil can have a significant effect on its composition. As a result, crude oils widely vary in volatility, density, viscosity and color. Crude oil may also contain dissolved inorganic gases, such as nitrogen, carbon dioxide, and hydrogen sulphide, at high pressure and temperature conditions. Water is another important constituent of produced crude oil. As water has limited miscibility with hydrocarbons, most of the water is usually found in the form of emulsified droplets or in a free water phase. The free water is usually separated at the well-head facilities, while the emulsified water is removed in the pre-refining operations.

In oilfield operations, crude oils are generally classified based on the viscosity (UNITAR definition) or the density (API definition), Table 2.1. Light oil or “conventional crude oil” is often produced by primary or secondary recovery process without the addition of

heat, chemicals or solvents. These oils have relatively low viscosity and density. Crude oil that is significantly more viscous and has a lower API gravity (higher density) is called “heavy oil”. These oils are typically produced by enhanced oil recovery techniques and require thermal stimulation or by addition of chemicals. Bitumen or “extra heavy crude oil” are near-solid materials that do not flow freely under ambient conditions. They are extremely viscous and are usually extracted from oil sands mining or through enhanced oil recovery techniques. Overall, the hydrocarbon (as opposed to heteroatom) content of the crude oil may be as high as 97 wt% in the case of light oil or as low as 50 wt% in heavy crude oil and bitumen.

Table 2.1: Classification of crude oils.

Crude Oil Type	**Viscosity(mPa·s)**	**Density (kg/m^3)**	**°API**
light oil	< 100	< 934	> 20
heavy oil	100 to 100,000	934-1000	10 to 20
bitumen	> 100,000	>1000	< 10

Hydrocarbon components in crude oil begin with methane (CH_4), the simplest of all hydrocarbons. Methane is the most common component in petroleum at high pressure and temperature conditions. Since methane contains one carbon atom, it is often referred to as C1. Similarly, the term C2 is used for ethane (C_2H_6), C3 for propane (C_3H_8), and so on. In general, the hydrocarbon components in a crude oil may extend up to C200. Hydrocarbons with seven and more carbon atoms are usually referred to as C7+ fraction or plus fraction.

The C7+ fraction is far more complex than lighter fractions due to the larger number of isomer combinations available to hydrocarbons with increasing carbon number as well as

the presence of heteroatoms. A particular C7+ component may belong to one of the following component classes: paraffins, naphthenes, aromatics, resins and asphaltenes.

Paraffins are straight chain alkanes or saturated hydrocarbons, where the carbon atoms are connected by single bonds. They may be unbranched (*normal*- or *n*-paraffins) or branched (*iso*- or *i*-paraffins).

Naphthenes, also called cycloalkanes, are similar to paraffins with one or more cyclic structures. The carbon atoms in the cyclic structures are connected by single bonds.

Aromatics are components with one or more cyclic structures containing double bonds. Benzene is the simplest aromatic component. Aromatics may be linked with substituted naphthene rings and/or paraffin side-chains.

Resins are very aromatic components and their structure is not well-defined. Primarily, they are polar, polynuclear molecules consisting of condensed aromatic rings, aliphatic side chains and few heteroatoms.

Asphaltenes are similar to resins but are larger, denser, more polar and aromatic, and have a higher heteroatom (S, N, O, Ni and V) content.

2.1.2 Whole Oil Characterization

Characterization is a technique to divide the complex multi-component crude oil into various pure components and pseudo-components of known properties. It is one of the first and important steps in modeling the phase behavior of crude oils. This step is performed because it is impossible to analytically determine the composition of each pure component in the crude oil. Usually, the composition of lower carbon number

components below C7 and its isomers is determined using gas chromatography, and the rest of the crude oil is reported as plus fractions. The plus fractions are divided into various pseudo-components. The properties of pure components are known, while the properties of pseudo-components are measured or calculated.

Characterization of the crude oil or the plus fraction into pseudo-components can be based on chemical composition, density, viscosity, boiling cut, H/C atomic ratio, carbon distribution, heteroatom content and solubility class (Altgelt and Boduszynski, 1994; Wauquier, 1995; Speight, 1999; Pedersen and Christensen, 2007). There is no universal characterization technique applicable to all types of oils or reservoir fluids. In general, characterization technique depends on the oil/fluid type and the required property information for pseudo-components. The common characterization techniques adapted for modeling the asphaltene phase behavior are outlined below.

Light oils can be characterized using distillation, where the components are separated primarily by the differences in their vapor pressure or boiling point. Vapor pressure is inversely proportional to the boiling point. The vapor pressure also decreases with increasing molecular weight, aromaticity and polarity. Distillation can be performed at atmospheric pressures or under vacuum depending on the crude oil type. For example, distillation is conducted at lower pressures for heavier oils to vaporize the high molecular weight components. As a result, several distillate fractions are separated from the oil with each fraction representing a boiling point range. The properties of each fraction are then measured. In some cases, the average boiling point of each distillate fraction is compared with *n*-alkane having a similar boiling point. Therefore, the properties of each fraction are assigned accordingly based on *n*-alkane properties. The heaviest fraction of oil cannot be distilled because it decomposes below its boiling point.

Vacuum distillation is usually adapted to obtain higher-boiling distillates and to have deeper cuts of the oils without undergoing decomposition. A standard procedure is

available for such characterization and is given in ASTM D2892 to obtain “true boiling point” (TBP) distribution of crude oil. Since the conventional or vacuum distillation techniques requires relatively large sample sizes and long operation times (for example, ASTM D2892 method is a 100 h procedure), the simulated distillation (SIMDIST) technique has been widely adopted recently. SIMDIST can largely reduce the sample size and saves time with additional advantage of being more operationally convenient and covering even higher temperatures than vacuum distillation. SIMDIST is based on gas chromatography (GC), which can handle samples up to about 540°C (1000°F). For very high boiling samples, vacuum thermal gravimetric analysis, high-temperature GC and supercritical fluid chromatography have been used. Among these various methods, GC-SIMDIST is well-established and adopted in ASTM D2887.

Heavy oils and bitumen characterization is not usually based on true boiling point fractions because these fluids possess large amount of high molar mass components that decompose before they boil. Therefore, these fluids are normally characterized according to molecular weight fractions (gel permeation chromatography), chemical family (liquid chromatography) or functional groups (absorption spectrometry). The most common methodology to characterize the heavy oils and bitumen based on chemical family is the saturates, aromatics, resins and asphaltenes (SARA) analysis.

SARA fractionation involves prior separation of asphaltenes from the crude oil by the addition of excess liquid hydrocarbon (typically 40:1, solvent:oil volume), such as *n*-pentane or *n*-heptane (ASTM D4124). Saturates, aromatics and resins fractions are then extracted from the deasphalted oil using liquid chromatography (ASTM D2007). Saturates are non-polar and consist of paraffins and naphthenes. Aromatics, resins and asphaltenes appear to form a continuum of polynuclear aromatic species of increasing molar mass, polarity and heteroatom content. Typical SARA compositions of various heavy oils and bitumen and their measured properties are provided elsewhere (Peramanu et al., 1999; Akbarzadeh et al., 2005).

2.2 Asphaltenes

2.2.1 Definition and Composition

Asphaltenes are usually defined as a solubility class of petroleum, which precipitate from crude oil by the addition of an excess amount of *n*-alkane solvents such as *n*-heptane or *n*-pentane and are soluble in aromatic solvents such as toluene or benzene. The precipitate obtained by adding *n*-pentane to the oil is called "pentane (C5)-asphaltenes", whereas the precipitate obtained by adding *n*-heptane is called "heptane (C7)-asphaltenes". When there is no precipitate, the oil is considered as "asphaltenes-free". In the literature, several standard test procedures are available for such asphaltenes extraction (ASTM D6560, ASTM D3279, ASTM D4124). Variations of these standard procedures have also been used (Alboudwarej et al., 2002; Kharrat et al., 2007). The part of crude oil after the removal of asphaltenes is called "deasphalted oil" or maltenes.

Asphaltenes are not a pure component and consist of tens of thousands of species which have similar solubility behavior but may have different chemical structures, sizes, and shapes. Nonetheless, asphaltene species share some common features; they are polynuclear aromatics that also contain *n*-alkane chains, cyclic alkanes, and heteroatoms such as sulphur, nitrogen and oxygen, as well as traces of heavy metals like nickel, vanadium and iron. Speight (1999) provided the elemental composition of asphaltenes extracted from various crude oils around the world, Table 2.2. Usually, the hydrogen to carbon (H/C) atomic ratios of C5-asphaltenes found to be 1.15 ±0.5% (Moschopedis et al., 1976). A typical asphaltene molecule may contain sulphur as thiophenes, thiols, sulphides, disulphides and oxidized forms. Nitrogen can exist as pyrroles and pyridines structures. Oxygen has been identified in carboxylic, phenolic and ketonic locations, and metals (nickel and vanadium) are present as porphyrins.

Asphaltenes are generally claimed to be the "highly polar" fraction in the crude oil. This statement is based on the fact that asphaltenes are insoluble in *n*-heptane, a non-polar

solvent. The asphaltenes are, however, easily soluble in relatively non-polar solvents like benzene, toluene and dichloromethane, whereas they are insoluble in polar solvents like water, glycerine and methanol. Hence, asphaltenes are non-polar chemically and relatively more polar when compared to other components of crude oil.

Table 2.2: Elemental composition of asphaltenes from world sources (Speight, 1999).

	Canada	**Iran**	**Kuwait**	**Venezuela**
Carbon (wt%)	79.0 - 88.7	83.7	81.6 - 82.4	81.1 - 84.7
Hydrogen (wt%)	6.9 -11.1	7.8	7.8 - 8.1	7.8 - 8.3
Nitrogen (wt%)	0.7 - 2.8	1.7	0.6 - 1.7	0.2 - 2.0
Sulphur (wt%)	0.3 - 8.1	5.8	7.4 - 8.0	2.7 - 6.9
Oxygen (wt%)	0.4 - 3.9	1.0	0.6 - 1.8	1.0 - 4.2
H/C Ratio	0.98 - 1.56	1.19	1.14 - 1.19	1.13 - 1.19
N/C Ratio	0.007 - 0.029	0.017	0.008 - 0.017	0.002 - 0.02
S/C Ratio	0.001 - 0.038	0.026	0.034 - 0.039	0.012 - 0.032
O/C Ratio	0.004 - 0.037	0.009	0.005 - 0.017	0.013 - 0.039

The physical properties of asphaltenes are sensitive to the extraction method and/or solvents used for separation since the amount and exact chemical composition of extracted asphaltenes will vary with the different procedures. For example, asphaltenes precipitated using *n*-heptane are more aromatic compared to asphaltenes precipitated using *n*-pentane (Ancheyta et al., 2002). In other words, the H/C atomic ratio of asphaltenes precipitated using *n*-heptane is lower than the asphaltenes precipitated using *n*-pentane. Hence, asphaltenes are defined operationally rather than by their chemistry.

A number of authors have characterized asphaltenes obtained from different methods such as: addition of various diluents (Kharrat, 2009); gel permeation chromatography

(Dettman et al., 2005); addition of the same solvent at different dilution ratios (Andersen et al., 1997; Yang et al., 2004; Nalwaya et al., 1999). For example, Yang et al. (2004) fractionated Athabasca asphaltenes into six sub fractions based on the dilution ratio of *n*-heptane to bitumen. Zhao and Shaw (2007) partitioned bitumen and heavy oil into several fractions using nano-filters to determine the composition and size distribution of asphaltene enriched nanostructures. Overall, it is inferred that the asphaltene composition varies continuously, but there is no dramatic change in the composition from fraction to fraction.

2.2.2 Molecular Structure

There is considerable debate on the molecular structure of asphaltenes, particularly on the size of the aromatic groups and how they are linked to other structural groups. Two fundamentally different views of the asphaltenes structure are discussed in the literature: the condensed (island) structure and the dispersed (archipelago) structure, Figure 2.1 and Figure 2.2, respectively.

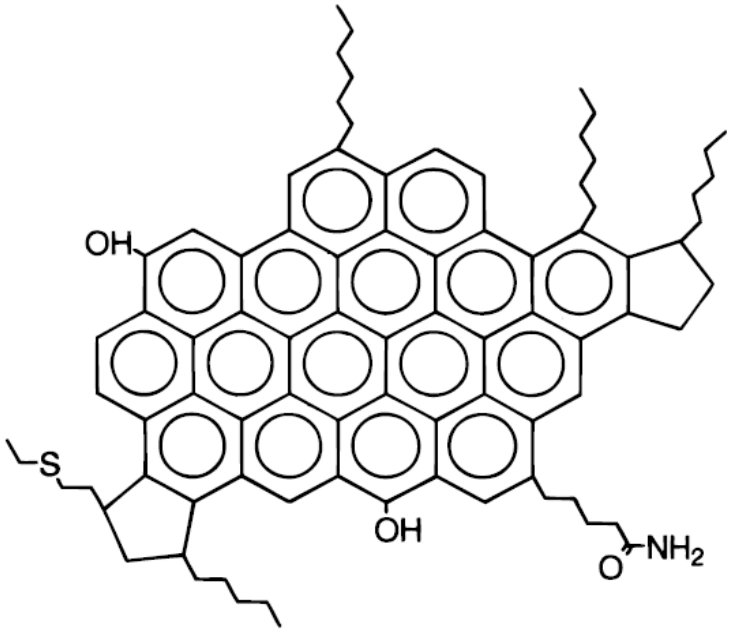

Figure 2.1: Hypothetical condensed asphaltene molecular structure (adapted from León et al., 2000).

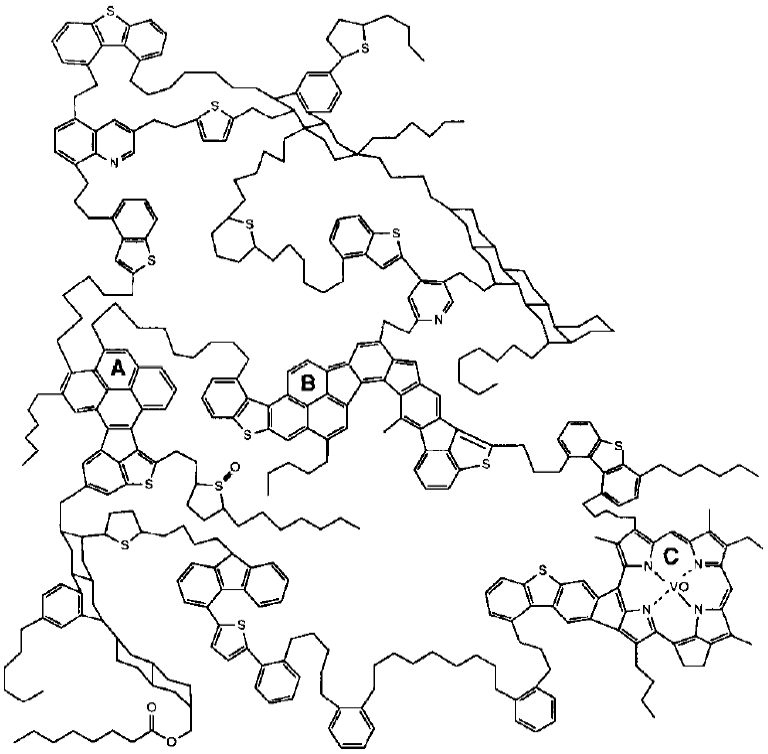

Figure 2.2: Hypothetical dispersed asphaltene molecular structure (adapted from Strausz et al., 1992).

The condensed structure represents a typical asphaltene molecule as a core aromatic group containing a large number of fused rings (comprised usually of more than seven rings) with aliphatic groups towards the periphery. A condensed structure interpretation is supported by data obtained from proton (^{1}H) nuclear magnetic resonance spectroscopy, X-ray diffraction and fluorescence depolarization experiments (Dickie and Yen, 1967; Betancourt et al., 2008; Mullins, 2010). The dispersed structure represents a typical asphaltene molecule as a collection of small aromatic groups linked by aliphatic bridges. The dispersed structure interpretation is based on data from pyrolysis, oxidation, thermal degradation and small-angle neutron scattering techniques (Strausz et al., 1999; Gray, 2003; Liao et al., 2009). Recently, high resolution mass spectrometry data suggests that both structures may actually exist in the oil (McKenna et al., 2010).

2.2.3 Self-Association and Molar Mass

The molar mass of asphaltenes had been a controversial issue for many years. Two of the main reasons for the controversy are: the polydisperse nature of asphaltenes and the association behavior of asphaltenes even at low concentrations. As a result, the application of any experimental technique to measure the molar mass is uncertain. The development of advanced mass spectrometry techniques in recent years has helped to reach a consensus on the asphaltene molecule (or monomer) molar mass. Mullins (2010) summarized the available experimental techniques (classified as mass spectrometry and molecular diffusion methods) to report the molar mass of asphaltene monomers in the range of 400 to 1000 g/mol.

Since asphaltenes can associate with each other even in dilute solutions, numerous studies have been carried out to investigate the self-association behavior. Self-association has been experimentally observed from the trends of asphaltene apparent molar mass with concentration. The apparent molar mass is the product of the monomer molar mass and the aggregation number of the self-associated asphaltenes. Some of the experimental methods used to observe the asphaltene self-association are vapor pressure osmometry (Yarranton et al., 2000), interfacial tension measurements from a drop volume tensiometer (Yarranton et al., 2000), small-angle X-ray and neutron scattering measurements (Xu et al., 1995; Spiecker et al., 2003), differential scanning calorimetry (Andersen and Birdi, 1991), dielectric spectroscopy (Maruska and Rao, 1987), two-step laser mass spectrometry (Pomerantz et al., 2009) and Fourier transform ion cyclotron resonance mass spectrometry (Rodgers and Marshall, 2007).

Vapour pressure osmometry provides what is probably the most direct measure of asphaltene association. For example, the apparent molar mass of asphaltenes in toluene increases from approximately 1000 to 5000+ g/mol as the concentration of asphaltenes increases from 2 to 40 g/L. In most cases, at concentrations above 10 g/L, the apparent molar mass approaches a constant value in the order of 5000 to 10,000 g/mol. Hence, the

self-associated asphaltenes consist of three to ten molecules per aggregate on an average. Also, the extent of asphaltene self-association has been found to decrease in better solvents (such as toluene), at higher temperatures and with increasing resin content (Yarranton, 2005; Yarranton et al., 2007).

The mechanism of asphaltene association is not well understood and likely depends on the type of asphaltene structure (Yarranton, 2005). With a condensed structure, the asphaltenes would likely form colloidal stacks of asphaltene molecules held together with π-π bonds. These stacks are believed to be dispersed in the solution via a surround layer of resins. With the dispersed structure, the self-association may resemble polymer systems. The aggregates could be considered as macromolecules, where the individual molecules are held together with π-π, acid-base and/or hydrogen bonding. The macromolecules are believed to be freely dispersed in solution just like any other molecule.

The relative significance of the forces holding the aggregates together is unknown. A molecular mechanics investigation of asphaltene aggregation has emphasized the importance of hydrogen bonding (Murgich, 2002). Hydrogen bonding between the asphaltene molecules is more likely due to heteroatoms in the functional groups. However, since asphaltenes consist mainly of carbon and hydrogen atoms, it is also important to consider van der Waals interaction forces. Although van der Waals forces are very weak, its overall contribution could be significant once the asphaltene molecules are highly packed (Rogel, 2000).

2.2.4 Properties

Both thermodynamic and dielectric properties of asphaltenes have been studied in the literature. Thermodynamic properties include molar volume or density, solubility parameter and heat capacity (Laštovka et al., 2008). Dielectric properties include

permittivity or dielectric constant and dipole moments (Sheu et al., 1994; Pedersen, 2000). The two most significant properties of asphaltenes for this thesis are density and solubility parameter.

2.2.4.1 Density

Gravimetric measurements are normally used to obtain the density of asphaltenes. The densities of solid asphaltenes from crude oil were reported to be between 1170 and 1280 kg/m³ (Rogel and Carbognani, 2003). The density of asphaltenes with a smaller H/C ratio (more aromatic) was larger than the asphaltenes with a larger H/C ratio. The effective liquid density of asphaltene in mixtures was measured using an indirect method (Yarranton and Masliyah, 1996). In this approach, the densities of solutions of different concentrations of asphaltenes in toluene were measured. The asphaltene density was back-calculated assuming zero excess volumes of mixing. The reported density by this method ranged from 1100 to 1200 kg/m³ for asphaltenes from a variety of sources.

2.2.4.2 Solubility Parameter

The definition of solubility parameter (δ) is given by the following equation (Hildebrand and Scott, 1950):

$$\delta = \left(\frac{-E}{v} \right)^{1/2} \tag{2.3}$$

where, E is the cohesive energy of the liquid and v is the molar volume at a given pressure and temperature. The unit of the solubility parameter is the square root of pressure units. Physically, the extent of miscibility of two components depends on the closeness of solubility parameter of those components. At temperatures below the normal boiling point and low pressures, the most used expression for solubility parameter is given by:

$$\delta = \left(\frac{\Delta H^{vap*} - RT}{v} \right)^{1/2} \tag{2.4}$$

where ΔH^{vap*} is the molar heat of vaporization (J/mol), R is the universal gas constant (8.314 J/molK), v is the molar volume (cm^3/mol), and T is the absolute temperature (K). For these units, the solubility parameter is reported in $MPa^{0.5}$.

Measured data for enthalpy of vaporization are available in the literature for pure components in most cases or can be determined from an equation of state. Hence, the solubility parameters for pure components are calculated for a given pressure and temperature. Barton (1991) and Hansen (2007) provided a complete list of solubility parameter data for most of the pure components. These references also present numerous empirical correlations to link the measurable physical properties (for example, viscosity, permittivity, refractive index, and surface tension) of a pure component to solubility parameter. For unknown compounds, solubility parameter can be obtained by measuring the heat of vaporization, vapor pressure, boiling point, heat of mixing and internal pressure. The influence of pressure and temperature on solubility parameter on pure hydrocarbon components and a few non-hydrocarbon gases has also been investigated (Verdier, 2006).

Solubility parameter correlations for crude oil as a whole are usually based on average molar mass of the oil (Chung, 1992; Zhou et al., 1996). Solubility parameter of oils with or without solution gases are also calculated by relating to either internal pressure (Verdier and Andersen, 2005) or refractive index (Buckley et al., 2007). Recently, Zuo et al. (2010) established empirical correlations for calculating the solubility parameters of oils with solution gas at high pressures and temperatures as a function of density.

The determination of solubility parameters of asphaltenes is uncertain due to their operational definition. Hirschberg et al. (1984) reported the solubility parameter of

asphaltenes as 19.50 $MPa^{0.5}$ with a correction for temperature dependence. Lian et al. (1994) used the miscibility of asphaltenes in various solvents to report the solubility parameter values ranging from 17.6 to 21.3 $MPa^{0.5}$. Yarranton and Masliyah (1996) determined the solubility parameter to be in the range of 19 to 21 $MPa^{0.5}$ by fitting their solubility model to asphaltene-toluene-*n*-heptane solubility data.

Andersen (1999) investigated eighteen different crude oils to plot the ratio of volume of precipitant to volume of oil against the ratio of volume of solvent to volume of oil. Based on the plot, solubility parameter of asphaltenes is calculated within 19 and 22 $MPa^{0.5}$ at ambient conditions. Wang and Buckley (2001) used asphaltene molar volume (or density) and solubility parameters as fitting parameters in their solubility model for predicting asphaltene precipitation. The fitted solubility parameter of asphaltene is within the range of 20.0 to 20.5 $MPa^{0.5}$. Verdier (2006) used density and internal pressure to determine the asphaltene solubility parameters in the range 20 to 23 $MPa^{0.5}$.

2.2.5 Surface Activity

Numerous studies have focused on the characterization of surface active materials at the water-oil interface that include asphaltenes. The surface activity of asphaltenes can be attributed to hydrophilic functional groups embedded in a hydrophobic hydrocarbon structure. For example, acidic and basic heteroatom groups containing oxygen, nitrogen and sulphur are hydrophilic. Hence, asphaltenes behave as surfactants and can adsorb at the water-oil interface. The adsorbed asphaltenes contribute to the formation of stable emulsions that make oil-water separation difficult and thereby causing problems in downstream operations (Stephenson, 1990).

The most cited evidences for the asphaltene surface activity is based on the interfacial tension measurements. An increase in concentration of asphaltenes reduced the interfacial tension between the model oil (for example, heptane-toluene mixtures) and

water systems (McLean and Kilpatrick, 1997; Yarranton et al., 2000). The reduction in interfacial tension has been observed in highly acidic or basic media, suggesting that both acidic and basic groups interact at the interface (Acevedo et al., 1992; Sheu et al., 1995).

Resins are also considered as a surface active component of the crude oil. For example, the most stable interfacial films and emulsions are created by a combination of asphaltenes and resins (Mohammed et al., 1993; Khristov et al., 2000). However, Gafonova and Yarranton (2001) reported addition of resins tend to destabilize the model emulsions. Using the thin liquid film-pressure balance apparatus, Taylor et al. (2002) observed that toluene-asphaltene films and toluene-bitumen films could be compressed to the same thickness (8.5 nm bilayer). Therefore, it has been concluded that the surface active materials at the bitumen-water interface were mainly asphaltenes. In addition, it was noted that upon removal of high molar mass asphaltenes, the bilayer decreased from 8.5 nm to 5.1-7.3 nm and the film stability was reduced.

The chemistry of surface active components at the water-oil interface has been examined in the past as well. Xu et al. (1999) reported that surface active components or the interfacial material in the bitumen-water system are polar and oxygen containing compounds. Wu (2003) developed an experimental methodology to isolate the interfacial material from Athabasca bitumen emulsified with heavy water (D_2O). The elemental analysis indicated that interfacial material contained H/C atomic ratio of 1.13 above the onset of precipitation, whereas the interfacial material isolated below the onset of precipitation consisted of carboxylic salts with H/C ratio of 1.32. A high resolution mass spectrometry analysis also indicated that interfacial material consists of highly condensed aromatics, rich in acidic O_2, O_2S, O_3S, O_4 structure classes and basic N, NS heteroatom structure classes (Stanford et al., 2007a, 2007b).

2.3 Asphaltene Precipitation

2.3.1 General Description

Asphaltenes precipitate upon changes in crude oil composition, pressure and temperature. Composition induced precipitation occurs when the oil becomes less aromatic due to the addition of gases or paraffinic solvents to the oil. For example, for conventional oil operations, typical injection gases for enhanced oil recovery processes, gas lift operations, and/or acidizing jobs consist of carbon dioxide, nitrogen, and light paraffinic hydrocarbon gases such as methane, propane and butane. These gases can induce precipitation when the dissolved gas concentration exceeds a certain limit at a given pressure and temperature (Kokal et al., 1992; Idem and Ibrahim, 2002; Jamaluddin et al., 2002; Creek et al., 2008; Badamchi-Zadeh et al., 2009). To take another example, heavy oils or bitumen are highly viscous and are therefore diluted with condensates, distillation cuts (naphtha), or light oil to reduce the viscosity for processing and transport. These diluents are usually rich in paraffinic components and may result in precipitation.

Pressure-induced precipitation can occur for some conventional crude oils. These oils are usually highly under-saturated and contain high concentration of light hydrocarbon gases such as methane, ethane, and propane, and also a higher concentration of light (paraffinic) liquid compounds that act as a poor solvent for asphaltenes. As the oil is depressurized during production, the relative molar volumes of the solution gas and light ends tends to increase significantly relative to the heavier components in the oil. Consequently, asphaltenes start to precipitate at a certain pressure called the upper asphaltene precipitation onset pressure.

At the bubble point, the oil has the highest content of dissolved gas by volume and therefore the maximum amount of asphaltene precipitation will occur (Hammami et al., 2000). Below the bubble point, solution gas and other volatile components will evolve from the oil as a gas phase resulting in the liquid phase becoming a better solvent for the

asphaltenes. Hence, the precipitated asphaltenes will start to redissolve into the oil. The pressure at which the last of the precipitated asphaltenes redissolve is called the lower asphaltene precipitation onset pressure. Temperature change has a minor effect on the onset and amount of precipitation when compared to pressure change.

The term “stability” is often used to describe the propensity of a crude oil to precipitate asphaltenes or, in other words, how well the asphaltenes are dissolved in the crude oil. An oil is considered unstable if asphaltenes precipitate at the specified conditions. For instance, an oil-solvent mixture is unstable at solvent contents above the onset of precipitation and stable below the onset. When oils undergo depressurization, oil is unstable between the upper and lower asphaltene precipitation onset pressures. Note, precipitation conditions do not appear to correlate to the asphaltene content of an oil. For example, a crude oil from Venezuela with 17.2 wt% asphaltenes was produced with no asphaltene related production problems, whereas the Hassi-Messaoud field in Algeria had numerous problems with only 0.15 wt% asphaltenes (Sarma, 2003).

2.3.2 Precipitation Onsets and Amount

At atmospheric conditions, the most common method to determine the precipitation onset is the titration of oil against the precipitating solvents (Andersen, 1999). Microscopic examination of an oil-solvent mixture is also adapted by some authors (SMS 1600; Buckley, 1996). The most common methods for oils under high pressure and temperature are light scattering technique with a near-infrared light source and high pressure microscope (HPM) systems (Hammami and Ratulowski, 2007). HPM allows direct visual observation of multiple phases present at elevated pressure and temperature. Overall, optical methods are usually limited to light oils with low asphaltene content because of the limitation on the opacity of oils. Other methods with physical property measurements are used when the low light transmittance is encountered.

Amount of precipitation is usually measured using filtration (Leontaritis et al., 1994) and centrifugation (Akbarazadeh et al., 2005; Tharanivasan et al., 2009) techniques for oils at atmospheric conditions. In these techniques, the oil is mixed with an appropriate solvent and filtered or centrifuged. However, various filtration techniques are adapted for oils at elevated pressures and temperatures to measure the precipitation amounts (Peramanu et al., 1999; Edmonds et al., 1999; Fahim et al., 2004; Negahban et al., 2005). HPM system coupled with post-filtration technique is adapted widely for such amount measurements (Hammami and Ratulowski, 2007).

2.3.3 Particle Size and Flocculation

Once precipitated, asphaltene particles tend to flocculate. The size of the flocs is likely an important factor in deposition because particles above a certain size would deposit (Eskin et al., 2011). Floc sizes of 300 nm to several hundred microns have been observed (Ferworn et al., 1993; Rastegari et al., 2004; Mullins, 2010). The mean particle size of asphaltenes from a mixture of asphaltenes and mixed solvents, and light oils (Alkafeef, 2001; Burya et al., 2001) appear to be at least one order of magnitude smaller than asphaltene flocs from heavy oils/bitumens (Ferworn et al., 1993; Nielsen et al., 1994).

The type of precipitant, temperature and hydrodynamics (shear) affect asphaltene particle size during flocculation (Bouts et al., 1995; Eskin et al., 2011). As the number of carbon atoms in the *n*-alkane precipitating solvent series increases, the mean particle size decreases (Ferworn et al., 1993). For a mixture of asphaltene in mixed solvent (typically a mixture of *n*-heptane and toluene), the mean particle size decreases as the volume ratio of *n*-heptane to toluene decreases (Yudin et al., 1998) or if resins are added to the mixture (Alkafeef, 2001). The mean particle size decreases with an increase in temperature while pressure appears to have no significant effect (Nielsen et al., 1994). The asphaltene mean particle size is expected to decrease with shear (Ferworn et al., 1993; Rastegari et al., 2004; Eskin et al., 2011). It was also observed that the asphaltene

flocs are generally unstable and even a slight shaking break the flocs into stable asphaltene particles of approximately one micron (Anisimov et al., 1995).

2.4 Asphaltene Precipitation Models

Asphaltene precipitation modeling has been the subject of much research over the past 30 years and is still a challenging topic because asphaltenes are a mixture of ill-defined components, they self-associate even at very low concentrations, and the form of asphaltenes in the crude oil (colloids or macromolecules) is still unknown. Experimental measurements for live oils (oils containing solution gas at high pressure and temperature conditions) are usually conducted at reservoir conditions or over a narrow range of temperatures close to reservoir conditions. For dead oils (solution gas-free oils at atmospheric conditions), the measurements are usually carried out over a defined range of concentration for a particular solvent. Based on differing oils, experimental approaches, and author viewpoints, a number of different models have been proposed in the literature for predicting the onset condition and the amount of asphaltene precipitation. The existing modeling approaches can be broadly classified into colloidal and thermodynamic models.

The colloidal models hold that the asphaltenes are dispersed in oil as solid colloidal particles. Each particle is a stack of asphaltenes, which is stabilized by resins adsorbed on its surface or concentrated around the asphaltenes (Dickie and Yen, 1967). The resins are believed to act as peptizing agents and maintain the asphaltenes in a colloidal dispersion (as opposed to a solution) within the crude oil. The resins are assumed to partition between the asphaltene particles and the asphaltenes-free part of the crude oil or solvent. Precipitation is believed to occur when the resins are stripped from the colloid allowing aggregation and physical separation. To model the precipitation, the phase stability of the system is related to chemical potential of the resins in both asphaltenes and oil (solvent) phases (Leontaritis and Mansoori, 1987). At the onset point of precipitation, where the

concentration of resins in the liquid phase is just enough to peptize asphaltenes, the chemical potential is called the critical chemical potential of the resins. The critical chemical potential of resins is calculated from the Flory-Huggins theory for polymer solutions and the measured onset data. The molar volume and solubility parameter are also required for the calculation. Given the critical concentration of resins in crude oil, asphaltene precipitation is predicted at other conditions. Wu et al. (1998) and Pan and Firoozabadi (1998) also presented a variation of the colloidal model to account for the asphaltene-resin interactions. Overall, the colloidal model predicts that precipitation is irreversible.

Thermodynamic models presume that the asphaltenes are part of a non-ideal mixture and their behavior is governed by conventional thermodynamics. The asphaltenes are assumed to behave as macromolecules that are able to self-associate and precipitation is considered to be liquid-liquid or liquid-solid phase transition. Thermodynamic models predict that precipitation is reversible. There are two main types of thermodynamic model applied to asphaltene precipitation: regular solution and equations of state models. Regular solution theory based models are usually semi-empirical and predict the effect of solvent addition on asphaltene precipitation with good accuracy. Equations of state based models are readily applicable for simulation with pressure and temperature effects. The main thermodynamic models are briefly outlined below.

2.4.1 Regular Solution Based Models

Regular solution theory is one of the approaches to model polymer-like systems. The basic assumption of this approach is no volume change in mixing. Regular solution theory has been modified to include a Flory-Huggins entropic contribution from the difference in molecular sizes (Flory, 1941; Huggins, 1941) as well as an enthalpy contribution from Scatchard-Hildebrand solubility theory (Scatchard, 1949; Hildebrand, 1949). This approach has been successfully applied to predict the solubility of

asphaltenes in asphaltene-solvent systems (Yarranton and Masliyah, 1996). The model parameters are mole fraction, molar volume and solubility parameter of each component in the system.

Hirschberg et al. (1984) first used this approach to model asphaltene precipitation by assuming an asphaltene component and a non-asphaltene component in the live crude oil. For a given crude oil containing solution gas, a vapor-liquid equilibrium (VLE) calculation is first performed to determine the amount and properties of both vapor and liquid phases. Then the liquid-liquid equilibrium (LLE) calculation is carried out on the liquid phase using regular solution theory assuming no influence of the precipitated asphaltenes phase on the previously calculated VLE.

Kawanaka et al. (1991) used a model for poly-disperse polymer solution and a molar mass distribution for asphaltenes. An interaction parameter has been introduced into the regular solution model to fit the asphaltene precipitation data (Andersen and Speight, 1999; Yang et al., 1999). Later, this approach was refined to predict the precipitation onsets and amounts from diluted crude oils (Cimino et al., 1995; Alboudwarej et al., 2003; Wang et al., 2004; Correra and Merino-Garcia, 2007; Creek et al., 2009).

Wang and Buckley (2001) adapted the regular solution approach to develop a two-component solubility model. The crude oil is characterized into asphaltene and non-asphaltene components. The required input parameters are molar volume and solubility parameter of the two components. The properties of non-asphaltene component are determined by relating those to refractive index through measured data or correlations (Buckley et al., 1998; Buckley and Wang, 2002). The properties of the asphaltene component are used as fitting parameters in the model. The model then calculates the free energies of mixing and thermodynamically predicts the appearance of a separate asphaltene phase in mixtures. This solubility model is specifically developed for modeling the precipitation from pure *n*-alkane diluted crude oils at ambient conditions.

Buckley et al. (2007) also summarizes various methods to determine the precipitation onset conditions for pure *n*-alkane diluted oils based on the solubility parameter of oil-solvent mixture, oil and solvents used for dilution. These methods require titration data (volume of each solvent required to precipitate asphaltenes) and refractive index measurements for the oil-solvent mixture. In addition, the two-component fluid characterization is an oversimplification and may not fit for direct use in compositional reservoir simulators.

Wang et al. (2004) developed an empirical methodology based on regular solution theory to predict the onset of asphaltene instability from live oils. The basis of the method is the correlation between solubility parameter and the refractive index so that a refractive index measurement can be used to determine the solubility parameter (Buckley, 1999). First the dead oil solubility parameter is determined from its refractive index. Then the live oil solubility parameter is determined from the dead oil refractive index, PVT data, and a relationship between the onset solubility parameter and the molar volume of *n*-alkanes or asphaltene instability trend (Creek et al., 2009). Hence, the solubility parameter of the live oil is compared with the solubility parameter at the onset of precipitation to determine the stability of the oil.

The advantage of Wang et al. (2004) model is that it avoids the use of molar mass of asphaltenes. However, the predictions are mainly governed by the calculated solubility parameters. A change in the onset solubility parameter along the depressurization path depends on the extrapolation of the asphaltene instability trend to lower molar volumes. The accuracy of the model depends on refractive index measurements. Density changes are accounted only through molar volume of dissolved gases with pressure. A more detailed characterization of crude oil and the information about distribution of component properties are necessary to obtain reliable predictions. Asphaltene self-association must be accounted as well to better describe the precipitation behavior. Buckley et al. (2007) also briefly investigated the asphaltene stability in crude oil

mixtures. However, the predictions are not reliable because the diluted solvents are not pure and limit the applicability of asphaltene instability trend relationship.

Kraiwattanawong et al. (2007) modified the Wang et al. (2004) model to more accurately account for the dissolved gas. The live oil solubility parameter was calculated by combining the dead oil solubility parameter (determined from the refractive index) and the dissolved gas solubility parameter using the volume average mixing rule at the reservoir conditions. The dissolved gas solubility parameter was estimated from its composition and individual pure component solubility parameters. The Peng-Robinson equation of state with volume correction was used to estimate the molar volume and composition of the live oil at reservoir conditions. By adapting the refractive index approach, it is not necessary to directly determine the solubility parameter of the oil or the molar mass distribution of the self-associated asphaltenes. However, these models do not predict asphaltene yields and can be challenging to apply when the oil composition changes; for example, when multiple liquid phases form.

Alboudwarej et al. (2003) and Akbarzadeh et al. (2005) developed a generalized regular solution model for predicting asphaltene precipitation from *n*-alkane diluted heavy oils and bitumens. The oil samples are characterized into SARA fractions. Asphaltenes were further divided into 30 sub-fractions based on gamma distribution function to account for the distribution of aggregates resulting from self-association. The generalized property correlations for molar volumes and solubility parameters of SARA fractions were developed. A liquid-liquid equilibrium was assumed between a heavy liquid phase (asphaltenes-rich phase including asphaltenes and resins) and a light liquid phase (oil-rich phase including all other components). The only unknown parameter in the model was the average molar mass of asphaltenes that was found by fitting the *n*-heptane precipitation data. Precipitation caused by blending of oils and due to depressurization was not investigated in their work.

2.4.2 Cubic Equations of State Based Models

Since compositional reservoir simulators are primarily based on various cubic equations of state (EoS) to calculate the phase equilibrium of hydrocarbon fluids, the EoS method certainly has an advantage over the regular solution based models for asphaltene precipitation. Traditional Soave-Redlich-Kwong and Peng-Robinson (PR) cubic equations of state have been widely used to model the asphaltene precipitation behavior. Few models accounted for self-association of asphaltenes directly or indirectly. Overall, EoS models are very useful for generating precipitation phase envelopes and are limited in application for precipitation due to dilution.

In the first and simplest cubic EoS model, asphaltenes are considered as either single or multiple heavy pseudo-components. The properties of characterized crude oil components are either calculated or estimated. The binary interaction parameters are adjusted to cause a liquid-liquid split at the observed asphaltene precipitation onset point. In some cases, solid phase fugacity models have been used in conjunction with cubic EoS because liquid-liquid equilibrium phase split may allow gas components to be associated with asphaltene phase. One of the main drawbacks of such EoS approach is the estimation of critical properties for the heavy components of crude oil and asphaltenes because these components decompose well before boiling point. The estimation of these properties are therefore carried out based on structural correlations (Gupta, 1986; Akbarzadeh et al., 2004), tuning the model to experimental data (Nghiem and Coombe, 1996) or by using the same critical properties as a pure heavy hydrocarbon (Qin et al., 2000). However, unrealistic property values are obtained for asphaltenes and heavy pseudo-components.

Du and Zhang (2004) developed a model based on PR equation of state. Asphaltenes are considered as a solid precipitating phase and traditional equilibrium calculations are performed to predict the crude oil phase behavior. The oil is characterized into pure components and 4 or 5 pseudo-components. One of the pseudo-components is

asphaltenes. It was assumed that the asphaltenes exist as monomers in bulk crude oil and are capable of associating with each other. The precipitation is believed to occur as a result of association. To account for the association, an additional term was added to the usual fugacity expression for any pure component. The additional term is negligible for all components except asphaltenes. The additional term is determined by fitting the precipitation onset or amounts. Hence, the amount of precipitation is calculated for a given pressure and temperature conditions. The major drawbacks of the model are the characterization of asphaltenes and the methodology to account for association. There is no distribution of asphaltene components of different sizes in the crude oil. The association is considered in terms of several polymer reactions and the equilibrium constants are lumped into a single fitting parameter.

Sabbagh et al. (2006) adapted the PR-EoS with group contribution methods to model asphaltene precipitation from solutions of toluene and an *n*-alkane and from *n*-alkane diluted heavy oils/bitumens. This model accounts for the asphaltene self-association behavior but as an externally determined input parameter. However, this model used unrealistic values for binary interaction and EoS parameters. Recently, Castellanos Díaz et al. (2011) tested the PR EoS to model the phase behavior bitumen and solvent mixtures. Specifically, heavy oil fluid characterization was examined with a focus on the extrapolation of SIMDIST data and the associated property correlations. The model successfully predicted the vapor-liquid equilibrium and liquid-liquid equilibrium behavior of propane-CO_2-bitumen system. However, the model could not predict the asphaltene precipitation yields from bitumen at high dilution with *n*-heptane. The authors attributed the model failure to the use of conventional mixing rules and symmetric interaction parameters for asphaltene components.

2.4.3 Association Equations of State Based Models

Equations of state for associating fluids have also been used to model asphaltene precipitation. Two well-known approaches in this category are cubic plus association (CPA) and statistical associating fluid theory (SAFT) equations of state. First consider CPA. In the CPA-EoS, an additional association term is added to classical SRK or PR EoS. Initially, the additional term is used to account only for hydrogen bonding contribution. Later, several modifications were made to the additional term for modeling specific pure component mixtures. The CPA-EoS requires at least five parameters for each self-associating component. For non-associating species, the usual three parameters critical temperature, critical pressure and acentric factor are sufficient. Experimental data are required to determine all these parameters.

CPA-EoS was first applied to model asphaltene precipitation from crude oils by Edmonds et al. (1999). Specifically, SRK-EoS is used with an additional term to describe the association of asphaltene molecules and their solvation by resin molecules. The oil is characterized into pure components, pseudo-components, single-component resins and single-component asphaltenes. The critical properties of the pseudo-components are tuned using the bubble point data of the oil. The additional term contains two temperature-dependent association constants. These constants are determined by fitting the measured precipitation onset data. The required input to the model are composition of live oil, total asphaltene content of stock tank oil precipitated by using *n*-heptane, asphaltene to resin ratio in wt% usually obtained from SARA analysis, one set of precipitation onset and/or amount data and the saturation or bubble point data (Yonebayashi et al., 2011).

Following the Edmonds et al. (1999) model, several improvements are made to CPA-EoS to better predict the asphaltene phase behavior. Recently, Li and Firoozabadi (2010a, 2010b) altered the characterization methodology by dividing the oil into pure, light pseudo hydrocarbon, heavy pseudo hydrocarbon and asphaltene components.

Precipitation is modeled as LLE above the bubble point and as VLE below the bubble point. Self-association between molecules and cross-association between asphaltenes and heavy components are described by thermodynamic perturbation theory. Although association is taken into account, asphaltenes are considered as a single component and a single molar mass is used for asphaltenes. Five association parameters are assigned based on several assumptions and one association parameter is used as a fitting parameter in the model.

SAFT was based on extensions and simplifications of Wertheim's first order perturbation theory for associating fluids. SAFT is widely applied for both polar and non-polar substances including polymers. In SAFT, molecules are modeled as chains of bonded spherical segments. Numerous forms of the SAFT equation of state have been proposed as well. These forms differ only in the segment term used to account for the van der Waals attraction between molecules. All forms use the same chain and association terms introduced in original SAFT-EoS by Chapman et al. (1990).

The Perturbed Chain version of SAFT (or PC-SAFT) is usually adapted to model asphaltene precipitation from crude oils (Gross and Sadowski, 2001). Briefly, asphaltene precipitation is modeled based on the molecular size and van der Waals interactions. For each non associating species in SAFT, the equation of state requires the three physical parameters:σ, the diameter of each molecular segment, m, the number of segments in the molecule, and ε/k, the interaction energy (van der Waals attraction) between each molecular segment. Two additional parameters are included for associating molecules: association energy and association volume.

Most pure component parameters are available in the literature or taken from the fits to the component's saturated liquid densities and vapor pressures. Parameters for heavy hydrocarbon or pseudo-components including asphaltenes are estimated from the average molar mass or correlated to measured refractive index at the precipitation onset.

Asphaltene precipitation due to dilution and depressurization effects has been modeled in the literature (Ting et al., 2003; Buenrostro-Gonzalez et al., 2004). Although the PC-SAFT model provides more flexibility in matching complex temperature-dependent behavior, it requires additional parameters to characterize association energies (Gonzalez et al., 2005; Vargas et al., 2009).

2.5 Effect of Emulsified Water on Asphaltene Precipitation

To date, all asphaltene precipitation models have been developed and tested on water-free crude oils. In reality, water is almost always associated with produced or extracted crude oil. Hence, it is necessary to determine and account for the effect of emulsified water on asphaltene precipitation.

Solubilized water may affect asphaltene self-association which in turn can affect asphaltene precipitation. Andersen et al. (2001) tested this idea with calorimetric measurements of asphaltene association. A sample of water-free toluene was placed in a calorimeter and asphaltene-toluene solution was added. The amount of heat absorbed due to the addition of the solution was measured and related to the aggregation behavior. The experiment was then repeated with an asphaltene-toluene solution containing trace amounts of water (~0.047 wt%). The data indicated a change in the amount of heat absorbed with a change in trace water concentration suggesting that asphaltenes do interact with water and change their aggregation behavior.

Murgich et al. (2002) conducted molecular simulation studies to investigate the aggregation behavior of asphaltenes in toluene with and without the presence of trace amounts of water. Their study concluded that the presence of water molecules promotes the association of asphaltenes due to its small size and high intrinsic polarity. In addition, it was reported that water may form bridging H bonds between the heteroatom of asphaltenes with a considerable span of energies. Khvostichenko et al. (2004) examined

the state of water molecules in asphaltene-toluene-water solution using infra-red spectroscopy measurements. They found that water molecules existed as both without forming hydrogen bonds (free water) and also as hydrogen- bonded water molecules (bound water).

Andersen et al. (2001) examined the effect of dissolved water on the solubility of asphaltenes in an organic solvent. An organic solution of either pure toluene or a solution of asphaltenes in toluene was placed above the water for a given amount of time. A sample of organic solution was extracted and the water content was measured with a Karl-Fischer titration apparatus. The water content of asphaltene-toluene solution was higher than that of the pure toluene solution indicating that the presence of asphaltenes increases the solubility of water in the solvent. Khvostichenko and Andersen (2008) also found that solubility of water in asphaltene-toluene solutions increases as the asphaltene concentration increases. However, their work does not indicate if there is any effect on the onset and the amount of precipitation when the crude oil is diluted with precipitating solvents.

Gelin et al. (2004) tested a live oil (oil containing solution gas under high pressure) with emulsified water to determine the effect of water on asphaltene precipitation. The precipitation was induced by isothermal depressurization of the live oil sample with and without emulsified water. The precipitation onset pressures were measured and compared and it was found that the onset pressure did not change with the presence of water but could not determine if the amount of precipitation was affected by the presence of water. It has also been speculated that chemical composition of precipitated asphaltenes in the presence of water may possibly differ from the precipitated asphaltenes in the absence of water and therefore affect the deposition behavior. However, there is no evidence to validate this speculation.

2.6 Summary

Asphaltenes precipitation has been the subject of research for decades. A number of models have been developed for asphaltene precipitation. The most successful models are equilibrium models based on either regular solution theory or equations of state. Equations of state have been applied to detecting the onset of asphaltene precipitation upon depressurization of the crude oil. They have not yet been successful in predicting asphaltene yields from the depressurization of light crude oils or the dilution of heavy oils. Furthermore, equation of state models must be fitted to match precipitation data for each diluent. Regular solution models, on the other hand, have been applied to asphaltene precipitation from diluted heavy oils and can successfully predict the effect of different diluents. However, these models have not been applied to blended oils or live oils undergoing depressurization. Neither the equation of state nor the regular solution based models have been applied to crude oils containing emulsified water.

One of the issues associated with regular solution models is the characterization of crude oils. The fluid is normally characterized into SARA fractions or one asphaltene component and one non-asphaltene component. For live oils, light gases and several additional pseudo-components are considered. The properties are either estimated from correlations or tuned to the experimental data. The characterization methodologies adapted for dead oils and live oils are not the same. Hence, there is no consistent approach to model the precipitation from diluted dead oils and live oils due to depressurization.

CHAPTER 3

Experimental Methods

In this chapter, the experimental methods used in this thesis are presented including composition measurements, dead oil (depressurized oils from which all solution gas has evolved) tests and live oil (oils containing solution gas under high pressure) experiments. Composition measurements include GC analysis, SARA fractionation, water content determination for crude oils, and elemental analysis for asphaltenes. Dead oil tests include density, asphaltene precipitation onset, and asphaltene yield measurements. Live oil tests involve sample preparation, gas-oil ratio measurement, density measurement, bubble point pressure determination, measurement of the onset pressure for asphaltene precipitation, and yield measurements.

Note, company-specific protocols and methodologies were used for some of the analyses as described in this chapter. Some details of these procedures are confidential and the procedures are described only as much as permitted.

3.1 Oil Samples

Nine different crude oil samples (Crudes A to I) and a light gas oil (LGO) were used in this thesis. The crude oil samples included four heavy oils/bitumens, three onshore conventional oils and two offshore light oils. Table 3.1 lists all of the oils tested in this thesis. All the data related to Crude A to D and LGO were measured by the author at the University of Calgary (UofC). Live oil tests conducted using Crude D at Schlumberger's DBR Technology Center (DBR), Edmonton, Alberta, Canada, were designed and supervised by the author. Crude E and Crude F data sets were obtained from National Center for Upgrading Technology (NCUT), Devon, Alberta, Canada. The data for Crude G, H and I were provided by Centro Tecnológico Repsol, Móstoles, Spain.

Crude A was a heavy oil blend obtained from Husky Oil Ltd.; two-thirds of the blend was from the Lloydminster area in Saskatchewan and one-third was from the Cold Lake area in Alberta. This blend was a feed to the Husky Lloydminster Upgrader and had been processed to remove contaminants such as, water, water-soluble salts, clay and sand.

Crude B was a coker-feed bitumen extracted from the Athabasca oil sands and was provided by Syncrude Canada Ltd. This bitumen had been treated to remove water and sand.

Crude C was an unprocessed bitumen produced by Cyclic Steam Stimulation recovery process in the Peace River area of Alberta and it was provided by Shell Canada Ltd. The water content of this sample was determined by Karl-Fischer titration (See Section 3.2.4) and was found to be 19 wt%. Therefore, the bitumen was treated at the UofC to remove the water using the dilution method (Alboudwarej et al., 2002). Briefly, the bitumen sample was first diluted with *n*-heptane (98% pure) in the ratio of 1.1 cm^3 of *n*-heptane to 1 g of unprocessed bitumen. The resulting mixture was maintained at about 70°C for 3 days in a separating funnel. At this condition, the density of oil was reduced sufficiently to allow the water to settle. The water was removed resulting in a water-free diluted bitumen. *n*-Heptane was then recovered from diluted bitumen in a rotary evaporator at 70°C and 34 kPaa (20″ Hg vacuum). Note that the light ends loss during evaporation was negligible. The water content of the treated bitumen was 1.5 wt%.

Crude D was a light crude oil from the Gulf of Mexico and was provided by DBR. This oil was originally supplied to DBR by British Petroleum. The water content of the sample was 0.4 wt%.

Crude E is another sample of bitumen extracted from the Athabasca oil sands. Crude F is a conventional crude oil from Alberta, Canada. Crudes G, H and I were obtained from the Gulf of Mexico, Venezuela and the Middle East, respectively. The water content of these samples was determined using the ASTM D4006 procedure and all were found to be less than 0.1 vol% of oil.

The light gas oil (LGO) was obtained from Shell Canada Ltd. This gas oil was a refinery product and it was free of any asphaltenes.

Table 3.1: Oil samples used in the thesis work.

Oil Sample	Source	Type	°API
Crude A	Lloydminster + Cold Lake	heavy oil	11
Crude B	Athabasca	bitumen	7
Crude C	Peace River	bitumen	8
Crude D	Gulf of Mexico	offshore light oil	30
Crude E	Athabasca	bitumen	9
Crude F	Alberta	conventional oil	32
Crude G	Gulf of Mexico	offshore light oil	21
Crude H	Venezuela	conventional oil	33
Crude I	Middle East	conventional oil	31
LGO	Shell Refinery	distillate fraction	22

3.2 Composition Measurements

3.2.1 C30+ Analysis by Gas Chromatography

Gas Chromatography (GC) analysis was performed on synthetic solution gas sample used to prepare live oil, flashed gas and flashed oil from live oil. The analysis was carried out at DBR.

For gas sample analysis, the GC equipment consisted of a sample injection loop, chromatographic columns, and detectors. Gas samples were injected by connecting the sample container to the pre-evacuated injection loop through valves. The injection loop was heated to 150°C to ensure there is no liquid condensate drop-out during sample injection. The injected sample was then split into two streams. One of the streams passed through two packed stainless steel columns (2m×1/8″ of Restek Rt-XL Sulfur and 15ft×1/8″ of molecular sieves 13×60/80 mesh) in series. Each column was connected to a common thermal conductivity detector (TCD). The Rt-XL sulfur column was used for trapping and isolating carbon dioxide, hydrogen sulfide, ethane, propane, *iso*-butane and *n*-butane. The molecular sieve column was used for separating oxygen, nitrogen and methane.

The other injected stream passed through a capillary column (60m×0.25mm×1μm Varian VF-1MS Fused Silica) that was connected to a flame-ionization detector (FID). FID is used to detect *n*-alkanes from C1 to C10, *i*-butane, *i*-pentane, methylcyclopentane, benzene, cyclohexane, methylcyclohexane, toluene, ethylbenzene, *o*-, *m*- and *p*-xylene. Helium was used as carrier gas for the analysis. The amount of each component was determined based on retention time of components in the column that was translated to chromatographic peak area. Based on the amount of injected sample, the two peaks from FID and TCD were then combined to obtain overall composition of gas sample. The repeatability of analysis was within ±1%.

Liquid samples were analyzed by using another GC equipped with a different capillary column (30m×0.25mm×0.25μm Varian VF-1MS Silica and 5m×0.25mm×0.25μm dimethylpolysiloxane) and FID. Helium was used as a carrier gas. Since the liquid samples contain heavy hydrocarbon components, the injected sample was vaporized by heating the injection loop to about 350°C. Note that only a part of injected sample was passed through the column for analysis. FID detects the hydrocarbon components with carbon numbers from C5 to C29. This includes all common isomers in this carbon

number range. Individual components with isomers were quantified based on the chromatographic peak area for carbon numbers from 5 to 8. These components include *i*-pentane, *n*-pentane, methylcyclopentane, benzene, cyclohexane, *n*-hexane, methylcyclohexane, toluene, *n*-heptane, ethylbenzene, *o*-, *m*-, *p*-xylene and *n*-octane. The components with same carbon number were grouped to obtain pseudo components ranging from C9 to C29. The mole fractions of the pseudo components were determined from the corresponding chromatographic peak areas. Then, by material balance, the amount of C30+ fraction was calculated.

3.2.2 SARA Fractionation – University of Calgary Procedure

Crude A to D, LGO and their blends were analyzed for saturates, aromatics, resins and asphaltenes (SARA) fractions using this method. A schematic of the SARA fractionation procedure performed at the UofC is shown in Figure 3.1. SARA fractionation consists of three main steps: topping of oil, asphaltenes extraction, and isolation of saturates, aromatics and resins fractions. All three steps are described below.

To perform a SARA fractionation on a dead crude oil, the oil was first topped to remove volatile components (C7 and less), if necessary. The presence of a volatiles fraction in the oil greatly affects the mass balance because SARA fractionation involves the addition and evaporation of various low boiling solvents (e.g., *n*-pentane or *n*-heptane, toluene, and acetone). Therefore, any components with normal boiling point less than these solvents would be lost during the evaporation steps. To separate the volatiles fraction, the crude oil was roto-evaporated at 60°C and 34 kPaa. At these conditions all the components in the oil sample with normal boiling point below toluene and C8 were evaporated. The residual oil was referred to as “topped” oil and used for SARA fractionation. Note that topping step was performed only for Crude D.

Following topping (if required), the next step was to precipitate asphaltenes from the crude oil by the addition of excess *n*-pentane at a ratio of 40 cm³ of *n*-pentane to 1 g of oil. The asphaltenes extraction procedure is a modified form of the ASTM D2007 procedure. A pre-weighed and clean 2 liter beaker was used for this addition process. Usually, about 40 g of topped oil was taken for SARA fractionation. After the addition of *n*-pentane with the oil, the beaker was covered with polyethylene and aluminium foil to prevent any evaporation. The *n*-pentane-oil mixture was sonicated for 45 minutes and left to settle for 24 hours at room temperature and pressure conditions (23±2°C, ~93 kPa). Then, the supernatant was poured through a pre-weighed Whatman #2 filter paper (8 micron pore size) and the residue was further mixed with *n*-pentane in the same beaker at a 4:1 ratio (cm³/g) of *n*-pentane to original oil. The beaker was again covered with polyethylene and aluminium foil. After sonicating the *n*-pentane-residue mixture for 30 min, the mixture was left to settle for 16 h. The final mixture was filtered using the same filter paper. The filter cake or precipitated asphaltenes were further washed on the filter paper with *n*-pentane three times per day for five days (Alboudwarej et al., 2002). For each washing, about 100 cm³ of *n*-pentane was used for a 40 g of original oil sample. After five days of washing, the filtrate was almost colorless for all of the samples.. The washed asphaltenes were then dried in a fume hood until there was no further change in mass. The dried asphaltenes after this step were referred as C5-"filter-washed" asphaltenes or simply C5-asphaltenes.

When the asphaltene extraction procedure is repeated with *n*-heptane as solvent, the extracted asphaltenes are referred to as C7-asphaltenes. For asphaltene extraction leading to complete SARA analysis, *n*-pentane was used as the precipitant. Asphaltene yields are reported as the mass of asphaltenes recovered after washing and drying divided by the mass of dead oil. After the asphaltenes were extracted from dead oil, the deasphalted oil or maltenes were recovered by evaporating the solvent from the solvent-maltene mixture (*i.e.*, filtrate) using a rotary evaporator operated at 35 kPaa and 40°C. The maltenes were dried in the fume hood until no further change in weight was observed.

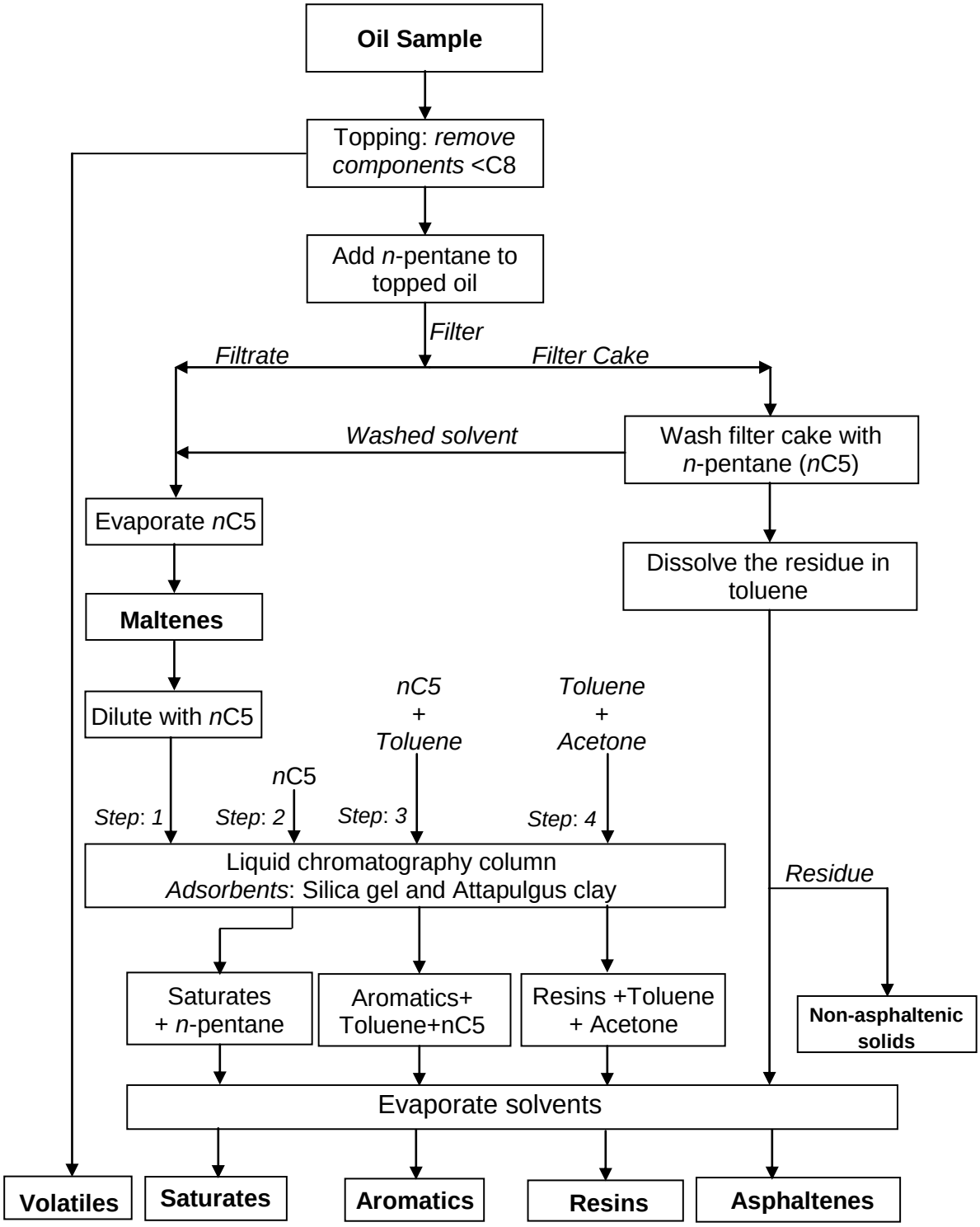

Figure 3.1: Flowchart of SARA fractionation method – University of Calgary Procedure.

Saturates, aromatics and resins (SAR) were then fractionated from maltenes based on liquid chromatography by modified ASTM D2887 procedure. In this technique, Attapulgus clay and silica gel were used as adsorbents to prepare two glass separation columns arranged one above the other. The upper column consisted of 100 g of clay and the lower column was packed with 200 g of activated silica gel. The columns were uniformly tapped softly using a rubber hammer on all sides to obtain a homogeneous packing. The columns were then flushed with 25 cm^3 of *n*-pentane to improve the wetting and solvent flow characteristics. The SAR separation was initiated by dissolving 5 g of maltenes in 25 cm^3 *n*-pentane and then poured into the top of the column. 500 cm^3 of *n*-pentane was then added to the columns. The resins adsorb on the clay, the aromatics adsorb on the silica gel, and the saturates pass through as a saturates-*n*-pentane mixture. Following *n*-pentane, about 1600 cm^3 of toluene-*n*-pentane mixture (1:1 v/v) was then added to the column to collect the aromatics fraction adsorbed by silica gel.

In the next step, the columns were separated. The lower column was refluxed with 200 cm^3 toluene for 2 hours in a soxhlet apparatus to recover any trapped aromatic fraction. The upper column was eluted with 800 cm^3 of toluene-acetone mixture (1:1 v/v) to recover resins-solvent mixture. Saturate, aromatic, and resin fractions were then individually recovered by evaporating the solvents of the respective mixtures in a rotary evaporator and then placed in fume hood until there was no significant change in their mass with time. Yields were calculated as the mass of each fraction divided by mass of maltenes taken for SAR fractionation. Finally, the saturates, aromatics, resins and asphaltenes contents of the oil were normalized and reported.

Asphaltene samples often contain non-asphaltenic solids (here referred to as “solids”), which included sand, clay and adsorbed organics. In order to determine the amount of solids in the precipitated asphaltenes, toluene was added in excess such that the concentration of precipitated asphaltenes was about 10 kg/m^3. The solution was sonicated for 1 h, left to settle for 2 h, and then centrifuged for 5 min at 4000 rpm (equivalent to

1640 Relative Centrifugal Force). The supernatant was decanted and the residue in the centrifuge tube (the solids) was dried and weighed. Toluene was also evaporated from the supernatant to recover "solids-free" asphaltenes.

Technical grade toluene was used for the SARA analysis. Acetone, *n*-heptane and *n*-pentane had a purity of 99%, 99.7% and 99.6%, respectively. At least two runs of analysis were conducted for unblended oils. Overall, the repeatability of the analysis for saturate, aromatic, resin and asphaltene fractions were ±2.1, ±3.1, ±2.7 and ±0.5 wt%, respectively. The experiments were not repeated for the blends and the error was assumed to be similar to that of the unblended oils.

3.2.3 SARA Analysis – DBR Procedure

Experiments related to live oil work were conducted at DBR, and hence Crude D was also analyzed for SARA fractions using a modified IP143 procedure (Kharrat et al., 2007). A schematic of DBR SARA fractionation procedure is shown in Figure 3.2. The dead oil sample was initially topped to constant mass by heating at approximately 80°C under vacuum. The topped sample was cooled to room temperature. A subsample (approximately 2 to 3 g) of the topped oil was then dissolved in excess (40 times by volume) of *n*-heptane and refluxed for 2 h, close to the boiling temperature of the solution (to melt co-precipitated waxes, if any). Subsequently, the solution was filtered hot using Millipore Fluropore 0.45 μm filter under vacuum. The filter was weighed prior to use. The filtrate consisted of deasphalted oil and *n*-heptane.

The filter was then folded to confine the precipitate (asphaltene + residual oil), loaded into a soxhlet apparatus, and thoroughly washed using hot *n*-heptane (~75°C) until the solvent in the upper section of the soxhlet became clear. Following this, the boiling flask containing *n*-heptane was replaced with another flask containing dichloromethane and the washed *n*-heptane was added to the filtrate. The extraction process was continued

with dichloromethane to dissolve all the asphaltenes from the filter. The solution (asphaltene + dichloromethane) was then concentrated by evaporating the dichloromethane and eventually transferred to a tared small vial for drying under nitrogen at 60°C. After drying, the vial was weighed and the asphaltene yield was calculated. Similarly, *n*-heptane was evaporated from the filtrate to quantify the amount of deasphalted oil or maltenes. In addition, the filter was dried in an oven at 40°C and weighed. The amount of non-asphaltenic solids in the sample was calculated from the initial and final mass of filter.

In order to determine the saturate, aromatic and resin fractions of the oil, the deasphalted oil (~0.3 g) was mixed with 1 or 2 cm^3 of *n*-heptane and fed into a liquid chromatographic column. The column was homogeneously packed with alumina, which was previously activated at 430°C for 24 hours and cooled to room temperature in a desiccator. About 250 cm^3 of *n*-heptane was pumped into the column to elute saturates and *n*-heptane. Aromatics and resins were adsorbed onto the alumina. Subsequently, a medium polar solvent (toluene) and a strong polar solvent (dichloromethane/methanol: 1:1 v/v) were loaded onto the same packed column in sequence to recover the aromatic and resin fractions, respectively. The corresponding effluents were collected in separate glass jars. Each solution was then subjected to rotary evaporation to remove the respective solvents. The saturate fraction was observed to be white and opaque just like candle wax; whereas, the aromatic and resin fractions appear to be brownish and very dark, respectively. Yields were calculated as the mass of each fraction divided by mass of maltenes taken for SAR fractionation. Then, the saturate, aromatic, resin and asphaltene contents of the oil were normalized.

All solvents used for the analysis were of 99.8% pure. The expected absolute error for the measured saturate, aromatic, resin and asphaltene content were assessed to be ±3.0, ±3.5, ±2.4 and ±0.3 wt%, respectively (Kharrat, 2010). The assessment was based on repeatability, operator dependence and inter-lab studies on several other oils.

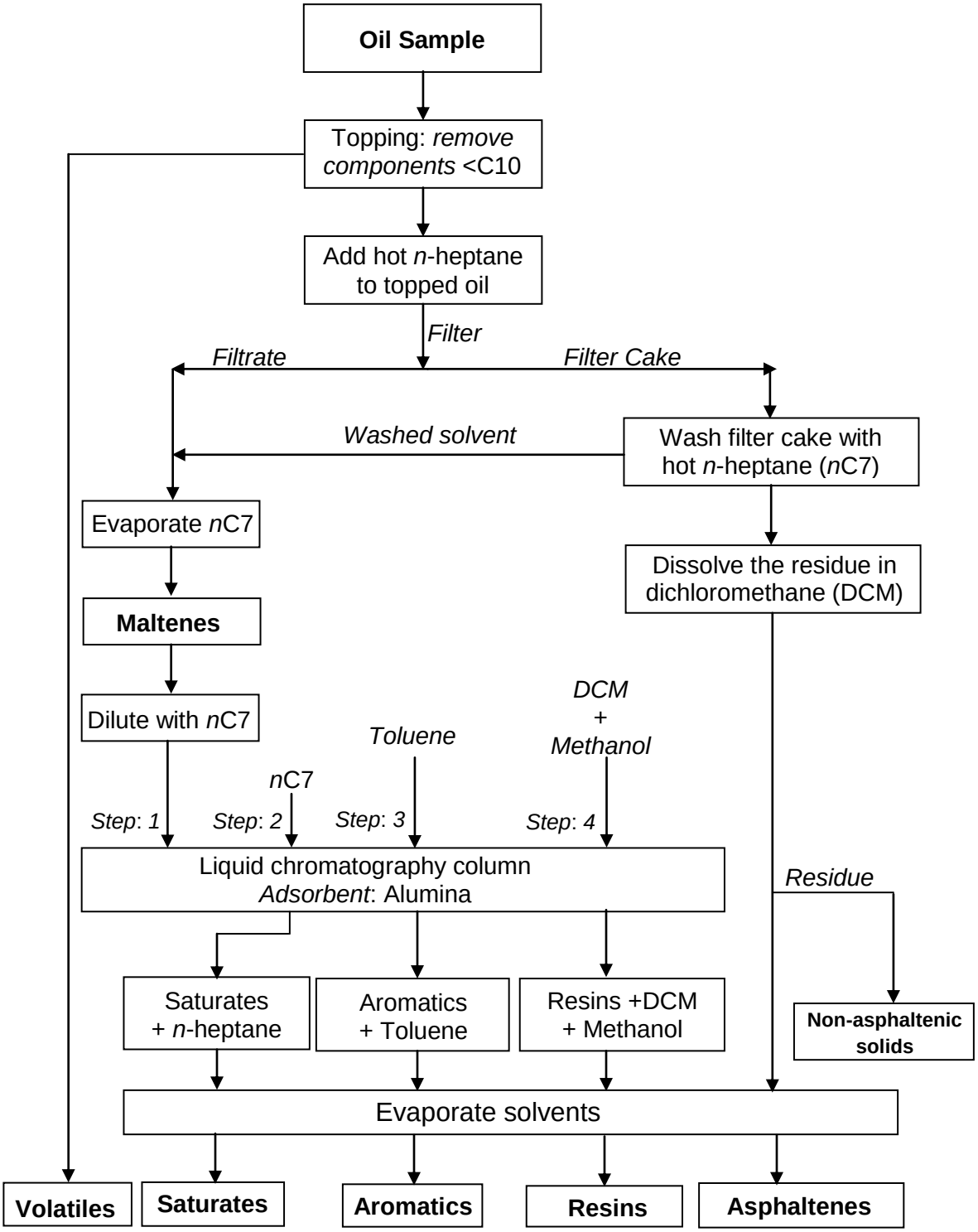

Figure 3.2: Flowchart of SARA fractionation method - DBR Procedure.

3.2.4 Water Content of Oil

The water content of oil samples was determined using a Karl Fischer Titrator (787 KF Titrio Metrohm). The reagent was Aqualine^{TM} complete 5, which contains iodine, sulphur dioxide and inidazole. The electrolyte solution used for the titrator was a mixture of 26 vol% 2-propanol and 74 vol% toluene. Luer-Lok tip syringes with a 20 gauge 1.5 inch needle were used to transfer about 1 cm^3 of the oil sample to the Karl-Fischer apparatus. Water percent in the sample was determined by comparing the volume (in cm^3) of titrator used for each sample with a calibration curve. The calibration curve was previously prepared by measuring the response of the apparatus to standard water samples, which were made with a known mass of water in a mixture of 26 vol% 2-propanol and 74 vol% toluene. Heavy oil/bitumen samples were diluted with toluene to facilitate the transfer of calculated volume of sample accurately from syringe to apparatus.

3.2.5 Elemental Analysis of Asphaltenes

Elemental analysis was carried out to determine the amount of carbon (C), hydrogen (H), nitrogen (N), sulphur (S), oxygen (O), nickel (Ni) and vanadium (V) in the asphaltenes.

3.2.5.1 CHNSO

The analysis was conducted at the Analytical and Instrumentation Laboratory, Department of Chemistry, University of Alberta, Edmonton, Alberta, Canada. The instrument used for the analysis is Carlo Erba EA 1108. It was calibrated using at least three samples of the organic analytical standard 2,5-Bis(5-tert-butyl-2-benzo-oxazol-2-yl)thiophene (BBOT) at the start of each analysis day. BBOT contains 72.52 wt% C, 6.09 wt% H, 6.51 wt% N, 7.44 wt% S and 7.43 wt% O. For samples containing smaller amounts of nitrogen and sulfur, enriched Phenanthrene OAS was used. This standard contains 93.25 wt% C, 5.65 wt% H, 0.44 wt% N and 0.59 wt% S.

3.2.5.2 Heavy Metals

Asphaltene samples were analyzed for two common heavy metals: nickel and vanadium. The analysis was performed at Alberta Research Council, Vegreville, Alberta, Canada. The analysis involved two steps. In the first step, the asphaltene sample (~ 0.1 g) was completely dissolved in 5 cm^3 of nitric acid and 2 cm^3 of hydrogen peroxide. A high-pressure closed vessel microwave acid digestion system (QWAVE-100 Microwave Sample Preparation System, Questron, Mercerville, NJ, USA) was used for this purpose. The sample digestion was conducted at 165°C for 30 minutes. In the second step, the digested sample was diluted with 50 cm^3 of deionized distilled water and subjected to Inductively Coupled Plasma-Mass Spectrometry (ICP-MS) analysis. The ICP-MS analysis was carried out using a Perkin-Elmer Sciex Elan DRC-II ICP quadrupole mass spectrometer. Conostan Metallo-Organic standard S-21 (Conoco Speciality Products Inc.) was used to calibrate ICP-MS.

3.3 Dead Oil Tests

3.3.1 Density Measurements

Densities of Crude A to D and LGO were measured with digital densitometer (Anton Paar DMA 46). The density meter uses a vibrating tube of a known volume to calculate the density. The period of oscillation of the vibrating tube corresponds to weight of sample and therefore density was calculated from sample weight and volume. The density meter was calibrated with two fluids; one fluid having a density higher than the unknown and the other fluid with lower density than the unknown. Hence, water and air were used for calibration at the same pressure and temperature conditions as the unknown. The instrument precision is ±0.5 kg/m^3. During each measurement, it was ensured to completely fill the vibrating tube with single phase fluid. At least 2 min were allowed to stabilize the period of oscillation. The reported densities were an average of three measured readings within the experimental error of ±2 kg/m^3.

For solids samples such as asphaltenes or highly viscous samples such as bitumen, an indirect method was used to calculate density as described elsewhere (Yarranton and Masliyah, 1996). In this indirect method, the actual samples were diluted in toluene to form a series of mixtures of increasing concentration and the density of each mixture was measured. The inverse of mixture density was plotted against the corresponding asphaltenes or bitumen mass fraction. The linear fit of the plotted data is of the form:

$$\frac{1}{\rho_{mix}} = \frac{1}{\rho_{tol}} + \left(\frac{1}{\rho_{asph/bit}} - \frac{1}{\rho_{tol}} \right) w_{asph/bit} \tag{3.1}$$

where, ρ_{mix}, ρ_{tol}, and $\rho_{asph/bit}$ are the mixture, toluene and average asphaltenes or bitumen densities (kg/m³), respectively, and $w_{asph/bit}$ is the asphaltenes or bitumen mass fraction. Therefore, the asphaltene or bitumen density is given by:

$$\rho_{asph/bit} = \frac{1}{S + I} \tag{3.2}$$

where, S is the slope and I is the intercept of the linear fit of Eq. (3.1).

3.3.2 Precipitation Onset Measurements

3.3.2.1 Microscopic Method

For Crude A to D, LGO and their blends, the onset of asphaltene precipitation from dead oils was determined from microscopic observations of samples of the crude oil or oil blends diluted with test amounts of *n*-heptane. A series of mixtures of increasing *n*-heptane concentration, from 0 wt% to 50 wt% were prepared. The diluted mixtures were then homogenized by sonicating for 45 min and left to equilibrate for 24 h at ambient conditions. Each mixture was then hand-shaken slightly to disperse any precipitate that

may have settled and a drop of the mixture was then transferred to a glass slide for examination in a transmission light optical microscope. The total magnification was approximately 400× which meant that particles size of about 1 μm or larger could be detected. The onset of precipitation was defined as the lowest mass fraction of *n*-heptane at which precipitated asphaltene particles were observed. A schematic of steps involved in the measurement is given in Figure 3.3. The repeatability for the onset measurements was within ±4 wt% of the reported amount of *n*-heptane at the onset.

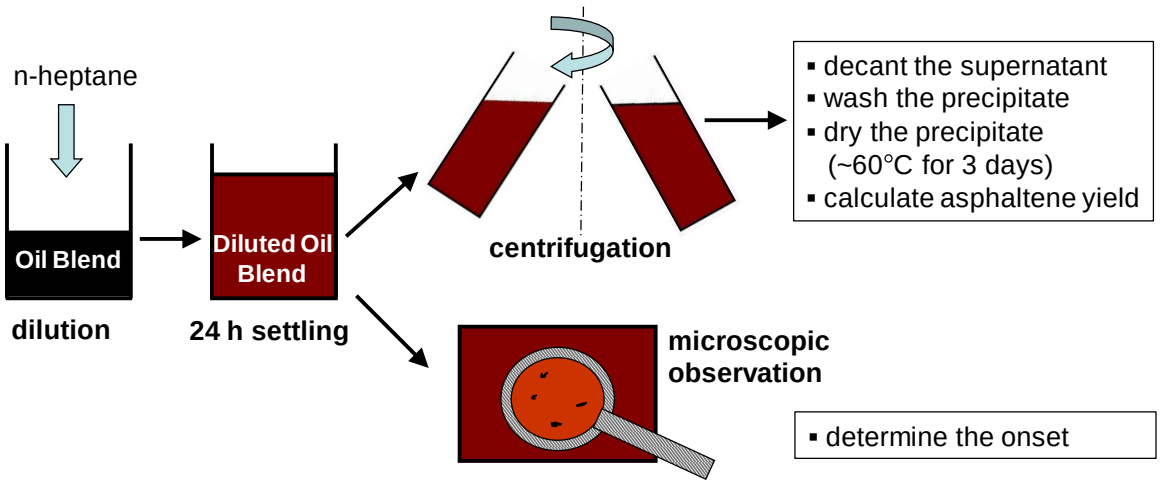

Figure 3.3: Schematic of the asphaltene precipitation onset and yield measurements.

For Crude G, H, I and their blends, precipitation onsets were measured by adapting the procedure from Shell (SMS 1600). The measurements for these samples were conducted at Rey Juan Carlos University, Móstoles, Spain. The oils and their blends were first diluted with toluene at three different dilution ratios (given in Chapter 5) and titrated with *n*-heptane to determine the onset of asphaltene precipitation. *n*-Heptane was added every 15 min, to allow the sample to stabilize between consecutive injections. For Crudes G, I and their blends, onset data were also collected by diluting the samples with *n*-

hexadecane without prior addition of toluene. The onset conditions were detected optically with the aid of a microscope. The procedure was similar to the procedure described above except the magnification of the microscope was approximately 70-100×. Hence, the minimum detectable particle size was about 1 μm. The onset measurements by this method were repeatable as well with a maximum relative standard deviation of ±5% of the volume of added solvent.

3.3.2.2 Light Transmittance Method

The precipitation onsets for Crude E, F and their blends were determined using a laser-based light transmittance technique (also commonly referred to as solid detection system "SDS"). The measurements were carried out at NCUT. In this method, the oil or blend sample was initially diluted with HPLC grade toluene to different ratios. A known mass of toluene diluted sample was then taken in a sample vial and titrated against *n*-heptane. The rate of *n*-heptane addition was 0.25 cm^3/min. All the contents in the vial were mixed well. A near-infrared laser light was passed through the oil-solvent mixture and its light transmittance was measured. The light transmittance increased monotonically with dilution until the onset of asphaltene precipitation after which the light transmittance decreased. Hence, the point at which the transmittance reached its maximum was taken to be the onset of precipitation. The *n*-heptane volumes for each toluene diluted sample at the onset were then extrapolated to determine the amount of *n*-heptane required to cause asphaltene precipitation from the oil sample without toluene. Note that precipitation is not instantaneous but may continue over at least several hours (Beck et al., 2005), which means that the continuous addition of *n*-heptane could lead to an overestimate of the onset. Because these data were not checked with another method, the potential error was not assessed; however, it is the comparison to the onset condition for blends versus individual crude oils that is of interest, and they were all measured with the same method. Overall, the repeatability of the measured onsets was within ±2% of the volume of *n*-heptane reported at the onset condition.

3.3.3 Precipitation Yield Measurements for Water-free Oil Samples

Asphaltene precipitation yields were measured for Crude A to D, LGO and their blends. Approximately, 2-10 g of crude oil or oil blend was diluted with *n*-heptane at a given ratio, sonicated for 45 min, and left to settle for 24 h at ambient conditions. Then the mixtures were centrifuged for 5 min at 4000 rpm (equivalent to 1640 Relative Centrifugal Force). The supernatant was decanted and approximately 30 cm^3 of *n*-heptane was added to wash the precipitate. Each mixture was again sonicated for about 15 min and centrifuged for 5 min at 4000 rpm. The supernatant was decanted and the washing step was repeated until the supernatant was almost colorless. Then the precipitate was dried in a vacuum oven at about 60°C until no significant change in the weight was noticed for 2 days. Asphaltene precipitation yields were reported as mass fractions; that is, the mass of precipitate per mass of oil sample. Figure 3.3 also presents the schematic of the steps involved in the yield measurement. The repeatability of the measured yields was within ±14% and ±5% of the reported yield data at low (*n*-heptane mass fraction < 0.6) and high (*n*-heptane mass fraction > 0.6) dilution ratios of oil or blend.

3.3.4 Water-in-Oil Emulsion Preparation

Water-in-oil emulsions were prepared for both Crude B and topped Crude D. The procedure begins by transferring 10 – 15 g of water-free sample into a pre-weighed and dried sample bottle. In order to facilitate the emulsion preparation process for the bitumen/heavy oil sample, the viscosity of the sample was reduced by adding a sufficient amount of *n*-heptane (0.7~1.0 cm^3/g of oil) and mixed well using a mechanical mixer. Note that the selected *n*-heptane concentration allowed for the desired viscosity reduction without inducing asphaltene precipitation. Light oil was used as is since it already had a low viscosity. Emulsions were then prepared by slowly adding the desired volume of deionized water to the sample while the mixture was homogenized with a CAT-520D homogenizer at approximately 17800 rpm for 5 minutes. Deionized water was obtained

from the University of Calgary water plant. Emulsion preparation was followed by drop size measurements using Carl Zeiss Axiovert S100 microscope set to 400 times magnification. Immediately after preparation, a drop of each emulsion sample was taken on a glass slide and placed on the glass slide under the microscope. The camera attached to the microscope was used to capture images of the emulsion. Image Pro image analysis software was used to determine the diameter of the emulsified water droplets in the captured image. In this work, approximately 350-450 drops were used in the measurement. The Sauter mean diameter (d_{32}) was then calculated by using the equation:

$$d_{32} = \frac{\sum f_i d_i^3}{\sum f_i d_i^2} \tag{3.3}$$

where f_i is the number frequency of droplets with diameter d_i.

3.3.5 Precipitation Yield Measurements for Water-in-Oil Emulsion Samples

Figure 3.4 summarizes the emulsion preparation and asphaltene precipitation yield measurements for the water-in-oil emulsion samples. The yield as a function of concentration was determined by diluting the water-in-oil emulsion samples with *n*-heptane to the desired dilution ratio, mixing well using a mechanical shaker for 5 minutes and leaving the sample undisturbed at atmospheric conditions for 24 hours. Each emulsion sample bottle was covered using a plastic cap with an inner Teflon lining to avoid any evaporation losses. After settling, the supernatant was carefully removed and the sediment was transferred to a vial and centrifuged at 4000 rpm (equivalent to 1640 Relative Centrifugal Force) for 5 minutes. As a result of centrifugation, the precipitate and the emulsified water were collected at the bottom of the vial. Any remaining supernatant was then decanted before adding approximately 30 cm^3 of *n*-heptane to wash the precipitate in the vial. A portion of the *n*-heptane was also used to collect any precipitate that remained in the original sample bottle or stuck to the transfer spatula.

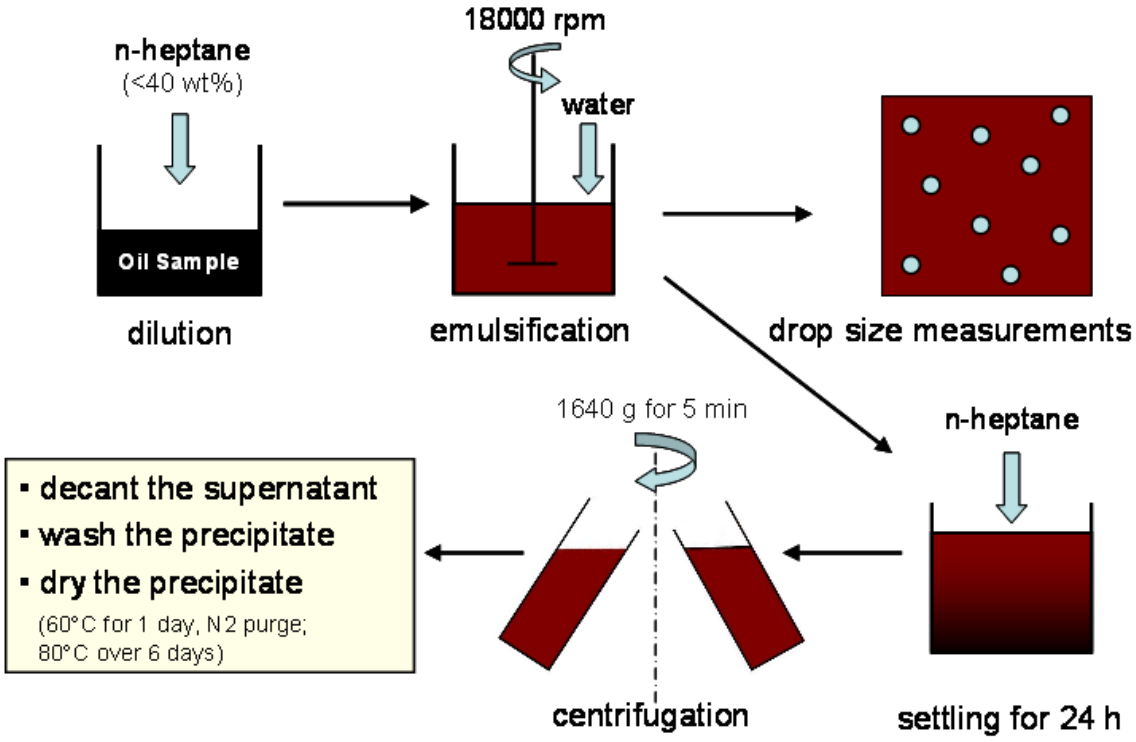

Figure 3.4: Block diagram for emulsion preparation and precipitation experiments.

The entire mixture was then shaken well using the mechanical shaker until all the precipitate was well dispersed before centrifuging for an additional 5 minutes. The *n*-heptane rich supernatant was decanted again and the washing step was repeated until the *n*-heptane supernatant was almost colorless. This process ensured that any maltenes trapped within the emulsion and asphaltene precipitate was removed prior to drying step. The precipitate was first dried at 60°C under flowing nitrogen for 24 hours. Then the temperature was slowly increased from 60°C to 80°C for 6 days under vacuum. Asphaltene precipitation yields were calculated as the mass of dried asphaltenes divided by mass of water-free oil sample.

3.4 Live Oil Experiments

All of the live oil experiments involved high pressure and temperature operating conditions. These experiments were carried out at DBR using their protocols and methodologies.

3.4.1 Live Oil Sample Preparation

The live oil test sample was created by recombining a dead oil (Crude D) with a synthetic solvent (hydrocarbon/non-hydrocarbon gases + light liquid hydrocarbons) mixture to match a known composition of the reservoir fluid. Following standard procedure, the recombination was based on matching a defined gas-oil ratio (GOR). The first step was to create a synthetic solvent mixture gravimetrically by adding pure components to a pre-cleaned and pre-evacuated stainless steel high pressure vessel. The pure components included CO_2, N_2, *n*-alkanes from C1 to C11, *i*-butane, *i*-pentane, methylcyclopentane (mcyclo-C5), benzene, cyclohexane (cyclo-C6), methylcyclohexane (mcyclo-C6), toluene, ethylbenzene (C2-benzene), *o*-, *m*- and *p*-xylene. All these chemicals were obtained from VWR International. Addition of gaseous components was carried out by converting the gases to a liquid state by using a booster pump. The mass of each component was weighed to the nearest 0.01 g of the required value. After the addition, the solvent mixture was conditioned to a predetermined pressure and a sub-sample was taken for GC analysis (Section 3.2.1) to verify whether the correct composition was prepared. Appendix B provides the composition of synthetic solvent (or solution gas) mixture. The density of synthetic solvent mixture was found to be 420 kg/m³ at 21°C and 68.3 MPa (See Section 3.4.4 for the measurement procedure). The calculated average molar mass of synthetic solution gas was 24.1 g/mol.

The next step was to prepare a recombined live oil sample with a desired gas-oil ratio (GOR). The recombination procedure involved transferring 260 g of dead oil into a high pressure cylinder and adding about 60 g of synthetic solvent mixture. The predetermined

volume of synthetic solvent mixture was calculated based on the desired GOR, pressure in the solvent vessel and density of solvent mixture. The recombination was carefully done such that there was no asphaltenes drop out. The recombined live oil was then homogenized by subjecting the recombination cylinder to 5 days of continuous rocking at the desired temperature and pressure (120°C and 103 MPa). Note that mixing is provided by the slow cyclic movement of a mixing ring sitting inside the recombination cylinder.

A sub-sample of 11.9 cm^3 of recombined live oil was then sampled into a pycnometer to verify the GOR and composition. The GOR measurement procedure is described later in Section 3.4.3. In the GOR apparatus, the recombined live oil was separated into flashed gas and flashed oil. The composition of flashed gas and flashed oil was then determined by GC as described in the Section 3.2.1. Their compositions are provided in Appendix C. Based on the composition, the average molar mass of flashed gas and flashed oil was calculated as 23.99 g/mol and 207.22 g/mol, respectively. The flashed gas density was then calculated to be 0.95 kg/m^3 at the flash apparatus operating conditions. Consequently, GOR, densities of flashed oil and flashed gas were used to calculate the amount of flashed oil and flashed gas in the recombined live oil and they were found to be 82.2 and 17.8 wt%, respectively. As a result, the composition of recombined live oil was determined (Appendix C).

3.4.2 Live Oil Sampling

The recombined live oil was sampled to facilitate the measurement of GOR and density. Sampling was carried out using a pycnometer and a positive displacement pump. The pycnometer is a small stainless steel container with a total volume of 75 cm^3 and with a maximum operating pressure of 12.4 MPa (1800 psi). The positive displacement pump is computer operated to accurately displace fluid under high-pressure conditions. The maximum operating pressure and total volume of pump are 138 MPa (20000 psig) and 500 cm^3, respectively. Mineral oil was used as a displacement medium for the pump.

The pycnometer was initially evacuated, weighed and connected to the live oil sample container through a high pressure valve. The connecting line between sample container and pycnometer was also evacuated. The positive displacement pump was connected to the sample container in order to transfer the fluid isobarically and to measure the transferred fluid volume. The initial pump volume was recorded. To avoid exceeding the maximum operating pressure and volume during sample transfer, the maximum volume of the live oil sample that can be transferred to the pycnometer was calculated using Boyle's law (i.e. $P_1V_1/T_1 = P_2V_2/T_2$; where subscripts 1 and 2 represent the conditions in the sample container and pycnometer, respectively).

First, the oil sample was filled in the connecting line. Then, the pycnometer valve was opened slowly to bleed the live oil sample. Any change in the live oil sample volume in the original container was translated to the volume change in the displacement pump. After transferring a required amount of sample, the pycnometer was detached from the sample container after closing the valves. The final pump volume was noted after transfer. The volume of sample taken in the pycnometer was calculated by subtracting the initial pump volume from the final pump volume. Any thermal effect during the sampling was assumed to be negligible.

3.4.3 Gas-Oil Ratio Measurement

Live oil GOR was measured using a single-stage flash apparatus or gasometer. During live oil preparation, the GOR is operated at 96.43 kPaa (13.98 psia) and 20.8°C. The live oil was first sampled into a pycnometer (Section 3.4.2). The pressure of the fluid in the pycnometer was calculated for a known volume of displaced fluid. The pycnometer was then connected to the gasometer where the sampled live oil was flashed to ambient pressure and temperature conditions. The flash process was carried out in a closed system. The evolved gas phase was circulated through the residual fluid (or flashed oil) for about one hour to achieve equilibrium between phases. The gasometer was equipped

with digital display of gas volume at ambient conditions. Hence, the flashed gas volume was calculated at standard conditions, 1 atm and 15.5°C. The calculated volume of flashed gas at the flash conditions was 1811.7 cm^3 (translates to 1693 cm^3 at standard conditions). The pycnometer with flashed oil was then weighed to calculate the mass of flashed oil. The density of the flashed oil was also measured using a digital densitometer (Anton Paar DMA 60). The volume of flashed oil was then calculated from its mass and density. The calculated volume of flashed oil was 8.7 cm^3. GOR of recombined live oil was reported in cm^3 of flashed gas per cm^3 of flashed oil at standard conditions.

3.4.4 Density Measurement

The density of fluids under high pressure and temperature was measured gravimetrically. Specifically, densities were measured for: a) live oil from the original recombination container, b) live oil after charging into PVT cell for bubble point measurement and c) live oil after charging the depressurization cell for onset pressure measurement.

The fluid is initially sampled from the appropriate container using the pycnometer (Section 3.4.2). The sample mass was calculated by subtracting the initial mass of pycnometer from the final mass after sampling. The volume of fluid sampled was obtained from the positive displacement pump reading. Therefore, the density of fluid at the sample pressure and temperature was calculated by dividing the mass of sample taken in the pycnometer by the volume of sample. The repeatability of the density measurements was within ±0.25%.

3.4.5 Bubble Point Pressure Determination

The bubble point or saturation pressure measurements were carried out on live oil at three different test temperatures, 80°, 100° and 120°C, using the DBR JEFRI visual PVT cell.

Experimental Setup

A schematic of the bubble point pressure measurement setup and the visual PVT cell is shown in Figure 3.5. The main body of the PVT cell consists of a Pyrex tube housed inside a steel shell with vertical tempered glass plates that permit visual observation of the internal Pyrex tube contents. The Pyrex glass tube is 15.2 cm long with an internal diameter of 3.2 cm. This translates into an effective working volume of approximately 120 cm^3. A floating piston and a magnetically coupled impeller mixer were mounted inside the Pyrex tube to allow for a mercury-free operation.

The volume of cell, and hence the pressure of the fluids under investigation, were controlled by a variable volume computer controlled positive displacement pump which allowed for the injection or the removal of the transparent displacing fluid (hydraulic oil). The same transparent displacement fluid is connected to the outer steel shell to maintain a balanced (minimal) differential pressure on the Pyrex tube. A magnetically coupled impeller mixer mounted on the bottom end cap was used to aid in the equilibration of the fluid under investigation. Note, the bottom end cap was designed to achieve two main goals: (a) shield the cell contents from any magnetic effects/flux and (b) provide for charging and sampling the test fluid.

The PVT cell was housed inside a temperature controlled, forced air circulation oven. The cell temperature was measured with a platinum thermocouple and was displayed on a digital indicator with an accuracy of 0.1°C. The cell pressure was monitored with a calibrated digital Heise pressure gauge accurate to ± 0.1 % of full scale. The maximum operating pressure and temperature for this PVT system is 103.4 MPa (15000 psia) and 200°C, respectively.

Procedure

Prior to the start of a measurement, the PVT cell was evacuated for two hours and then pressure tested with nitrogen at the maximum test pressure and temperature conditions.

The temperature of the air bath was set to test temperature and allowed to equilibrate. The bubble point pressure test was then initiated by charging a known volume of the recombined live oil from the sample cylinder to the PVT cell. The fluid should be in a single liquid phase (without any gas/solids) during injection. Hence, the pressure and temperature of the live oil should be well above the expected saturation and asphaltene onset pressures.

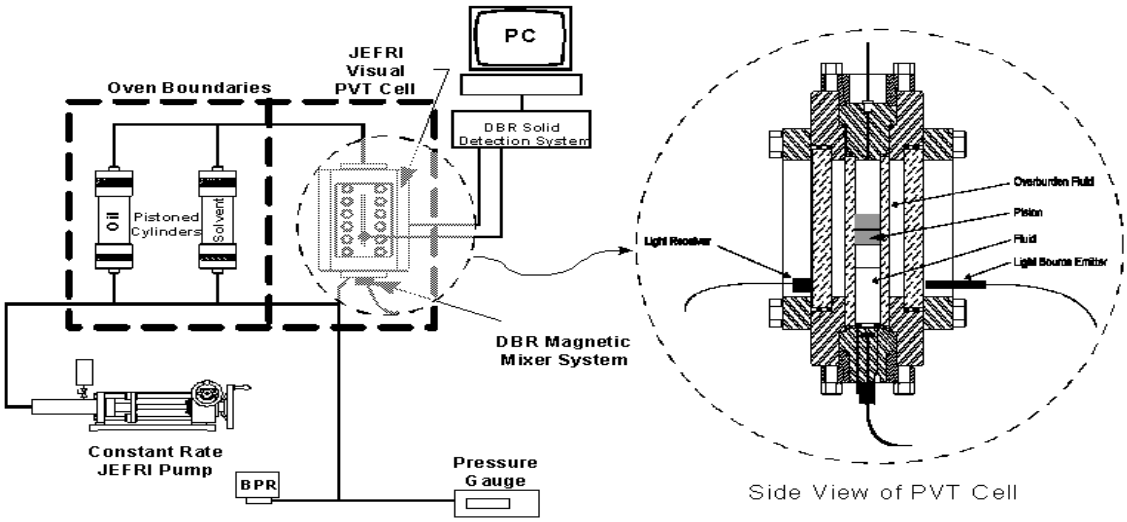

Figure 3.5: Schematic of bubble point pressure measurement setup and the visual PVT cell (courtesy of DBR Technology Center, Schlumberger).

The live oil fluid density was measured at the starting test temperature and pressure using a pycnometer (See Section 3.4.4). The fluid in the PVT cell was allowed to equilibrate for approximately 30 minutes until the temperature of fluid was the same as the cell. The initial height of the fluid was recorded with a cathetometer. The volume of the fluid was calculated based on the fluid height and the internal diameter of cell and the mass of fluid

in the cell determined from the volume and density measurements. Since this is a closed system, the mass of test fluid was assumed constant throughout the experiment.

The experiment was conducted by gradually expanding the fluid isothermally in several pressure steps by displacing the floating piston. At each pressure step, the fluid was allowed to equilibrate for approximately 15 minutes (for conventional oils) or until there was no change in pressure/volume of fluid. After equilibration at each step, the volume of fluid and the cell pressure was measured. The density of single phase fluid was calculated from its mass and volume at this particular pressure. This procedure was repeated a number of times until the first appearance of observed gas phase. The pressure and volume at this point was noted as this condition was used to differentiate between the single phase and two regions. Subsequently, the pressure was reduced in small steps into the two-phase region. Both gas and liquid phase volumes were measured for every equilibration step. The experiment was conducted until the relative volume of fluid was about 2, where the relative volume of fluid was defined as the ratio of the total volume of fluid (liquid and vapor) to the total volume of fluid at the saturation pressure. The measured total volume of fluid was plotted against the fluid pressure at each discrete step. The intersection of straight-line-fits for both single and two phase regions provided an estimate of the saturation pressure. Appendix D provides all the measured data to determine the bubble point pressure for the test temperatures 80°, 100° and 120°C.

In order to determine the bubble point pressure more accurately, the following methodology was used (Pedersen and Christensen, 2007):

a) The single phase data of pressure-volume plot was fitted with a polynomial equation of the form:

$$V_{tot} = aP^2 + bP + c \tag{3.4}$$

where, V_{tot} is the total volume of fluid in the cell at pressure P. This form of fitting equation is only applicable to conventional oils.

b) Y-function or Y-factor was calculated for the data below the observed two-phase region, based on the following equation:

$$Y = \frac{(P_{sat*} - P)/P}{(V_{tot} - V_{sat*})/V_{sat*}} \tag{3.5}$$

where, P_{sat*} is the pressure at which two phases were first experimentally observed; and V_{sat*} is the volume of fluid at P_{sat*} and it is calculated from Eq. (3.4). The Y-factor is a measure of the ratio between the relative changes in pressure and total volume in the two-phase region. As gas takes up more volume than liquid, volumetric changes will be larger with decreasing pressure in the two-phase region than in the single-phase region. Hence, oils that release large volumes of gas with decreasing pressure will have a small Y-factor, whereas oils that release only small amounts of gas with decreasing pressure will have a large Y-factor.

c) For the two-phase region, the calculated Y-factor was plotted against the total pressure P. If the experimentally observed P_{sat*} corresponds to the actual bubble point pressure, the data in the Y-factor plot was expected to show a linear trend. Otherwise, P_{sat*} values were changed to obtain a linear fit of the Y-factor data with pressure. During this tuning, V_{sat*} was calculated from Eq. (3.4). The P_{sat*} value that corresponds to best linear fit was considered as bubble point or saturation pressure at the test temperature.

3.4.6 Asphaltene Onset Pressure Measurements

Experimental Setup

A schematic of the experimental setup was shown in Figure 3.6. The experimental setup consists of two high pressure cylinders with floating pistons: a depressurization cell and a receiving cell. The maximum operating pressure and temperature conditions of these cells were 138 MPa and 200°C. These two cylinders were placed in an air-bath to

maintain temperature to within ±1°C. One end of the depressurization cell was connected to a computer controlled positive displacement pump and the other end was connected to a high pressure microscope (HPM) system. The receiving cell was connected to the HPM system and manually operated by a positive displacement pump. All the connections in the experimental set up were made using 1/8″ stainless steel tubing.

The visual identification and confirmation of phase changes was made possible with the HPM. The HPM system consists of a cell with two sapphire windows, a long focal length camera of high resolution (~2 μm), and a white light source. The HPM has a low-dead volume (<1 cm^3) and a small adjustable gap (100-400 μm) between the windows. The thin gap allows visualization in dark crude oils; it may also hinder the flow of large-sized particles and/or water droplets (i.e., >400 μm). The HPM could withstand temperatures up to 200°C and pressures less than 138 MPa. The HPM cell was connected to the bottom of the depressurization cell inside the same air-bath oven.

Procedure

Initially, the pre-cleaned depressurization and receiving cells were evacuated and the temperature of the air-bath was set to the desired value. Then, 50 cm^3 (~37 g) of the live fluid was isobarically charged to the depressurization cell from the storage cylinder using a positive displacement pump. The time allowed for equilibration of the fluid in the cell was about 24 h. Depressurization tests were started at 100 MPa and stopped at about 0.7 MPa (~100 psia) above the the bubble point pressure for each test temperature. Hence, the pressure of the cell was lowered isothermally at a slow rate while the cell contents were being mixed continuously and vigorously at ~1400 rpm.

The depressurization process was carried out by withdrawing the fluid from the depressurization cell to the receiving cell at a very slow rate. At defined pressures, the depressurization was temporarily halted to allow for a sub-sample of the recombined live oil to be transferred to the HPM for visual inspection. The visual inspection was made by

observing through the microscope, by taking still images and by recording a video. This process could be repeated at different temperatures to generate a complete pressure-temperature (PT) diagram with asphaltene precipitation onset envelope.

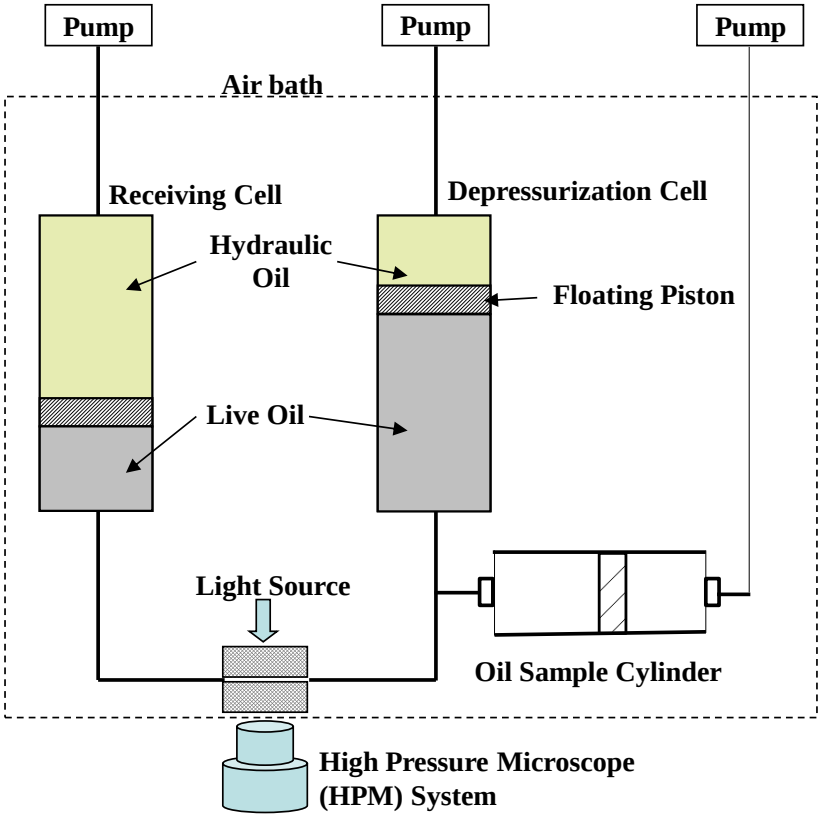

Figure 3.6: Schematic of experimental setup for detecting asphaltene onset pressure from live oils.

3.4.7 Precipitation Yield Measurements for Live Oil

The HPM only provides information about the asphaltene precipitation onset pressure. In order to determine the amount of precipitation at a pressure during isothermal depressurization, the precipitate was collected by adapting the following procedure.

Another stainless steel cylinder was connected to the receiving cell. A pre-weighed Millipore 0.22 μm silver mesh filter was placed along the connection. A motorized high-pressure displacement pump was used to displace the contents from receiving cell to the newly connected cylinder passing through the filter. The filtration was carried out at a pressure approximately 0.7 MPa (100 psi) above the bubble point pressure of the fluid to avoid the formation of vapor that may interfere with the measurement. While a portion of the precipitate was collected on the filter, most of the precipitate stuck to the walls of depressurization cell, receiving cell and the tubing (for example, see Figure 3.7). The filter was removed after filtration to collect the filtered portion of the precipitate (filter cake). The sticky precipitate or the adhered material was recovered by flushing toluene through the entire system. The toluene was then evaporated to obtain the precipitate retained within the cells and tubing.

Asphaltene yield was calculated from the amount of asphaltenes collected in the filter and the amount of asphaltenes from the toluene rinse. Since, both filter cake and the rinse contained trapped oil, corrections were required to determine the correct asphaltene yield. For the filter cake, the asphaltene content was measured by washing the filter cake with *n*-heptane at 75°C. The asphaltenes in filter cake were therefore precipitated from both the live oil during depressurization and from the trapped oil during the washing. To account for the latter, the maltene content was calculated by subtracting the asphaltene content from the mass of filter cake. Then, the asphaltene content of the trapped oil was back-calculated from the maltene content based on the composition of the flashed oil. Finally, the trapped oil asphaltene content was subtracted from the total asphaltene content of the filter cake to obtain the amount of asphaltenes precipitated only from live oil depressurization. A similar correction was applied to the toluene rinse material after the toluene was removed. The asphaltene yields were reported in grams of precipitated material for 100 g of live oil or wt%. Appendix E provides the yield calculation details for the experiments conducted at 80, 100 and 120°C.

Figure 3.7: Asphaltenes collected on the filter after the depressurization experiment conducted at 80°C.

CHAPTER 4

Modified Regular Solution Model

The asphaltene precipitation modeling in this thesis is based on a previously developed regular solution approach. In this chapte, the approach is presented along with the previously developed methodology to characterize heavy oils. Modifications to the characterizations for blends and live oils are presented in the relevant chapters later on.

4.1 Modified Regular Solution Model

The modified regular solution model (Alboudwarej et al., 2003; Akbarzadeh et al., 2005; Yarranton et al., 2007) includes a Flory-Huggins entropic contribution from the difference in molecular sizes as well as an enthalpy contribution from regular solution or Scatchard-Hildebrand solubility theory. A liquid-liquid equilibrium is assumed and the equilibrium ratio, K_i^{hl}, for any given component is given by:

$$K_i^{hl} = \frac{x_i^h}{x_i^l} = \exp\left\{ \begin{array}{l} \frac{v_i^h}{v_m^h} - \frac{v_i^l}{v_m^l} + \ln\left(\frac{v_i^l}{v_m^l}\right) - \ln\left(\frac{v_i^h}{v_m^h}\right) + \\ \frac{v_i^l}{RT}(\delta_i^l - \delta_m^l)^2 - \frac{v_i^h}{RT}(\delta_i^h - \delta_m^h)^2 \end{array} \right\} \tag{4.1}$$

where x_i^h and x_i^l are the heavy and light liquid phase mole fractions, R is the universal gas constant, T is absolute temperature, v_i and δ_i are the molar volume and solubility parameter of component i in either the light liquid phase (l) or the heavy liquid phase (h), and v_m and δ_m are the molar volume and solubility parameter of either the light liquid phase or the heavy liquid phase. The terms containing only molar volumes are the

entropic contribution and the terms containing solubility parameters are the enthalpic contribution.

Once the equilibrium ratios are known, the phase equilibrium is determined using standard techniques (Rijkers and Heidemann, 1986; Alboudwarej et al., 2003). Briefly, the phase equilibrium calculations are performed as follows:

1) The fluid mixture is appropriately divided into pure and pseudo components. The properties (molar volume and solubility parameter) of each component are determined. Both the fluid composition and the properties of each component are inputs to the calculation.
2) The equilibrium ratios or the *K* values of each component are initiated using the fluid composition.
3) The amounts of heavy and light liquid phases are calculated using the Rachford-Rice method.
4) The composition of the heavy and light liquid phases is updated and normalized.
5) Convergence is checked using the bisection method.
6) The *K* values for each component are updated using the new composition.
7) Return to Step No. 3 until the desired convergence is achieved.

In the phase equilibrium calculation, it was assumed that only asphaltenes and resins partition to the heavy phase; that is, the equilibrium is between an asphaltene-rich phase including asphaltenes and resins (the heavy liquid phase) and a solvent-rich phase including all components (the light liquid phase). This assumption is thermodynamically incorrect but is a reasonable approximation for heavy liquid phases with high asphaltene content and it provides a more stable flash calculation with much faster convergence. Asphaltene-rich phases have been found to contain approximately 95 wt% asphaltenes and resins (George, 2009).

To use this model, the mole fraction, molar volume, and solubility parameter of each component in the mixture must be specified. For a complex fluid like a crude oil, the fluid must be divided into pure components and pseudo-components to adequately represent the fluid without using an extremely large set of components.

4.2 Characterization

Characterization is the division of the fluid into components and pseudo-components and the assignment of properties to each component. For the regular solution model, the required properties are molar mass and density (to determine molar volumes) and the solubility parameter. In this thesis, characterizations are required for three types of fluid mixtures:

1) asphaltenes in solvents
2) solvent diluted heavy oils or crude oil blends
3) live oils

Characterization methodologies for the first two fluid mixtures have been developed previously (Alboudwarej et al., 2003; Akbarzadeh et al., 2005) and are presented here. A new methodology is required for live oils and is presented in Chapter 6.

4.2.1 Asphaltenes in Pure Solvents

The mass fractions of the pure solvents and the asphaltenes are controlled variables in the experiments and therefore are known. The molar mass and density of pure solvents are either known or calculated using well-established Hankinson-Brobst-Thomson (HBT) technique (Reid et al., 1989; Perry and Green, 1997). The HBT technique accounts for the effects of both temperature and pressure. Solubility parameters at 25°C were obtained from Barton (1991) and Hansen (2007). The effect of temperature on the solubility of *n*-

alkanes was required for some studies and was accounted for using an expression developed for *n*-alkanes by Akbarzadeh et al. (2005):

$$\delta = \delta_{25°C} - 0.0232(T - 298.15) \tag{4.2}$$

Note, the slope of -0.0232 $MPa^{0.5}/K$ is consistent with the order of magnitude of the derivative of the solubility parameter ($d\delta/dT \approx$ -0.03 $MPa^{0.5}/K$) found for hydrocarbons in general (Barton, 1991). Pressure effects on density and solubility parameter are discussed in Chapter 6. Properties at 25°C for the solvents used in this thesis are summarized in Table 4.1.

Table 4.1: Properties of pure components at 25°C and 1 atm.

Component	**Molar Mass (g/mol)**	**Density (kg/m^3)**	**Solubility Parameter ($MPa^{0.5}$)**
n-heptane	100	678	15.2
n-hexadecane	226	771	16.3
toluene	92	864	18.3

Asphaltenes are more challenging to characterize because they are a mixture of many thousands of chemical species and they are known to self-associate (Yarranton, 2005). Here, they are treated as macromolecular nano-aggregates of monodispersed monomers. The asphaltene fraction was divided into 30 sub-fractions, each representing a different aggregate size range and the number of monomers in an aggregate or the aggregation number (r) is described by the relation:

$$r = \frac{M}{M_m} \tag{4.3}$$

where M is the molar mass of the particular asphaltene aggregate or the sub-fraction, and M_m is the monomer molar mass of the asphaltenes. The gamma distribution function (Whitson, 1983) was then used to describe the molar mass distribution of the aggregates according to Eq. (4.4) as:

$$f(M) = \frac{1}{M_m \Gamma(\beta)} \left[\frac{\beta}{(\bar{r} - 1)} \right]^{\beta} \times (r-1)^{\beta-1} \exp\left[\frac{\beta(1-r)}{(\bar{r} - 1)} \right] \tag{4.4}$$

where $\bar{r}$ is the average aggregation number of asphaltene fraction defined as the average molar mass of all self-associated asphaltene sub-fractions ($\overline{M}$) divided by the monomer molar mass, that is given by $\frac{\overline{M}}{M_m}$. β is a parameter that determines the shape of the distribution. The molar mass of an asphaltene monomer and the largest asphaltene aggregate were assumed to be 1800 and 30,000 g/mol, respectively. Note, the asphaltene monomer molar mass of 1800 g/mol is at the upper end of recent estimates of asphaltene monomers and may represent an already aggregated component (Groenzin and Mullins, 2007).

The molar mass of an asphaltene sub-fraction (M) is the associated molar mass (rM_m) of that pseudo-component as calculated from the gamma distribution. Its molar volume was determined from Eq. (4.5) (Alboudwarej et al., 2003):

$$v = 1.493 M^{0.936} \tag{4.5}$$

where v is the molar volume (cm^3/mol) of asphaltene sub-fraction. Its solubility parameter was determined from Eq. (4.6) (Yarranton and Masliyah, 1996; Akbarzadeh et al., 2005; Yarranton et al., 2007):

$$\delta_a = \left(\frac{1000A(T)M}{v} \right)^{1/2} \tag{4.6}$$

where, A is the heat of vaporization of asphaltene, $A(T) = 0.579\text{-}0.00075T$ (J/kg); T is the absolute temperature (K) and δ_a is the solubility parameter ($MPa^{0.5}$) of asphaltene sub-fraction. Both the molar volume and the solubility parameter of the asphaltenes were assumed to be independent of pressure.

All of the model parameters are fixed except for the average aggregation number, $\bar{r}$, and the shape factor, β, of the asphaltene molar mass distribution. For asphaltenes in a pure solvent, the average aggregation number can be determined from the average measured molar mass using vapor pressure osmometry (Yarranton et al., 2007). The value of β is chosen as 2.5.

In defining a value for β, it is important to note, at any given molar mass, there is a mixture of asphaltene components with different solubility parameters, molar volumes, and other properties (Speight, 1999). This multi-dimensional array of properties is not accounted for explicitly in the model but the effect has been projected onto a one-dimensional distribution of molar mass. The error in this simplification is rectified to some extent when the shape of the distribution is adjusted to fit the data; that is, all of the asphaltenes of a given solubility, irrespective of their other properties, are allocated to a given molar mass and density. At this time, there is insufficient compositional and physical property data to justify using multiple distributions of properties.

4.2.2 Solvent Diluted Heavy Oils or Crude Oil Blends

The heavy oils or crude oil blends did not contain light components and based on simulated distillation data were equivalent to a C16+ residue; that is, they contained only

components with a normal boiling point equivalent or greater than *n*C16 (560 K). These dead oils were characterized into four pseudo components: saturates, aromatics, resins and asphaltenes.

Table 4.2 provides a summary of the average molar mass, density, and solubility parameter for saturates, aromatics, and resins at 25°C and 1 atm. Note that Akbarzadeh et al. (2005) demonstrated that using average properties for the saturates, aromatics, and resins introduced negligible error into the precipitation calculations, possibly because their mole fraction in the diluted oil was relatively small compared with the diluted solvent of the crude oil.

Table 4.2: Properties of saturates, aromatics, and resins at 25°C and 1 atm.

Components	**Molar Mass (g/mol)**	**Density (kg/m^3)**	**Solubility Parameter ($MPa^{0.5}$)**
saturates	460	880	16.4
aromatics	522	990	20.3
resins	1040	1044	19.3

The following curve fit equations were developed by Akbarzadeh et al. (2005) for the densities of the saturate and the aromatic fractions of an Athabasca bitumen sample as a function of absolute temperature in K:

$$\rho_{sat} = 1078.96 - 0.6379\ T \tag{4.7}$$

$$\rho_{aro} = 1184.47 - 0.5942\ T \tag{4.8}$$

where ρ_{sat} and ρ_{aro} are the densities of saturates and aromatics in kg/m^3, respectively. The following correlations were developed by Akbarzadeh et al. (2005) to estimate the solubility parameters of saturates and aromatics at other temperatures:

$$\delta_{sat} = 22.381 - 0.0222\,T \tag{4.9}$$

$$\delta_{aro} = 26.333 - 0.0204\,T \tag{4.10}$$

where δ_{sat} and δ_{aro} are the solubility parameters of saturates and aromatics. The solubility parameter of saturates was updated based on a more extensive data set at 23°C than was previously available to obtain the following:

$$\delta_{sat} = 23.021 - 0.0222\,T \tag{4.11}$$

In the above equations, the saturate and aromatic densities and solubility parameters were assumed to be independent of pressure. For live oils, a pressure dependence will be introduced for solubility parameter of saturates and aromatics in Chapter 6. The density of the resins was assumed to be independent of temperature and pressure.

The asphaltenes were characterized as was done for the mixtures of asphaltenes and pure solvents. However, the average molar mass of asphaltenes cannot be measured in a mixture like a crude oil. Therefore, the average aggregation number is used as a fitting parameter to match the asphaltene yield from a crude oil diluted with *n*-heptane. Thereafter, the average aggregation number (or average associated molar mass) is fixed. For most crude oils we have examined, a shape factor of 3.5 provides a good fit to the data; however, there are some exceptions and it is better to adjust the shape factor to fit the available data. A β of 3.5 was used for all solvent diluted heavy oil or crude oil blends cases in this thesis unless otherwise stated.

4.3 Example Application of Model

The application of the modified regular solution model is demonstrated using asphaltene precipitation data for a Lloydminster heavy oil (Akbarzadeh et al., 2005). The reported saturates, aromatics, resins, asphaltenes (SARA) and solids content of heavy oil are 23.1, 41.7, 19.5, 15.3 and 0.4 wt %, respectively. Asphaltene precipitation yield data were available for *n*-heptane-diluted and *n*-pentane-diluted heavy oil at 23°C and 1 atm.

The model inputs are the composition of heavy oil in terms of SARA fractions, the amount of solvent (*n*-heptane or *n*-pentane), and the average molar mass of asphaltenes. The only unknown parameter of the model is the average molar mass of the asphaltenes ($\overline{M}$). This parameter is determined by fitting the precipitation data for *n*-heptane diluted heavy oil. The precipitation of asphaltenes from the *n*-pentane diluted heavy oil is then predicted.

The specific steps to be followed are given below:

1. The heavy oil-solvent mixture is divided into five pseudo-components: solvent, saturates, aromatics, resins, and asphaltenes. The normalized fluid composition in terms of weight fractions is calculated based on the solvent-heavy oil dilution ratio and the amount of SARA fractions. In this case, *n*-heptane is the solvent.
2. Asphaltenes are further divided into 30 sub-fractions based on the gamma function as described in Eqs. 4.3 and 4.4. The parameters required to complete the specifications for the gamma function are the average molar mass of asphaltenes, $\overline{M}$, and the shape factor, β. Table 4.3 shows the calculated molar mass distribution for a given average molar mass of 3620 g/mol and shape factor of 3.5. Hence, the fluid is characterized into a total of 34 pseudo components. Note, the molar mass of each asphaltene sub-fraction is taken as the arithmetic average of the highest and lowest molar mass of that particular sub-fraction.

3. For a given pure solvent, the molar mass, density and solubility parameter are obtained from the literature. The HBT technique is used for calculating the molar volume or density of solvent at the given pressure and temperature conditions. The effect of temperature in the solubility parameter is accounted for using Eq. 4.2.
4. The properties of SAR fractions are taken from Table 4.2. The densities of saturates and aromatics at temperatures other than 25°C are calculated from Eqs. 4.7 and 4.8, respectively. The solubility parameters of saturates and aromatics at other temperatures are calculated from Eqs. 4.11 and 4.10, respectively. The properties of resins are assumed to be independent of temperature.
5. The molar volume or density of each asphaltene sub fraction is calculated from the molar masses in Table 4.3 using Eq. 4.5 and the solubility parameter is determined from Eq. 4.6.
6. Equilibrium calculations are then performed using Eq. 4.1 and standard techniques (Rijkers and Heidemann, 1986; Alboudwarej et al., 2003). A bisection method is used for model convergence.
7. The amount of asphaltenes precipitation is calculated at the desired pressure and temperature (25°C, 1 atm) conditions for a range of *n*-heptane mass fraction in the heavy oil-solvent mixture.
8. The calculated yield data for *n*-heptane diluted heavy oil is compared to the measured data. The measured data is fitted by changing the input average molar mass of asphaltenes. The fitting is carried out by comparing the average absolute deviation (AAD) in the yield (See Appendix A for the definition of AAD). The fitted molar mass for the current example is 3620 g/mol and the AAD is 0.31%.
9. The fitted average molar mass of asphaltenes is used as the input parameter for predicting the precipitation yield data for *n*-pentane diluted heavy oil. In other words, steps 1 through 7 are repeated with *n*-pentane as solvent and using the fitted average molar mass of the asphaltenes as the input. %AAD for the prediction is 0.66.
10. The predicted yield data is compared to the measured data (see Figure 4.1).

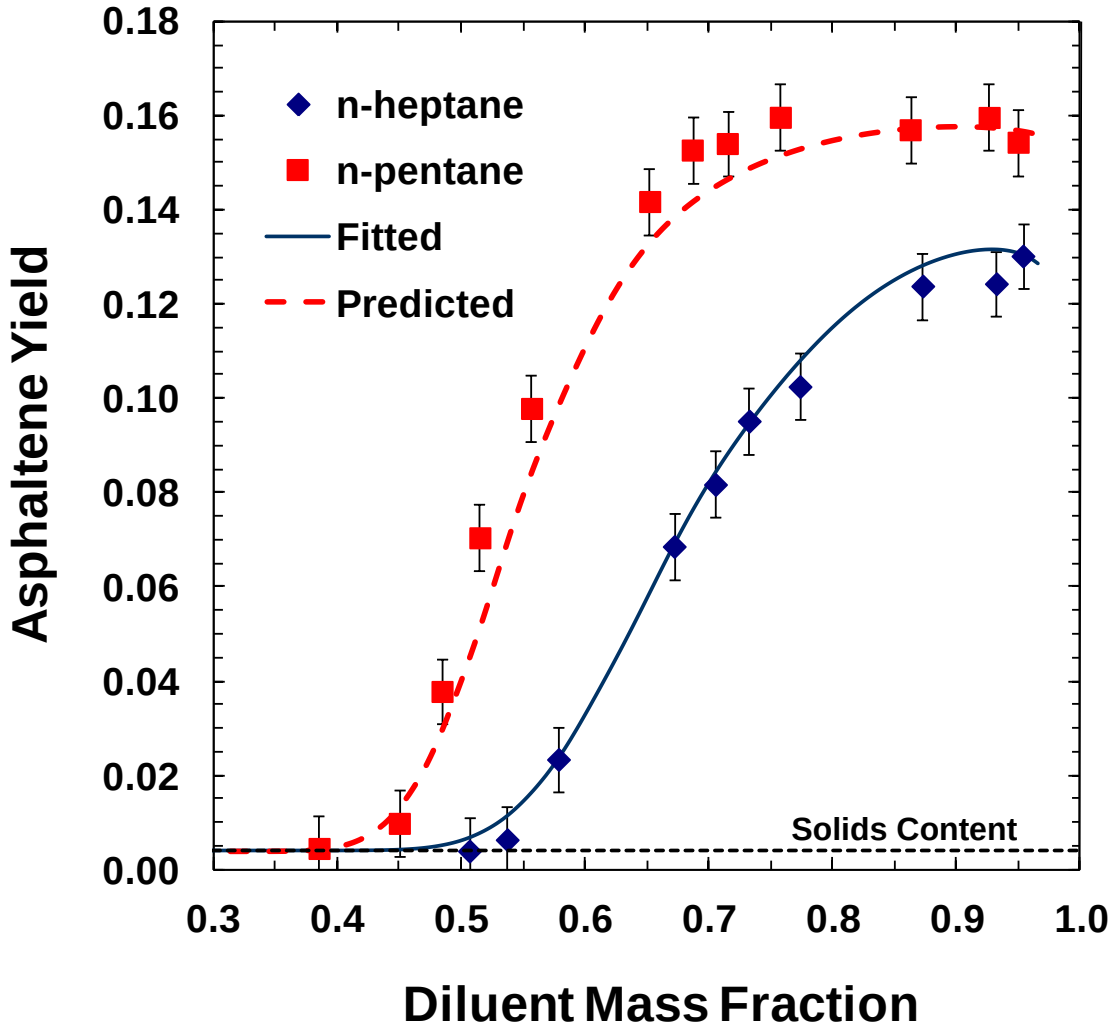

Figure 4.1: Measured and modeled asphaltene precipitation yields (in mass fraction) for Lloydminster heavy oil diluted with *n*-heptane and *n*-pentane. The data is from Akbarzadeh et al. (2005).

Table 4.3: Molar mass distribution of asphaltenes.

Asphaltene Subfraction	Molar Mass (g/mol)	f(M)	Mass Fraction	Mole Fraction
	1800	0	0	0
1	2469	3.08E-04	1.25E-01	1.82E-01
2	3201	4.70E-04	3.75E-01	4.21E-01
3	4088	2.86E-04	2.92E-01	2.57E-01
4	5006	1.11E-04	1.37E-01	9.89E-02
5	5934	3.46E-05	5.00E-02	3.04E-02
6	6866	9.39E-06	1.56E-02	8.16E-03
7	7801	2.33E-06	4.36E-03	2.01E-03
8	8738	5.42E-07	1.13E-03	4.65E-04
9	9675	1.20E-07	2.76E-04	1.03E-04
10	10613	2.57E-08	6.46E-05	2.19E-05
11	11551	5.34E-09	1.46E-05	4.54E-06
12	12489	1.08E-09	3.19E-06	9.20E-07
13	13428	2.16E-10	6.81E-07	1.83E-07
14	14367	4.22E-11	1.42E-07	3.56E-08
15	15306	8.13E-12	2.92E-08	6.86E-09
16	16245	1.55E-12	5.89E-09	1.31E-09
17	17185	2.92E-13	1.17E-09	2.46E-10
18	18124	5.45E-14	2.31E-10	4.58E-11
19	19064	1.01E-14	4.49E-11	8.47E-12
20	20003	1.85E-15	8.64E-12	1.56E-12
21	20943	3.38E-16	1.65E-12	2.84E-13
22	21882	6.13E-17	3.13E-13	5.14E-14
23	22822	1.11E-17	5.87E-14	9.27E-15
24	23762	1.98E-18	1.10E-14	1.66E-15
25	24701	3.54E-19	2.04E-15	2.97E-16
26	25641	6.30E-20	3.76E-16	5.28E-17
27	26581	1.12E-20	6.90E-17	9.34E-18
28	27521	1.97E-21	1.26E-17	1.65E-18
29	28460	3.47E-22	2.29E-18	2.90E-19
30	29400	6.08E-23	4.15E-19	5.08E-20

CHAPTER 5

Modeling of Asphaltene Precipitation from Crude Oil Blends[1]

The objective of this work was to adapt the modified regular solution model presented in Chapter 4 to predict the onset and amount of asphaltene precipitation from crude oil blends diluted with pure *n*-alkanes or a mixture of toluene and *n*-heptane. Asphaltene precipitation tests were conducted on nine different crude oils, a gas oil and their blends. Oils and blends were characterized in terms of SARA fractions. The inputs required for the model were the SARA composition of the blend and the distribution of asphaltene aggregates resulting from self-association. Therefore, appropriate mixing rules were developed in this study to determine the SARA fractions of the oil blend and its asphaltene distribution.

SARA analysis was performed on both the feedstocks and the blends to test a proposed weight average mixing rule for the SARA fractions of a blend. The distribution of asphaltenes in unblended crude oils was determined by fitting the model to its asphaltene yield data when diluted with *n*-heptane. The fitting parameter in the model was the average aggregation number of asphaltenes in the source oils. For blends, two approaches were tested to calculate the distribution of asphaltenes aggregates: 1) molar mass distribution was determined from the gamma function using the average aggregation number of the source oils; 2) the final distribution calculated as a sum of two feedstock asphaltene distributions.

---

[1]Contents of this Chapter published as: Tharanivasan, A., Svrcek, W. Y., Yarranton, H. W., Taylor, S. D., Merino-Garcia, D., Rahimi, P., "Measurement and Modeling of Asphaltene Precipitation from Crude Oil Blends", *Energy Fuels*, **23** (8), 3971-3980, 2009.

5. 1 Experimental

Three independent data sets were used in this study: 1) measured by the author at the University of Calgary (UofC); 2) provided by the National Centre for Upgrading Technology (NCUT); 3) provided by Centro Tecnológico Repsol (Repsol). All nine crude oil samples (Crudes A to I) and the light gas oil (LGO) listed in Table 3.1 of Chapter 3 were considered in this work. The UofC data set consisted of Crude A to D and the LGO. NCUT data set consisted of Crudes E and F. Repsol data set consisted of Crudes G, H and I. Descriptions of each oil blend prepared from Crude A to I and LGO are provided in Table 5.1.

Table 5.1: Blends of crude oils considered in this study.

Oil 1	Oil 2	Oil Blends (wt% oil 1/wt% oil 2)	Solvent	Data Set
Crude A	LGO	75/25, 50/50, 25/75	*n*-heptane	UofC
Crude B	LGO	75/25, 50/50, 25/75	*n*-heptane	UofC
Crude C	LGO	75/25, 50/50, 25/75	*n*-heptane	UofC
Crude A	Crude D	75/25, 50/50, 25/75	*n*-heptane	UofC
Crude E	Crude F	50/50, 40/60, 30/70, 20/80, 5/95	*n*-heptane	NCUT
Crude G	Crude H	50/50, 25/75, 15/85	toluene + *n*-heptane	Repsol
Crude G	Crude I	75/25, 50/50, 25/75, 20/80, 10/90	toluene + *n*-heptane	Repsol
Crude G	Crude I	75/25, 50/50, 25/75	*n*-hexadecane	Repsol

UofC – Measured by the author at the University of Calgary

NCUT – Provided by National Center for Upgrading Technology

Repsol – Provided by Centro Tecnológico Repsol

SARA fractionation was performed on all of the crude oil feedstock samples and for the blends from the UofC and NCUT data sets. Specifically, SARA fractionation at the UofC was carried out based on the procedure described in Section 3.2.2 of Chapter 3. SARA fractionation for NCUT crudes and blends were based on a modified ASTM D2007 procedure. SARA fractionation for Repsol crudes were also conducted using the modified ASTM D2007 procedure at the Rey Juan Carlos University, Móstoles, Spain. Table 5.2 provides the SARA composition for all of the feedstock samples. Precipitation onset measurements were performed for all three data sets (See Section 3.3.2 of Chapter 3). Asphaltene yield experiments were only performed for the UofC data set (Crudes A to D and their blends) based on the procedure mentioned in Section 3.3.3 of Chapter 3.

5.2 Adaptation of the Modified Regular Solution Model for Crude Oil Blends

Three initial assumptions were made in an effort to model crude oil blends: 1) the masses of the SARA fractions are additive; 2) the average aggregation number of the mixed asphaltenes is a mole average of the average aggregation number of the asphaltenes from each crude oil; 3) the average aggregation number of the asphaltenes is independent of asphaltene concentration.

The first assumption may seem obvious as a consequence of the conservation of mass. However, SARA fractions are solubility and adsorption classes. The solubility or adsorption of any component is affected by the other components in the mixture. Hence, the amount of a solubility class in a blend is not necessarily the sum of the amount of that class in each crude oil. The second assumption reflects that the aggregation number and the corresponding average molar mass are number averages. The third assumption presumes that asphaltene self-association in crude oils is only weakly dependent on concentration and can be ignored in the phase equilibrium calculations.

Table 5.2: Characterization data for oils tested in this study.

Oil	Source	Data Set	°API	Composition (wt%)					
				Volatiles	Saturates	Aromatics	Resins	C5-Asphaltenes	Solids
Crude A	Lloydminster + Cold Lake	UofC	11	-	29.0	42.2	15.8	13.0	0.0
Crude B	Athabasca	UofC	7	-	17.8	46.2	18.4	17.3	0.3
Crude C	Peace River	UofC	8	-	18.2	42.7	21.5	17.6	0.0
Crude D	Gulf of Mexico (topped)	UofC	20	-	50.3	30.5	14.6	4.0	0.6
Crude E	Athabasca	NCUT	9	-	17.3	39.7	25.8	16.9	0.0
Crude F	Alberta Conventional Crude	NCUT	32	-	61.1	29.6	5.3	4.0	0.0
Crude G	Gulf of Mexico	Repsol	21	12.6	25.3	40.9	4.9	16.3	0.0
Crude H	Venezuela	Repsol	33	21.5	36.6	33.1	5.4	3.5	0.0
Crude I	Middle East	Repsol	31	25.7	34.2	33.5	3.2	3.5	0.0
LGO	Shell Refinery	UofC	22	-	60.9	36.6	2.4	-	0.0

UofC – Measured by the author at the University of Calgary

NCUT – Provided by National Center for Upgrading Technology

Repsol – Provided by Centro Tecnológico Repsol

A fourth assumption involves the interaction of asphaltenes from different crude oils. Two alternative assumptions were evaluated: 1) the asphaltenes interacted and the final molar mass distribution was determined from the gamma function using the average aggregation number of the feedstocks (Gamma Function Method); 2) the asphaltenes did not interact with each other and the final distribution was a sum of the two feedstock distributions (Additive Method).

Table 5.3: Properties of pure components and pseudo components at 25°C and 1 atm.

Component	**Molar Mass (g/mol)**	**Density (kg/m^3)**	**Solubility Parameter ($MPa^{0.5}$)**
n-heptane	100	678	15.2
n-hexadecane	226	771	16.3
toluene	92	864	18.3
volatiles	86	657	14.9
saturates	460	880	16.4
aromatics	522	990	20.3
resins	1040	1044	19.3

Based on these assumptions, the following initial modeling approach was attempted:

1. The composition of the blend is the mass average of the feedstock crude compositions in terms of volatiles and SARA fractions.
2. The generalized properties of the pseudo-component fractions (Table 5.3) apply to the blends as well as the feedstock crudes.

3. The average associated molar mass of asphaltenes in each feedstock is determined by fitting the asphaltene yields of the crude oil diluted with *n*-heptane (as per original Akbarzadeh et al. (2005) methodology).
4. The distribution of asphaltene molar masses in the mixture is calculated using either the gamma function method or the additive method.
5. The onset and amounts of asphaltene precipitation for the given blend are predicted based on the calculated blend composition and asphaltene distribution.

The proposed modeling approach for blends is summarized in Figure 5.1. The validity of the model assumptions and the proposed methodology are discussed below.

5.3 Results and Discussion

5.3.1 Testing the Model Assumptions

Two model assumptions were tested before considering the blend data: the additivity of the SARA fractions and the effect of dilution on the asphaltene aggregation number.

Additivity of SARA Fractions:

SARA analyses were performed on all of the UofC and NCUT blends and the calculated blend compositions were compared with these measured compositions. Figure 5.2a shows the mass fraction of each SARA component for blends of Crude A and the LGO which contains no asphaltenes. Figure 5.2b shows the mass fraction of each SARA component for blends of Crude A and Crude D, both of which contain asphaltenes. In both cases, the calculated SARA fractions (lines) are in good agreement with the data. Similar behavior was observed for other blends of Crude B/LGO and Crude C/LGO. The average absolute deviations (See Appendix A) of the calculated composition from the measured composition are summarized in Table 5.4. The AAD's are all less than approximately 2 wt%, which is within the experimental error (See Section 3.2.2).

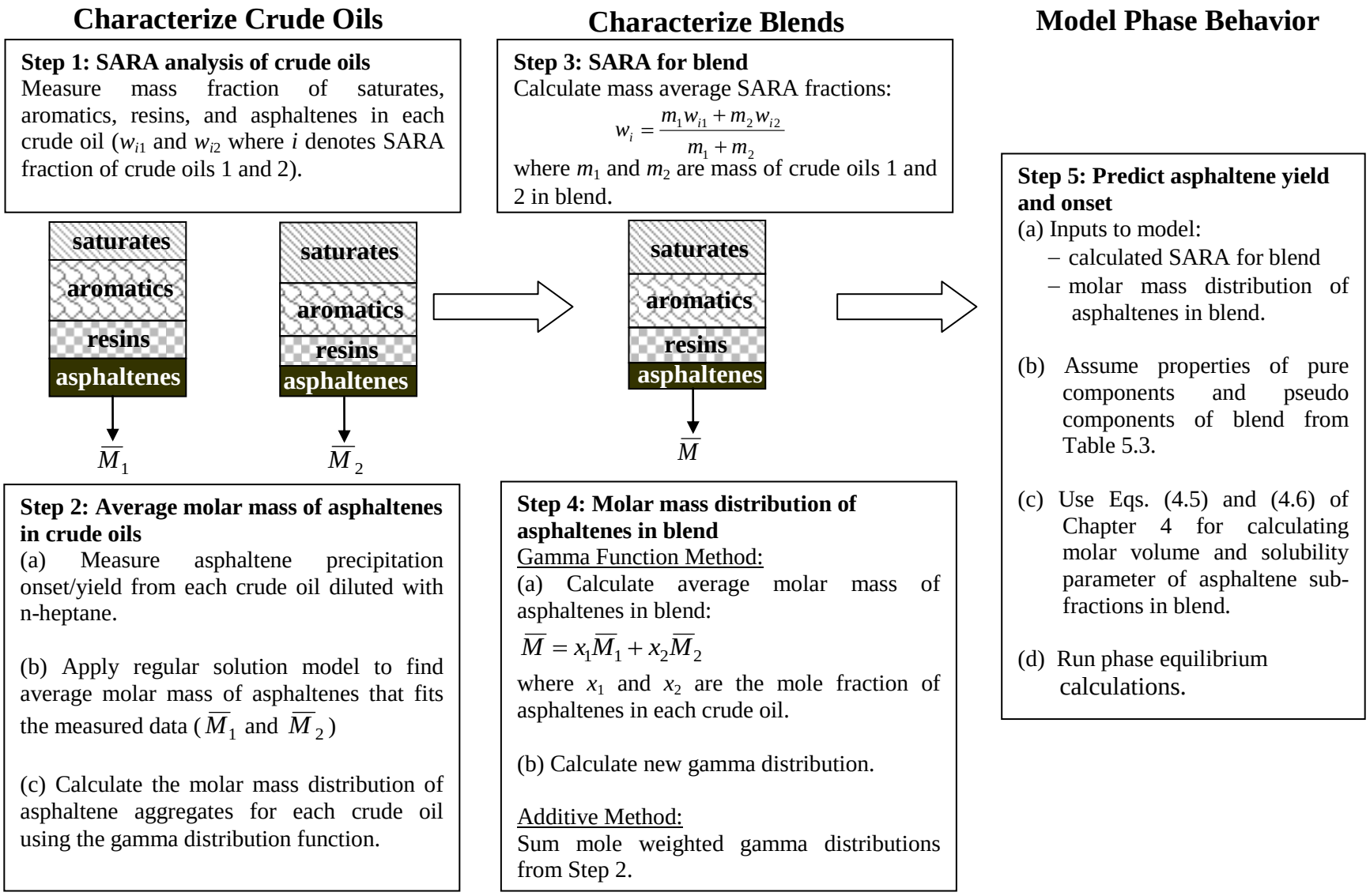

Figure 5.1: Flowchart of the proposed methodology to model crude oil blends.

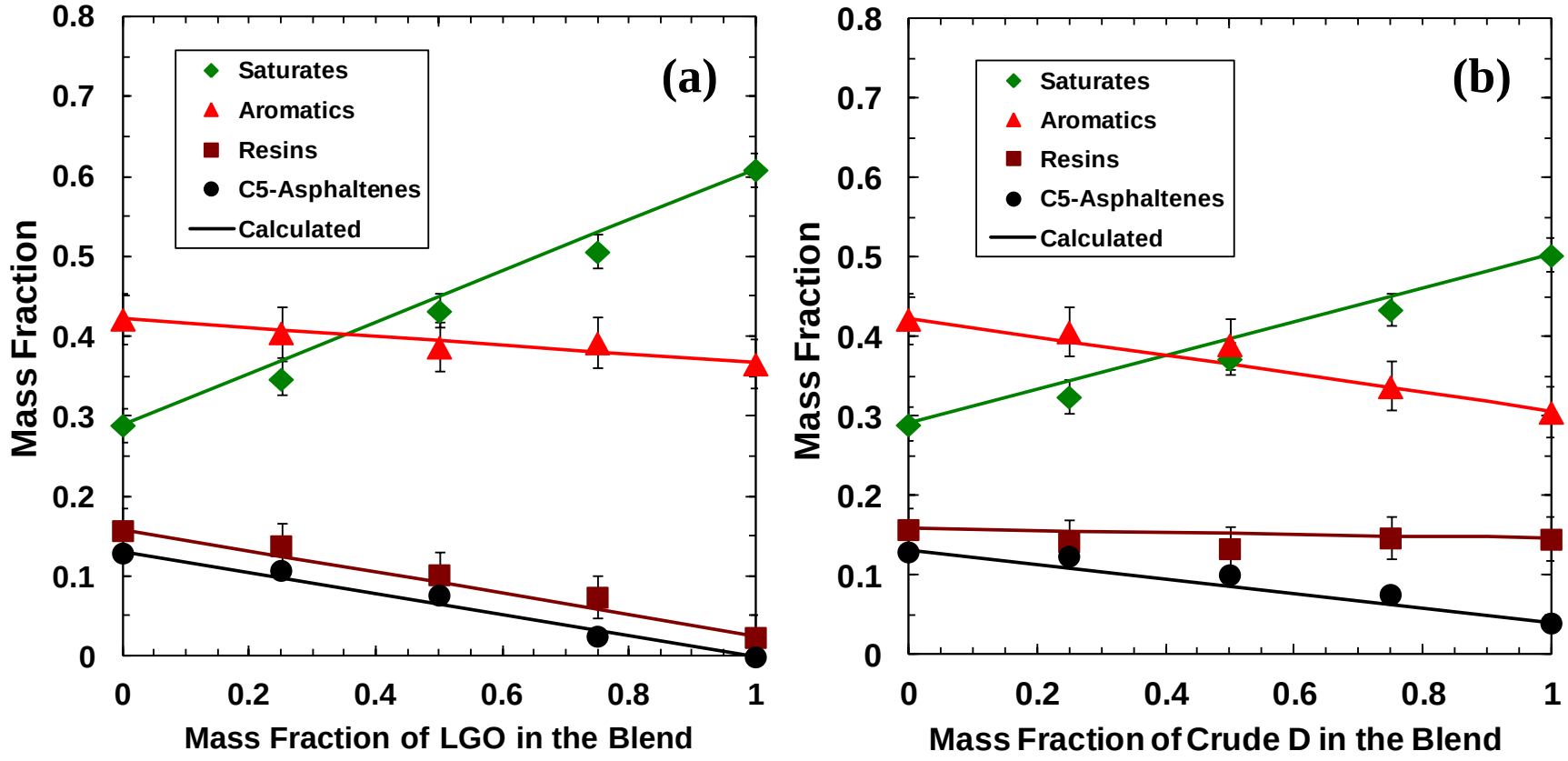

Figure 5.2: Comparison of measured and calculated SARA composition data for the blends of: a) Crude A and LGO; b) Crude A and Crude D.

Table 5.4: Average absolute deviation of each component of the blends tested at UofC.

Components	%AAD for Blends of			
	Crude A/LGO	**Crude B/LGO**	**Crude C/LGO**	**Crude A/Crude D**
saturates	2.1	0.9	1.7	1.9
aromatics	0.7	0.8	1.1	1.4
resins	1.4	1.1	1.4	1.0
C5-asphaltenes	1.0	0.4	1.0	1.6

One set of blend data did not appear to demonstrate the additivity of the SARA fractions. Figure 5.3 shows the mass fractions of each SARA fraction for blends of Crude E and Crude F. The calculated fractions for saturates and asphaltenes (dashed lines) were in good agreement with the data, whereas the other two fractions were not. All of the aromatics and resins data follow a linear trend except for the unblended Crude E data. It seems likely that there is an error in the SARA analysis for Crude E but, unfortunately, the sample was no longer available to redo the analysis. Therefore, the Crude E aromatic and resin contents were estimated by extrapolating the blend compositions (solid lines on Figure 5.3). The estimated SARA fractions for Crude E were 18.6, 49.7, 14.3 and 17.4 wt%, respectively. The AAD for the calculated blend SARA fractions were 0.6, 0.6, 0.5 and 0.2 wt%.

Effect of Dilution on Asphaltene Aggregation Number:

The blends tested at Repsol, Crude G/Crude H and Crude G/Crude I, were first diluted with toluene and then *n*-heptane was added to precipitate the asphaltenes (Table 5.1). Three different toluene-oil mixtures were used: 18.2, 50.0 and 72.7 wt% of toluene in crude oil prior to adding *n*-heptane. From 40 to 95 wt% *n*-heptane was then added to the

mixtures of crude oil and toluene, resulting in solvent (*n*-heptane and toluene) contents of approximately 55 to 98 wt%. These extreme dilutions provide a good test of the model assumption that asphaltene association is insensitive to asphaltene concentration in crude oils.

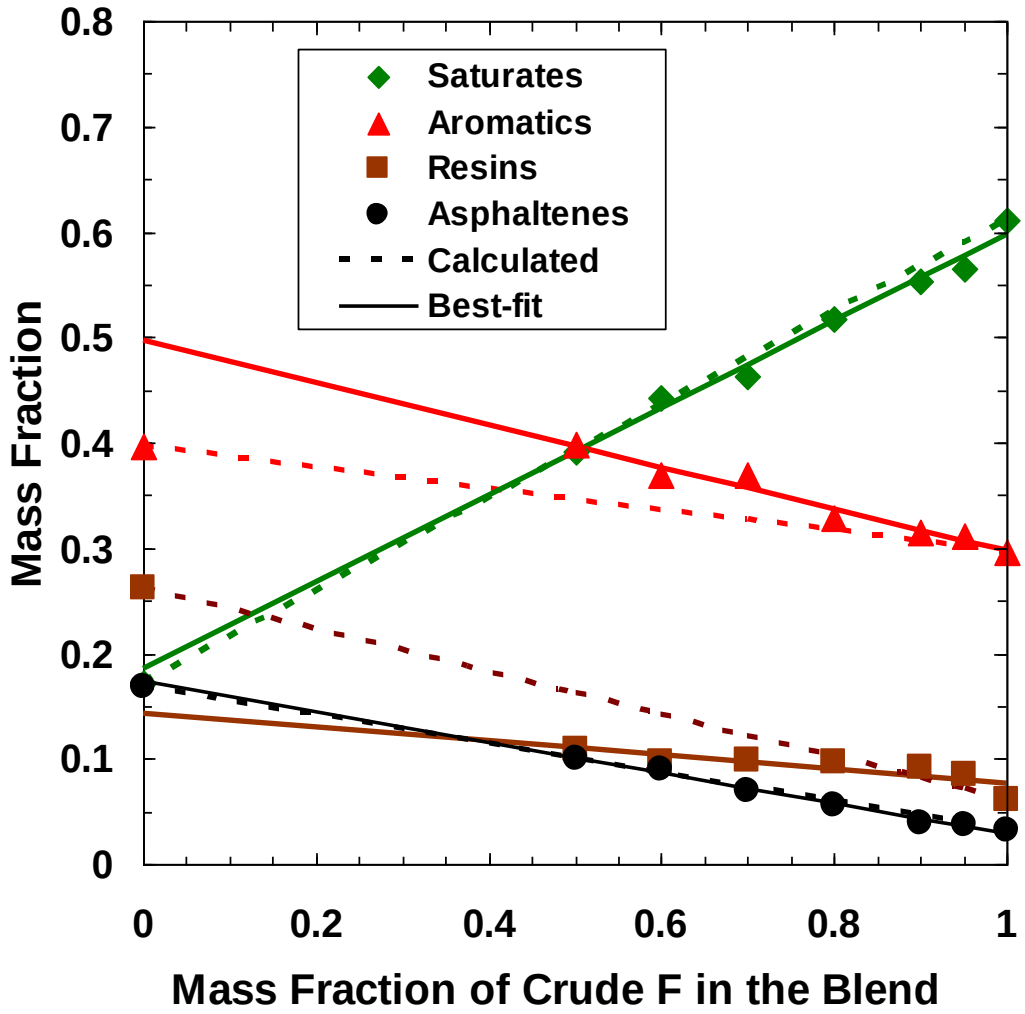

Figure 5.3: Comparison of measured, calculated, and fitted SARA composition data for blends of Crude E and Crude F.

Figure 5.4 shows the onset of precipitation for the toluene diluted crude oils. The asphaltene average aggregation number was adjusted to fit the 18.2 wt% toluene data in each case (corresponding to average asphaltene molar masses of 3340, 3125 and 2860 g/mol for Crudes G, H, and I, respectively). The average aggregation number was then fixed to predict the onset condition at the higher toluene contents (solid lines in Figure 5.4). The predicted onsets were found to underestimate the measured onsets. Furthermore, the deviation between the predicted and measured onsets increased with an increase in concentration of toluene in toluene-oil mixture. In other words, with the assumption of constant molar mass, the predicted trends in onset versus toluene wt% do not fit the data well and are non-linear, contrary to expectations from the oil compatibility model (Wiehe and Kennedy, 2000).

To correct for this deviation, the average aggregation numbers were adjusted to fit both 50.0 wt% and 72.7 wt% toluene data. The corresponding average asphaltene molar masses are plotted against asphaltene concentration in Figure 5.5. The data indicate that the apparent molar mass decreases slightly with decreasing concentration. The trends for Crudes H and I are very similar to what has been observed for mixtures of asphaltenes and resins in toluene (Yarranton et al., 2007), also shown on Figure 5.5. It is likely that at extreme dilutions (< 10 to 15 kg/m^3 asphaltenes), the average aggregation number decreases.

The trend for Crude G is anomalous with the molar mass beginning to decrease below a relatively high asphaltene concentration of 60 kg/m^3. The SARA analysis for this crude oil is unusual with 16.2 wt% asphaltenes and only 4.9 wt% resins. The asphaltene content is high for Gulf of Mexico oil and the resin-to-asphaltene ratio is very low. Hence, it is possible that the asphaltene content is overstated or that only a relatively small portion of the asphaltenes is associating. On the other hand, the onset of precipitation is more difficult to detect at high dilutions and the amount of *n*-heptane at the onset may be overestimated. A lower molar mass would be required to fit the

overestimated onset. Hence, the apparent decrease of molar mass at 40 kg/m³ may be an artifact arising from an incorrect onset measurement at this high dilution condition.

The aggregation numbers used to fit each data point were used in the evaluation of the blends presented later. Overall, changes in aggregation number are not expected to be significant unless the solvent mass fraction exceeds 60 wt%. For most crude oils, a fixed aggregation number can be used unless the oil has been highly diluted with a good solvent such as toluene first.

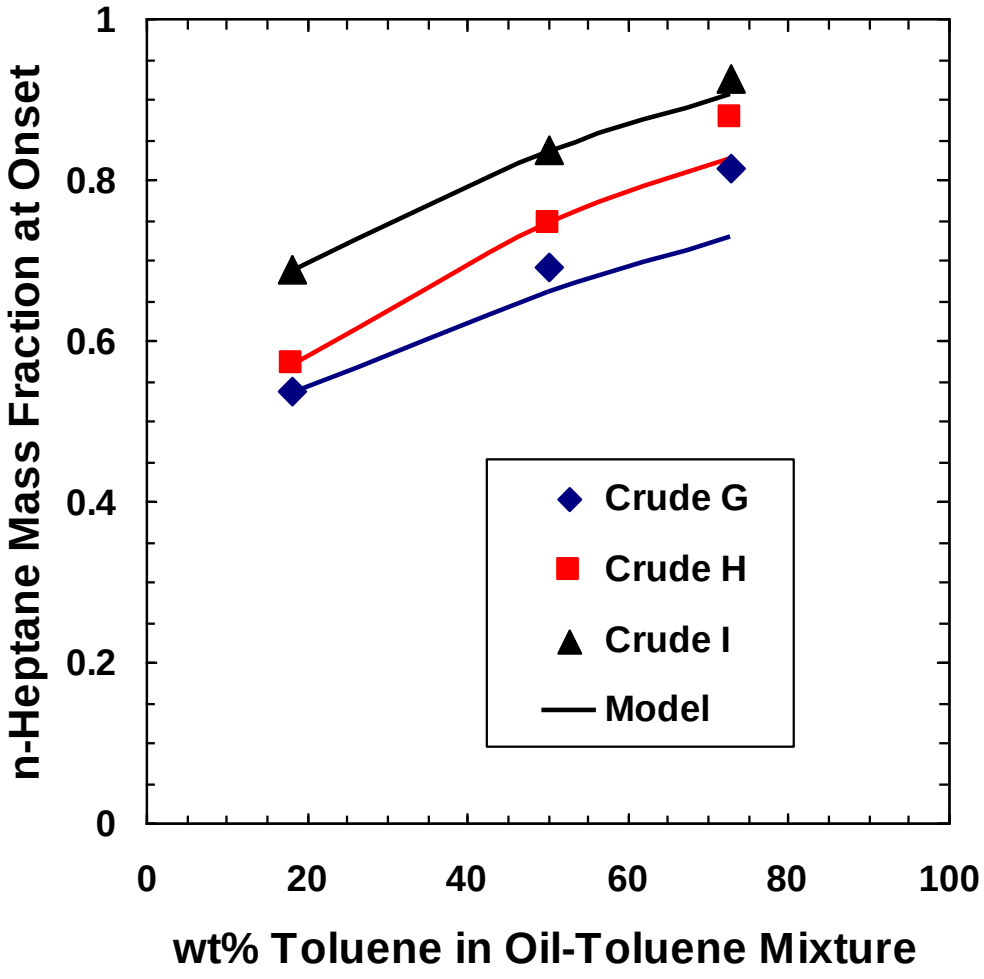

Figure 5.4: Measured and predicted onsets for toluene diluted crude oils.

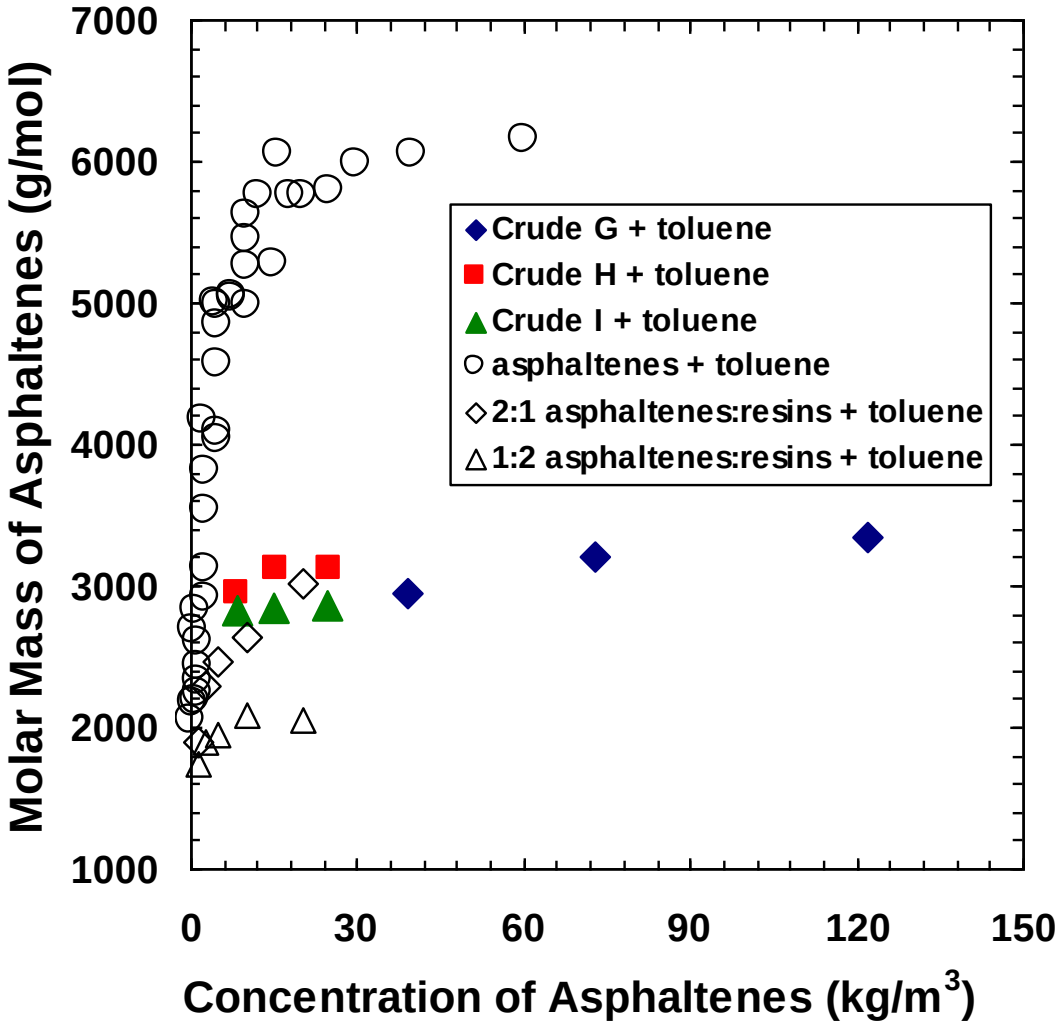

Figure 5.5: Variation in average associated molar mass of asphaltenes in Crude G, Crude H and Crude I with toluene dilution. Solid symbols are fitted molar masses; open symbols are measured data for C5-Athabasca asphaltenes and resins in toluene (Yarranton et al., 2007).

5.3.2 Blend Stability

The validity of the remaining model assumptions and the model methodology could only be evaluated indirectly based on predictions of asphaltene yields and onsets for blends. The methodology is tested on blends where one crude oil contains asphaltenes while the second oil is asphaltene-free. Then, the assumptions for averaging the asphaltene molar mass distributions are tested based on blends of crude oils where both oils contain asphaltenes.

Blends Where Only One Oil Contains Asphaltenes:

Three blends were evaluated: Crude A/LGO, Crude B/LGO, and Crude C/LGO. The asphaltene yields for the three sets of oils and blends are shown in Figures 5.6a to 5.6c, respectively. The first step was to tune the model to match the yields for the unblended crude oils diluted with *n*-heptane. The asphaltene aggregation numbers (expressed as an average molar mass) required to fit the data for Crude A, Crude B and Crude C were 3450, 3300 and 3450 g/mol, respectively. The shape factors (β) of the distribution found to fit the data were 3.5 for Crudes A and B and 2.0 for Crude C. The fitted model results are shown in Figure 5.6 (solid lines).

The asphaltene yields from the blends were then predicted using the methodology described in Section 4.3 of Chapter 4. Since the LGO contained no asphaltenes, the asphaltene aggregation number in each crude oil was assumed to be unaffected by blending. The model predictions (dashed lines) and the measured precipitation yield data for Crude A/LGO, Crude B/LGO, and Crude C/LGO blends are compared in Figures 5.6a to 5.6c, respectively. The predicted yield data matched the measured data reasonably well with an average absolute deviation for the predicted yields of 0.18, 0.33 and 0.32%.

Blends Where Both Oils Contain Asphaltenes:

The following blends were evaluated: Crude A/Crude D, Crude E/Crude F, Crude G/Crude H, and Crude G/Crude I. Crude A/Crude D blends are discussed first because both yield and onset data were available only for this system.

Figure 5.7 shows the asphaltene yields for Crude A/Crude D blends. The yields for Crude A and Crude D were fitted (solid lines) with average asphaltene molar masses of 3420 and 3060 g/mol, respectively. The asphaltene yields for the blends (dashed lines) were predicted using asphaltene molar mass distributions determined with the Gamma Function Method and the Additive Method. The results were the same in both cases except at the onset of precipitation (discussed later). Figure 5.7 shows that the asphaltene yields were reasonably well predicted for all three blends, although yields near onsets were slightly underestimated and the yields at high dilutions of *n*-heptane were slightly overestimated. The AAD of the predicted yields for Blend 75/25, Blend 50/50 and Blend 25/75 were 0.53, 0.50 and 0.38%, respectively.

Figure 5.8 shows the amount of *n*-heptane at the onset of asphaltene precipitation for the Crude A/Crude D blends. Note that above 50% Crude D in the blend, the onsets could not be measured because the concentration of non-asphaltenic solids was too high to differentiate the asphaltene aggregates in microscopic images near the onset condition. The onsets were predicted using the Gamma Function Method and the Additive Method. The threshold for model onset detection was set as 0.01 wt%. Figure 5.8 shows that the Additive Method (solid lines) predicted the onsets better than the Gamma Function Method (dashed lines).

The same methodology was applied to blends of Crude E/Crude F diluted with *n*-heptane and Crude G/Crude I diluted with *n*-hexadecane, presented in Figures 5.9 and 5.10, respectively. The onsets for Crudes E, F, G, and I were fitted with average asphaltene molar masses of 3030, 2925, 3560 and 2970 g/mol, respectively. Again, the Additive Method provided better predictions of the onset condition for the blends than the Gamma Function Method.

Similar results were obtained for blends of the toluene diluted crude oils: Crude G/Crude H and Crude G/Crude I, shown in Figures 5.11 and 5.12, respectively. In this case, the

average molar masses of asphaltenes in Crude G, Crude H and Crude I at each dilution were determined as discussed previously and shown in Figure 5.5. The Additive Method provided the best predictions but tended to overestimate the amount of *n*-heptane at the onset of precipitation. The reason for this discrepancy is not certain but the assumption that the average asphaltene aggregation number is a molar average of the aggregation numbers of the crude oils may break down at high dilutions. At these dilutions, the self-association becomes sensitive to asphaltene concentration and hence may vary as the amount of *n*-heptane varies.

In every case, the Additive Method provided better onset predictions than the Gamma Function Method. This observation suggests that the asphaltene fractions from each crude oil do not interact with each other within the time frame of the experiments; that is, the distributions are added together without alteration. However, recall that the onset of precipitation is governed by the largest asphaltene aggregates which precipitate first. Hence, it is possible that the asphaltenes do interact but that the largest aggregates are not significantly altered under the conditions used in this study. In other words, the gamma function is an inadequate description of the mixtures. Finally, the regular solution model assumes the system is at equilibrium. There may be kinetic effects to self-association and precipitation (Beck et al., 2005; Maqbool et al., 2009) which would not be captured with this approach. Experiments on a longer time scale are required to assess if kinetics have a significant effect.

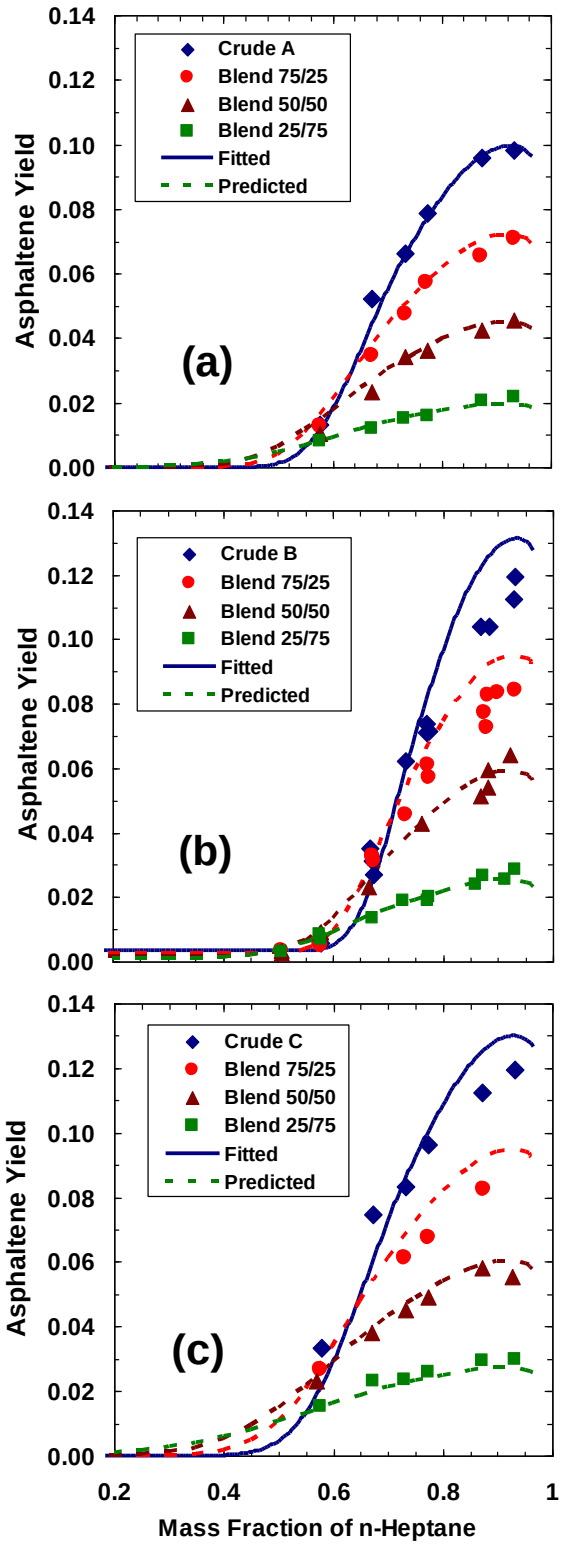

Figure 5.6: Asphaltene precipitation yields (in mass fraction) for crude oil blends at 23°C: a) Crude A/LGO; b) Crude B/LGO; c) Crude C/LGO.

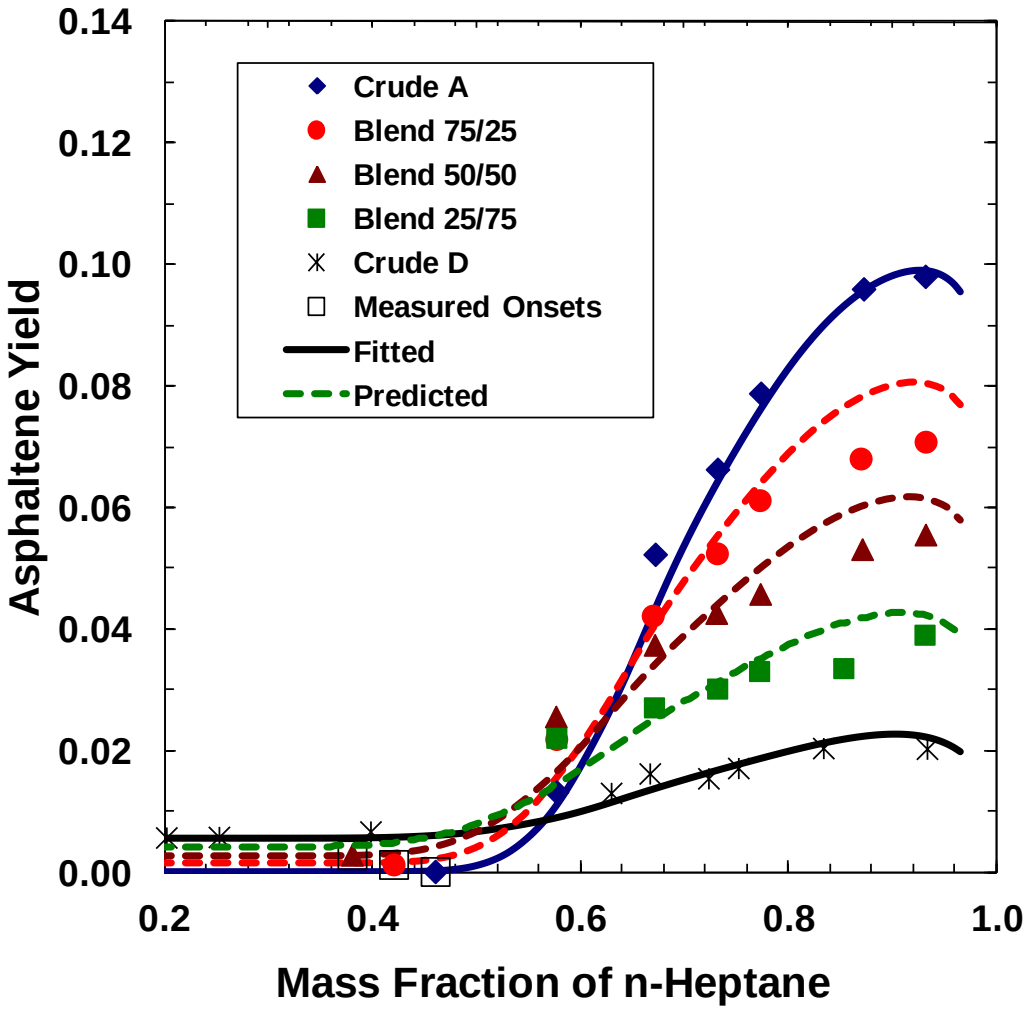

Figure 5.7: Asphaltene precipitation onset and yields (in mass fraction) for Crude A, Crude D, and their blends at 23°C.

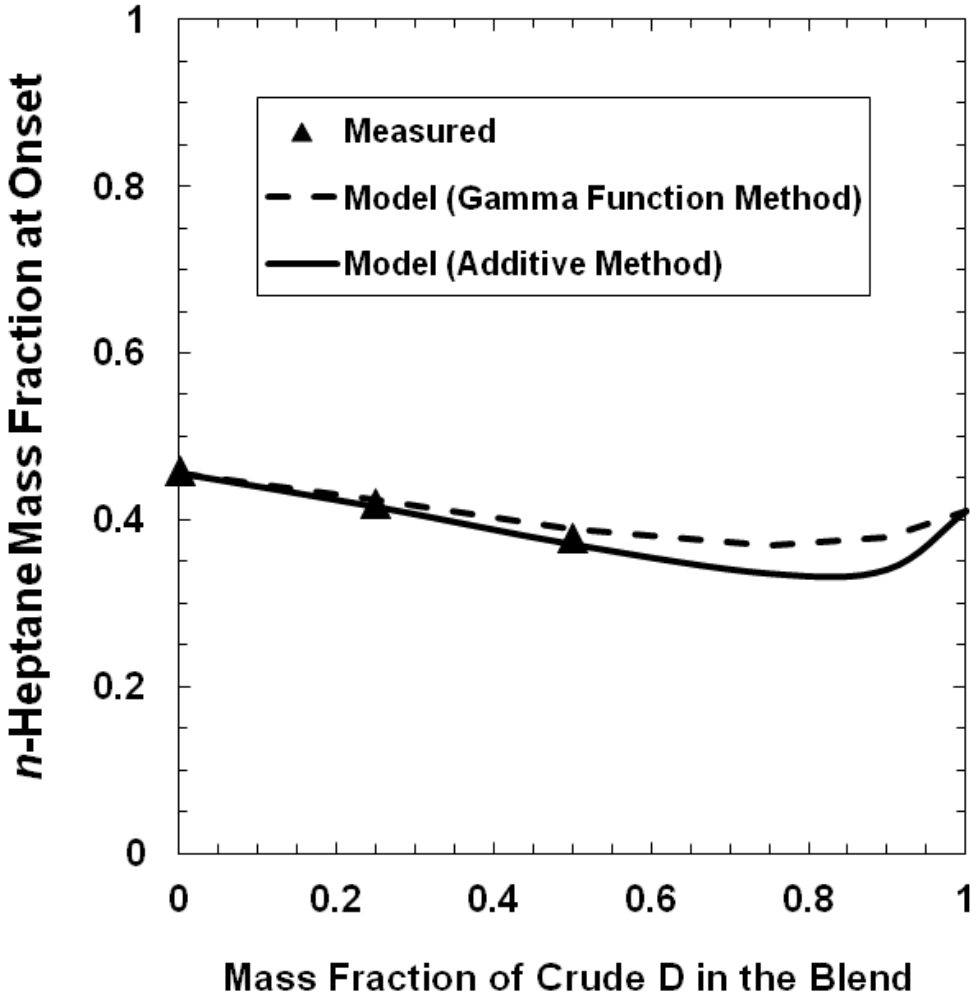

Figure 5.8: Asphaltene precipitation onsets for blends of Crude A and Crude D at 23°C.

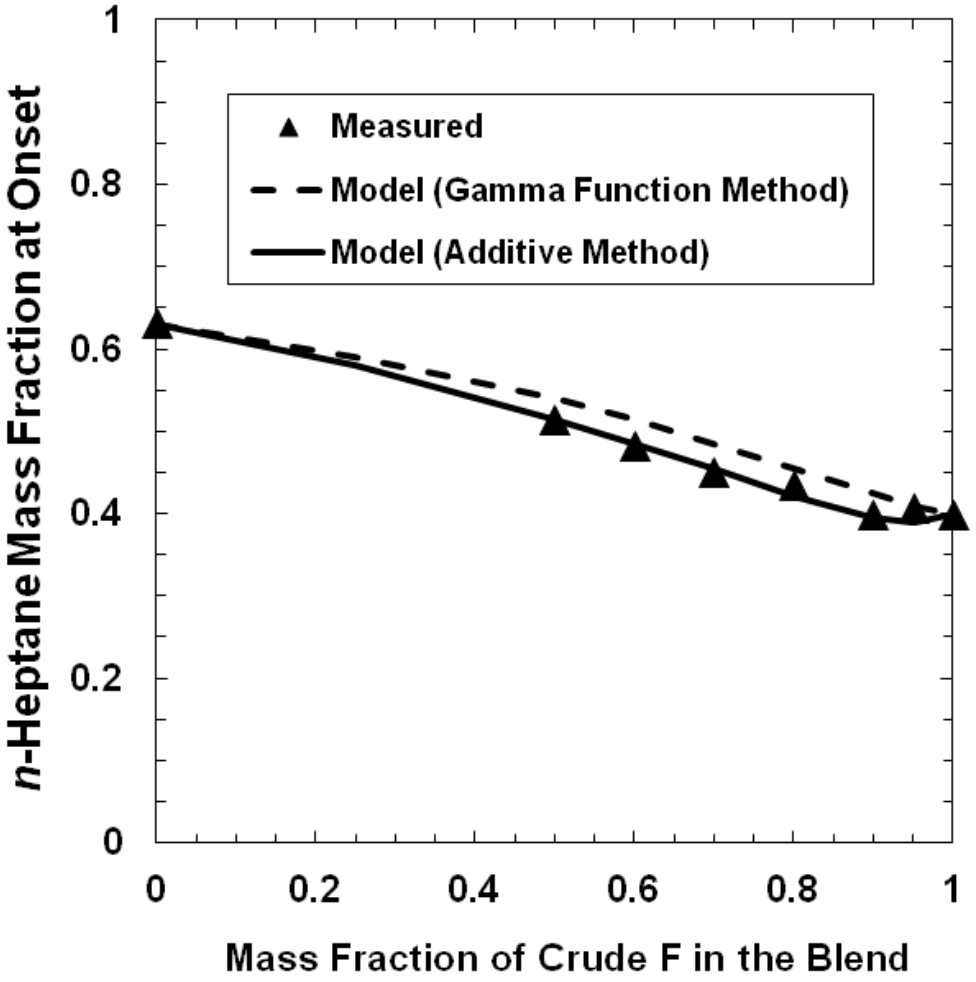

Figure 5.9: Asphaltene precipitation onsets for blends of Crude E and Crude F at 25°C.

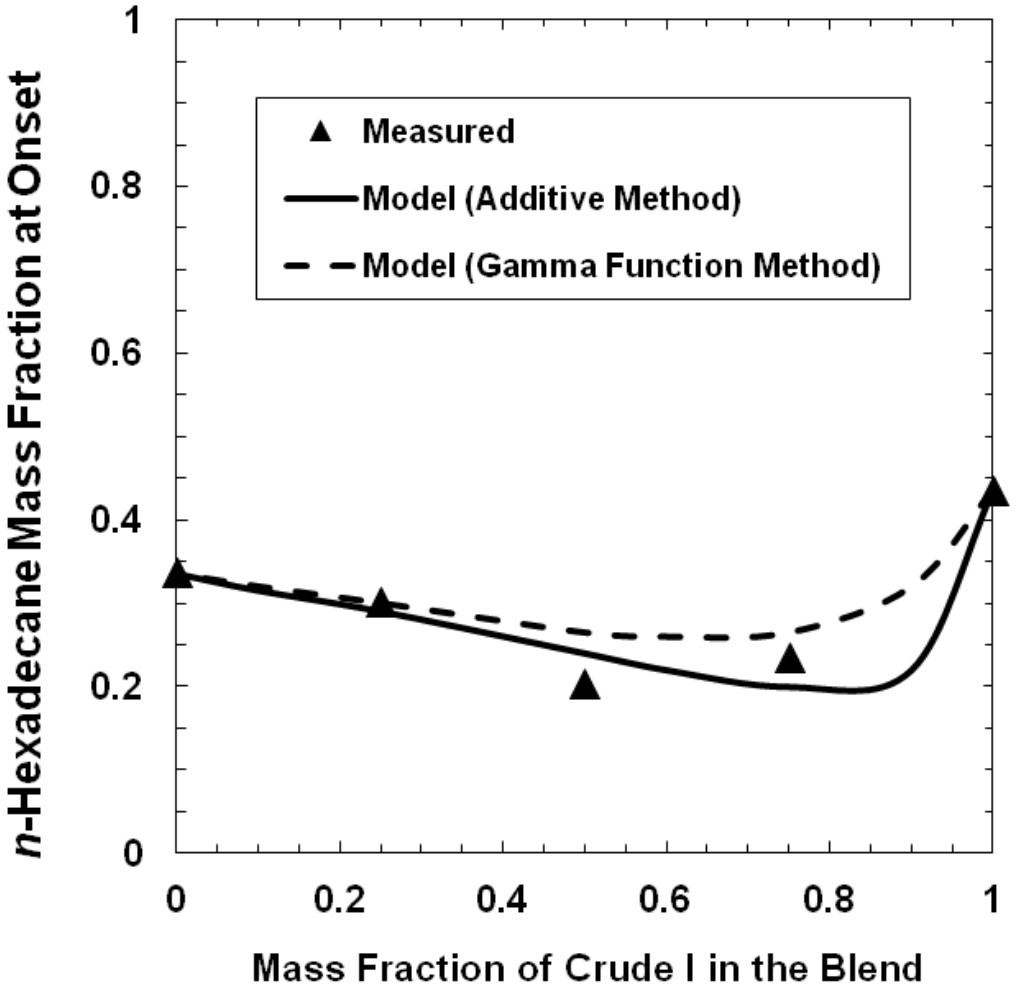

Figure 5.10: Asphaltene precipitation onsets for blends of Crude G and Crude I at 25°C.

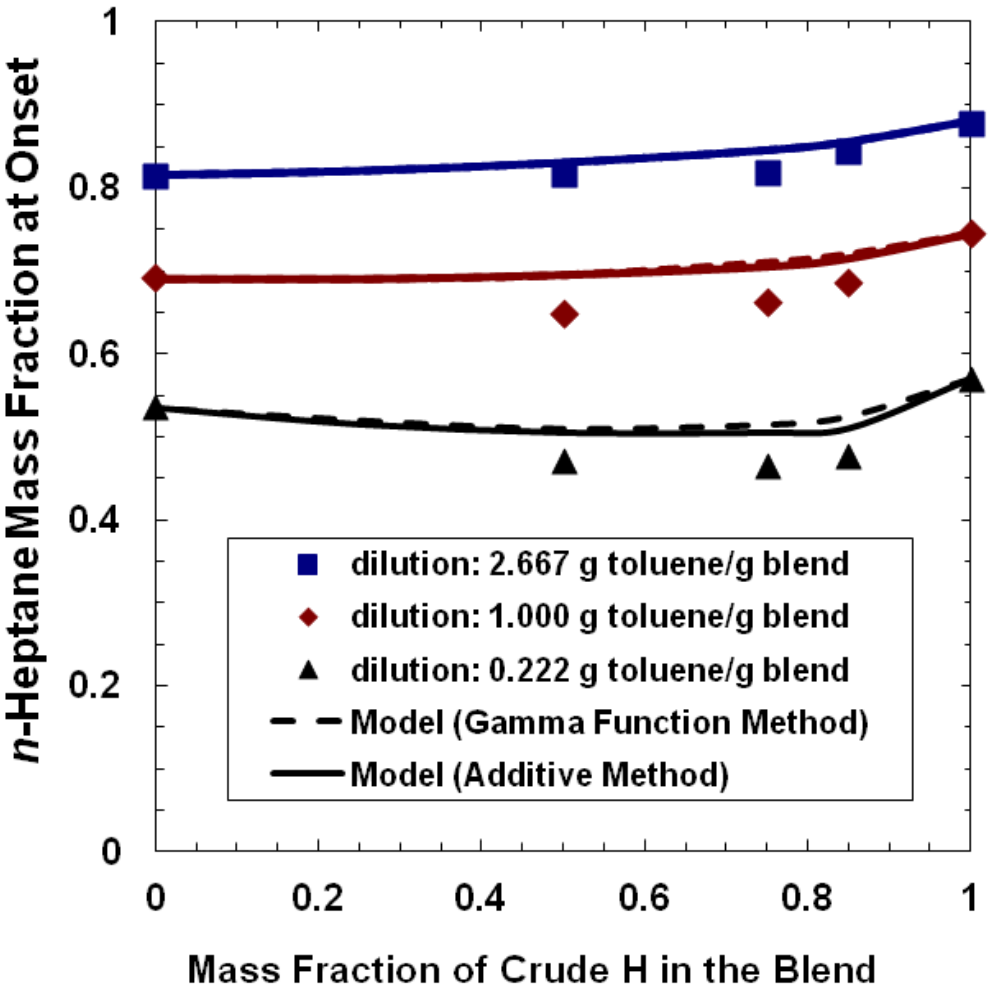

Figure 5.11: Asphaltene precipitation onsets for blends of Crude G and Crude H at different dilution ratios of toluene at 25°C.

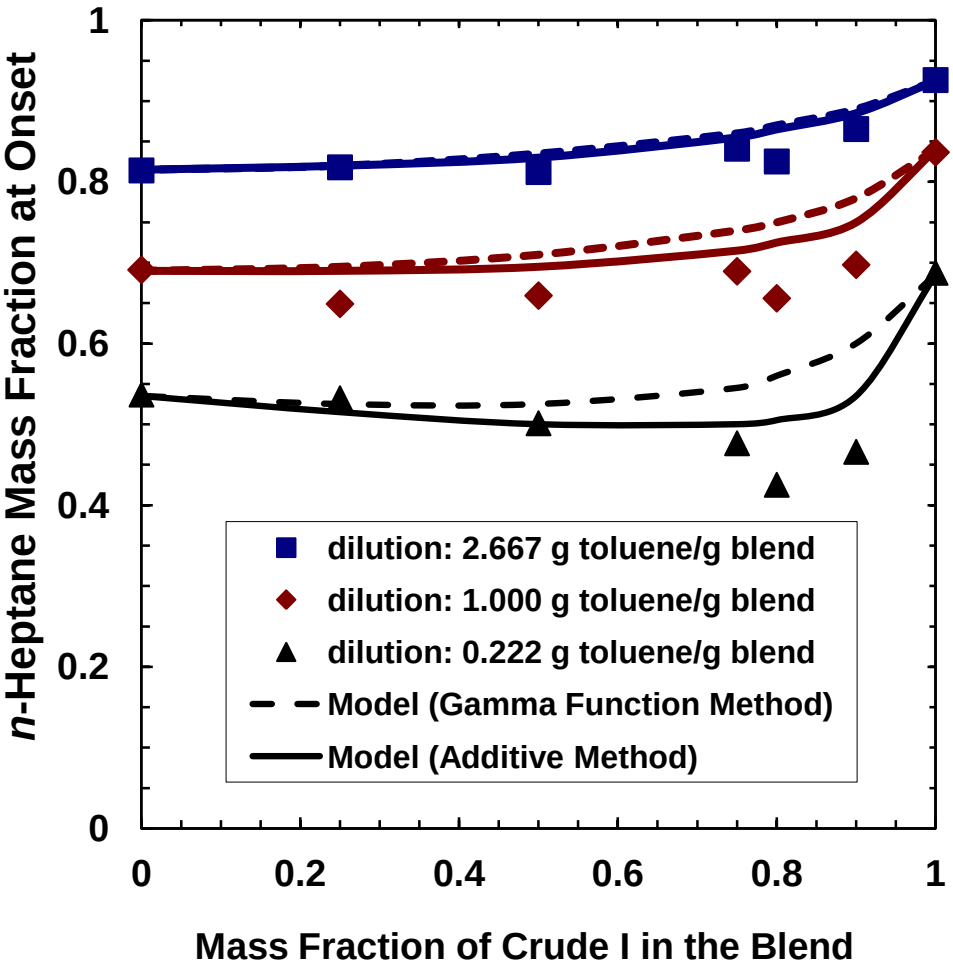

Figure 5.12: Asphaltene precipitation onsets for blends of Crude G and Crude I at different dilution ratios of toluene at 25°C.

5.4 Summary

Blends of eight crude oil mixtures involving nine different crude oils and a gas oil were evaluated in this study. A methodology was developed to use a regular solution approach to model the onset and amount of asphaltene precipitation from the blends diluted with *n*-heptane. It was shown that the composition of the blends could be determined using a mass average of the crude oil SARA analyses. The average aggregation number of the asphaltenes was a molar average of the crude oil asphaltene aggregation numbers. The molar mass distribution of the asphaltenes in the blend was determined by summing the mole weighted distributions from crude oils. The results indicate that, over the time frame of the experiments, the asphaltenes from different crude oils did not interact with each other. While these results must be tested over longer time scales, the data supports models that assume no such interaction.

The mass fraction of *n*-heptane required to initiate precipitation was predicted with an average absolute deviation of 0.53% or less for a range of blends. The model was also able to predict when blends are less stable than the constituent crude oils. The model was less successful at very high asphaltene dilutions; for example, when toluene had been added to the crude oils prior to *n*-heptane addition. At these high dilutions, asphaltenes tend to dissociate and the assumption that the average asphaltene aggregation number is constant breaks down.

CHAPTER 6

Application of Regular Solution Based Model to Asphaltene Precipitation from Live Oils[2]

In this chapter, the regular solution approach for dead oils (depressurized oils from which all the solution gas has evolved) is adapted to model asphaltene precipitation from live oils (oils containing dissolved solution gas) caused by depressurization. The objective is to test if a common characterization methodology can be used to model asphaltene precipitation from both compositional change and depressurization. The model inputs are the mass fraction, molar mass, density, and solubility parameters for each component.

A Gulf of Mexico crude oil is characterized into components and mass fractions are assigned based on GC and SARA analysis. Densities for pentane plus and SARA fractions are obtained from published data. For lighter components, effective densities are determined from extrapolated *n*-alkane data. Solubility parameters of each component are determined as a function of temperature and pressure. The only unknown parameter is the average molar mass of the asphaltene nano-aggregates in the oil which is used to fit the measured precipitation onset pressure data.

6.1 Experimental

All the experiments related to dead oil were conducted by the author at the University of Calgary, and the live oil experiments carried out at Schlumberger's DBR Technology Center were designed and performed under the supervision of the author. The

[2]Contents of this chapter published as: Tharanivasan, A., Yarranton, H. W., Taylor, S. D., "Application of Regular Solution Based Models to Asphaltene Precipitation from Live Oils", *Energy Fuels*, **25** (2), 528-538, 2011.

experiments were performed based on the procedures described in Chapter 3 and a schematic of the experiments performed in this study is given Figure 6.1.

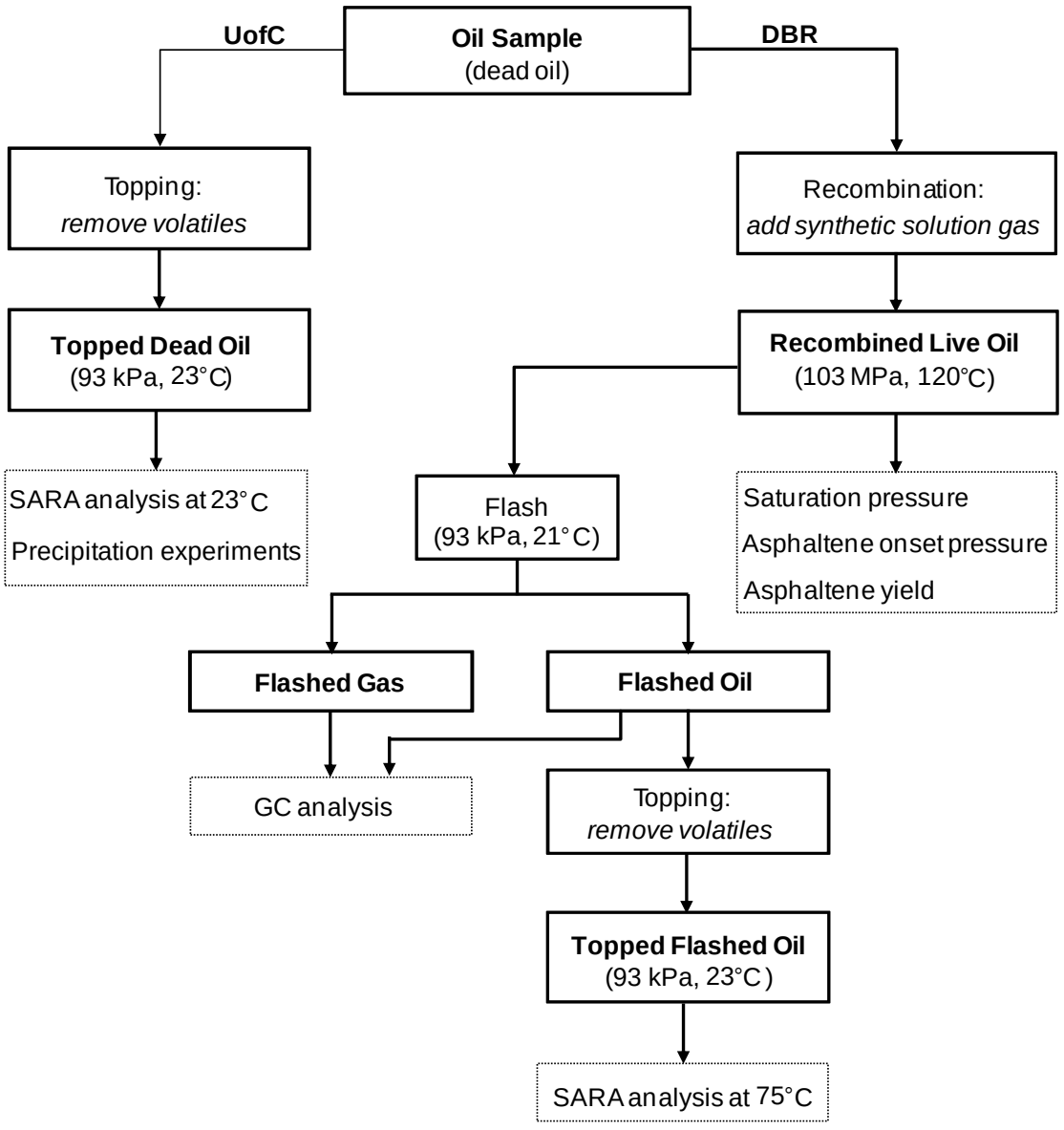

Figure 6.1: Flowchart of the live oil related experiments conducted in this study (UofC = measurements made by the author at the University of Calgary; DBR = experiments carried out at DBR under the supervision of author).

Dead oil tests were conducted using a solution-gas free light crude oil sample (Crude D) obtained from a Gulf of Mexico reservoir. The topped dead oil was used for the dead oil precipitation experiments. The topped oil was approximately 92 wt% of the original dead oil sample. Table 6.1 provides the SARA analysis of topped dead oil. The measured density of the topped dead oil sample was 854.7 kg/m³ at 23°C and 1 atm.

Table 6.1: SARA analysis of topped dead oil at 23°C.

Component	**wt%**
saturates	50.3
aromatics	30.5
resins	14.6
C5-asphaltenes	4.0
solids	0.6

The recombined live oil was used for the live oil depressurization experiments including onset measurement with the high pressure microscope and yield measurements using a filter and post solvent rinse of the equipment. The live oil test sample was prepared by recombining the untopped dead oil sample with a synthetic solution gas to match the desired GOR and live oil gas composition. The recombined live oil was prepared at 103 MPa (14900 psig) and 120°C. The composition of recombined live oil is provided in Table 6.2. The GOR for the recombined live oil was measured to be 195 m³/m³ (1093 SCF/STB) at standard conditions. The density of the recombined live oil at 103 MPa and 120°C was determined from gravimetric analysis and was 757.1 kg/m³. The flashed oil density was measured with an Anton Paar density meter and was 847.7 kg/m³.

6.2 Oil Characterization

6.2.1 Recombined Live Oil

The data available for the live oil characterization were (see Tables 6.2 and 6.3):

- composition of recombined live oil
- composition of flashed oil
- SARA analysis of topped flashed oil
- density and molar mass of SARA fractions from several other dead oils (Akbarzadeh et al., 2005).

A merged composition was required that included the SARA fractions corresponding to the available physical properties. The topped oil sample made up approximately 78% of the flashed oil sample and hence was equivalent to a C11+ fraction, Table 6.3. However, based on simulated distillation data, the dead oil samples used for the SARA fraction properties were approximately equivalent to C16+ fractions.

First, a merged analysis (Column D) was created by replacing the C11+ fractions (in Column B) with the topped oil SARA analysis (Column C), Table 6.2. Then, the C11 to C15 fractions were added back into the analysis. Their mass was deducted from the saturate and aromatic fractions, 76% from the saturates and 24% from the aromatics. The 76:24 split was based on the proportion of aromatic and cyclic species in the C6 to C8 fractions. Finally, several fractions were lumped (Column E) to reduce the total number of fractions to 17, Table 6.2. Appendix F provides the detailed composition calculation for Columns D and E of Table 6.2.

Table 6.2: Composition of recombined live oil.

Component (A)	Live Oil (wt%) (B)	Topped Oil SARA (wt%) (C)	Merged (wt%) (D)	Lumped for C16+ SARA (wt%) (E)
CO2	0.004	-	0.004	-
N2	0.129	-	0.129	-
C1	9.453	-	9.453	9.59
C2	1.599	-	1.599	1.60
C3	2.502	-	2.502	2.50
i-C4	0.673	-	0.673	0.67
n-C4	1.891	-	1.891	1.89
i-C5	1.129	-	1.129	1.13
n-C5	1.710	-	1.710	1.71
C6	2.479	-	2.479	3.03
mcyclo-C5	0.550	-	0.550	-
benzene	0.060	-	0.060	-
cyclo-C6	0.362	-	0.362	-
C7	2.550	-	2.550	2.97
mcyclo-C6	0.796	-	0.796	-
toluene	0.221	-	0.221	-
C8	3.105	-	3.105	4.68
C2-benzene	0.090	-	0.090	-
m&*p*-xylene	0.288	-	0.288	-
o-xylene	0.182	-	0.182	-
C9	3.171	-	3.171	-
C10	3.812	-	3.812	8.67
C11	3.378	-	-	-
C12	3.016	-	-	6.26
C13	3.115	-	-	-
C14	2.854	-	-	7.48
C15	3.065	-	-	-
C16	2.664	-	-	-
C17	2.562	-	-	-
C18	2.554	-	-	-
C19	2.487	-	-	-
C20	2.154	-	-	-
C21	2.185	-	-	-
C22	1.946	-	-	-
C23	1.843	-	-	-
C24	1.732	-	-	-
C25	1.658	-	-	-
C26	1.549	-	-	-
C27	1.556	-	-	-
C28	1.474	-	-	-
C29	1.503	-	-	-
C30+	19.952	-	-	-
saturates	-	50.12	31.70	19.97
aromatics	-	27.61	17.46	13.76
resins	-	19.43	12.29	12.29
asphaltenes	-	2.84	1.80	1.80

Table 6.3: Lumped composition of flashed oil and density of components at 21°C.

Component (F)	Flashed Oil (wt%) (G)	Flashed Oil (cum wt%) (H)	Merged for C16+ SARA (wt%) (I)	Lumped for C16+ SARA (wt%) (J)	Density (kg/m³) (K)
C3	0.16	0.16	0.16	0.16	505.3
i-C4	0.09	0.25	0.09	0.09	554.4
n-C4	0.40	0.65	0.40	0.40	568.6
i-C5	0.51	1.15	0.51	0.51	618.9
n-C5	0.96	2.11	0.96	0.96	625.7
C6	2.27	4.39	2.27	2.83	658.7
mcyclo-C5	0.56	4.94	0.56	-	730.0
benzene	0.06	5.00	0.06	-	877.0
cyclo-C6	0.37	5.37	0.37	-	777.0
C7	2.86	8.24	2.86	3.29	683.4
mcyclo-C6	0.90	9.14	0.90	-	768.0
toluene	0.25	9.39	0.93	-	865.0
C8	3.73	13.12	3.73	5.56	702.4
C2-benzene	0.11	13.23	-	-	-
m&*p*-xylene	0.35	13.58	-	-	-
o-xylene	0.22	13.80	-	-	-
C9	3.85	17.65	3.85	-	716.1
C10	4.67	22.32	4.67	10.60	729.7
C11	4.15	26.47	4.15	-	739.4
C12	3.70	30.17	3.70	7.69	749.1
C13	3.83	34.00	3.83	-	756.1
C14	3.51	37.50	3.51	9.18	763.0
C15	3.77	41.27	3.77	-	768.0
C16	3.27	44.54	-	-	-
C17	3.15	47.69	-	-	-
C18	3.14	50.82	-	-	-
C19	3.05	53.88	-	-	-
C20	2.65	56.52	-	-	-
C21	2.68	59.21	-	-	-
C22	2.39	61.60	-	-	-
C23	2.26	63.86	-	-	-
C24	2.13	65.99	-	-	-
C25	2.04	68.02	-	-	-
C26	1.90	69.93	-	-	-
C27	1.91	71.84	-	-	-
C28	1.81	73.65	-	-	-
C29	1.85	75.49	-	-	-
C30+	24.51	100.00	-	-	-
saturates	-	-	24.53	24.53	891.3
aromatics	-	-	16.90	16.90	1008.8
resins	-	-	15.09	15.09	1044.4
asphaltenes	-	-	2.21	2.21	1089.0

6.2.2 Flashed Oil

A similar procedure was used to obtain a composition for the flashed oil that included the C16+ SARA fractions, Table 6.3. First, a merged composition was calculated including SARA fractions and lumping higher aromatics with toluene. Second, several components were lumped following the same approach used for the live oil. Appendix G provides the detailed composition calculation for Columns I and J of Table 6.3.

6.2.3 Dead Oil

The dead oil had an asphaltene content of 4.0 wt%, almost double that of the flashed oil. The dead oil is approximately 90% of the mass of the flashed oil and therefore the difference in asphaltene contents is larger than can be accounted for by mass balance. One possible explanation is that the wax appearance temperature (measured at DBR) of the live oil was approximately 35°C and therefore wax precipitation could affect the apparent asphaltene content. However, the wax would likely be removed in the washing procedure. Another possibility is that the different washing temperatures (23°C for the dead oil versus 75°C for the live oil) led to different asphaltene yields for the dead oils. Asphaltene yield is known to decrease with increasing wash temperature (Alboudwarej et al., 2002).

Table 6.4: Composition of topped dead oil after characterization.

Component	**wt%**
C11- C15	19.0
saturates	31.3
aromatics	30.5
resins	14.6
asphaltenes	4.0
solids	0.6

Note that all of the asphaltene contents and yields at DBR were determined with a 75°C wash and all of the contents and yields at UofC were determined with a 23°C wash and therefore the data from each lab are self-consistent. For modeling purposes, the asphaltene content measured at DBR was used for the live oil data collected at DBR and the asphaltene content measured at the UofC was used for the dead oil data collected at the UofC.

The topped dead oil is equivalent to a C11+ fraction. As before, SARA properties were assigned to the C16+ fraction. Average molar mass, density, and solubility parameter were calculated at ambient conditions for the C11-C15 fraction. The SARA analysis for modeling the topped dead oil is provided in Table 6.4.

6.3 Property Data and Estimation

The properties required for the modified regular solution model are the molar volume (or density and molar mass) and solubility parameter for each component. For the live oil study, the density and solubility parameters were determined at temperatures of 80, 100, and 120°C and pressures from 10 to 100 MPa. For the dead oil density check, the properties were determined at 21°C and 101 kPa.

6.3.1 Molar Mass

The molar mass of the pure components are known. The molar mass of the saturates, aromatics, and resins of various crude oils were previously found to be reasonably consistent with each other (Akbarzadeh et al., 2005) and therefore the following average values were applied to the C16+ fractions:

saturates	460 g/mol
aromatics	550 g/mol
resins	1040 g/mol

The average molar mass of the asphaltene nano-aggregates is a function of composition and temperature (Moschopedis et al., 1976; Yarranton et al., 2000). Since the average molar mass of the asphaltene nano-aggregates in the oil cannot be measured directly, it is used as a fitting parameter.

6.3.2 Density

The challenge in predicting the density of the oil from pure component properties is how to handle the light components, such as methane, which exist as a vapor when pure but as a liquid in the oil. The problem can be handled either by using a mixing rule that accounts for a volume change upon mixing or by using effective densities. Effective density is the density of the component when it is part of a liquid mixture. The advantage of using effective liquid densities is that, by definition, there is no volume change with mixing. Hence, effective densities are consistent with the regular solution approach. The densities of the dead and live oils are then determined as follows:

$$\rho_{oil} = \left[\sum \frac{w_i}{\rho_{ei}} \right]^{-1} \tag{6.1}$$

and the volume fraction of each component is given by:

$$\phi_i = \frac{w_i \rho_{oil}}{\rho_{ei}} \tag{6.2}$$

where ρ_{oil} is the density of the oil, and ρ_{ei}, w_i, and ϕ_i are the effective density, mass fraction, and volume fraction, respectively, of component *i*.

Densities were obtained for all of the pure components from the National Institute of Standards and Technology (NIST) standard reference data base (NIST, 2008). For

pentane and higher carbon number hydrocarbons, the hydrocarbon is in the liquid phase for most of the range of conditions of interest and it was assumed that the effective density and the pure component density were identical. Methane and ethane are in the gas or near critical region at the conditions of interest and hence effective densities were required. Propane and butane approach the critical region and therefore effective densities were estimated but compared with liquid phase densities where possible. Different methods were developed for the pentane plus fractions and for the butanes and lower fractions as outlined below. Another set of correlations was used for the saturates, aromatics, resins, and asphaltenes, also described below.

6.3.2.1 n-Pentane and Higher Carbon Numbers

Since the densities were not always available at exactly the desired temperature and pressure, the density data was curve fit at each of several temperatures using a pressure dependent compressibility as follows:

$$\rho = \rho_0 \exp\{\alpha_1 P + \alpha_2 (1 - \exp(-\beta P))\} \tag{6.4a}$$

where ρ_0 is the density in kg/m³ at 101 kPa, α_1 is the compressibility at high pressure, $\alpha_2=\Delta\alpha/\beta$, $\alpha_1+\Delta\alpha$ is the compressibility at low pressure, β is the decay rate from the low to high pressure compressibility, and P is the pressure in kPa. The parameters, ρ_0 and α_2 were found to be temperature dependent and were fit with the following expressions:

$$\rho_0 = a_0 + b_0 T + c_0 T^2 \tag{6.4b}$$

$$\alpha_2 = a_1 T^n \tag{6.4c}$$

where a_0, a_1, b_0, c_0, α_1 and n are fit parameters and T is temperature in K. Note that curve fits were performed rather than using a more generalized correlation in order to obtain a more precise fit over the liquid phase conditions of interest.

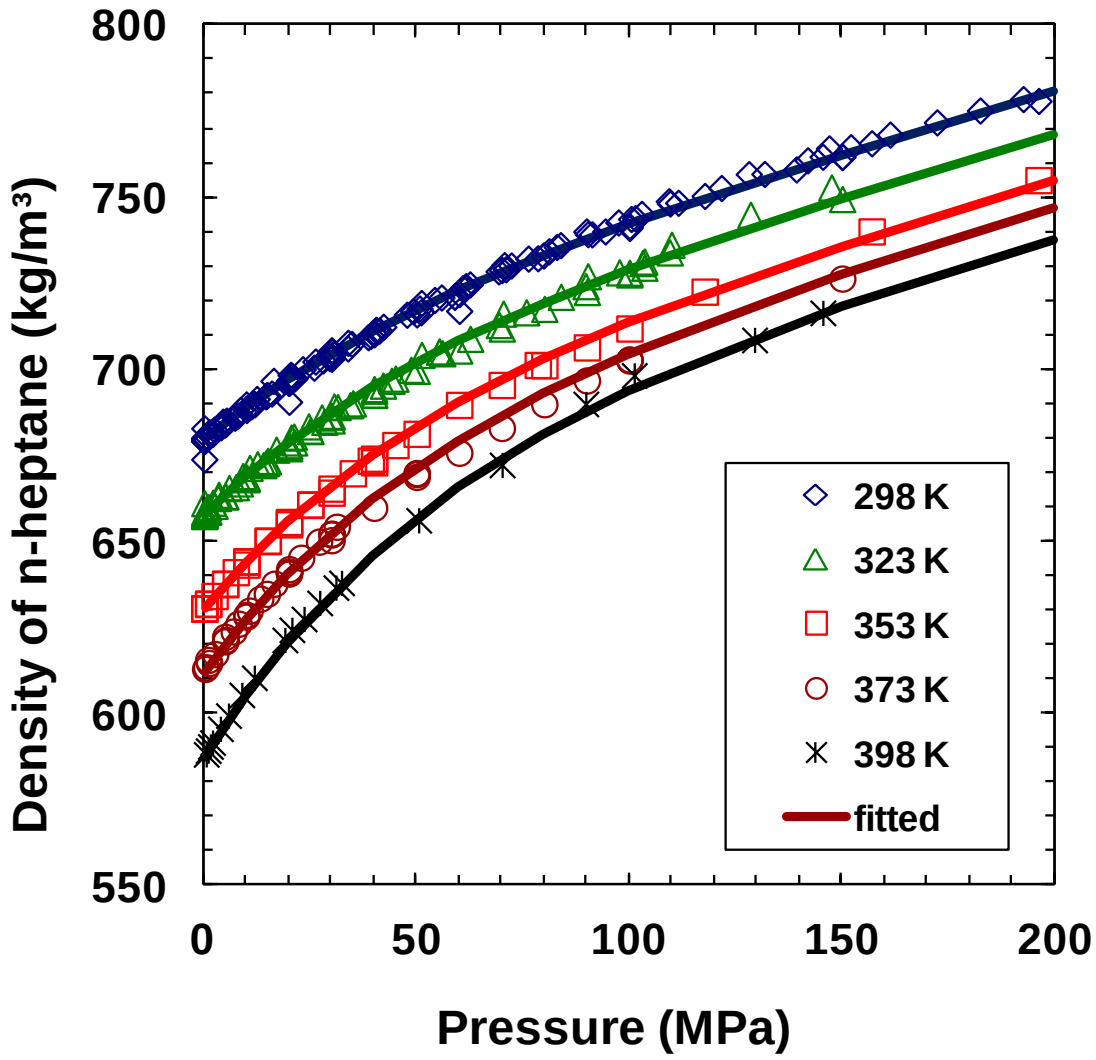

Figure 6.2: Fitted liquid density data for *n*-heptane. Symbols are data from NIST. Solid lines are fits using Eq. 6.4a.

Table 6.5: Parameters for fitting pure component densities.

Component	a_0 (kg/m^3)	b_0 (kg/m^{3}K)	c_0 (kg/m^{3}K^2)	α_1 (kPa^{-1},×10^6)	a_1 (×10^{10})	n	β (kPa^{-1},×10^4)	AAD (kg/m^3)
n-pentane	647.70	0.7408	-0.002785	0.85	0.000095	5.087	0.30	2.8
n-hexane	841.31	-0.3645	-0.000883	0.58	0.254	3.732	0.28	1.1
n-heptane	867.45	-0.4104	-0.000737	0.45	0.669	3.585	0.20	0.9
n-octane	841.27	-0.1762	-0.001014	0.40	2.99	3.327	0.17	0.9
n-decane	883.36	-0.3419	-0.000629	0.40	8.12	3.118	0.16	1.1
n-dodecane	883.36	-0.2562	-0.000698	0.40	2.05	3.322	0.16	1.1
n-tetradecane	883.27	-0.1661	-0.000822	0.40	1.00	3.410	0.16	0.8
n-hexadecane	883.36	-0.1399	-0.000815	0.40	0.14	3.749	0.16	0.7

The parameters used to fit the data are provided in Table 6.5. Figure 6.2 shows fitted *n*-heptane liquid densities at 298, 323, 353, 373, and 398 K. For all components, the goodness of fit or the average absolute deviation for the fitted data was generally within the scatter of the data, less than 1.1 kg/m³ in all cases except for *n*-pentane, Table 6.5. The average absolute deviation for *n*-pentane was higher at 2.8 kg/m³ because there was significant scatter in the data set.

The densities of other components, such as toluene, which were only required at 21°C and 101 kPa, were taken directly from the NIST data base (NIST, 2008). High pressure data was not available for *i*-pentane. Instead, it was estimated to be 98.9% of the density of *n*-pentane based on the ratio of the density of *i*-pentane to *n*-pentane at 101 kPa.

6.3.2.2 Methane, Ethane, Propane, n-Butane, and i-Butane

To estimate the effective density of the light *n*-alkanes, the molar volumes of the higher *n*-alkanes at a given temperature and pressure were plotted versus molar mass. Molar volumes were used because the data followed a trend that was easily fit with a quadratic equation which was then extrapolated to estimate the molar volume of the lower *n*-alkanes, Figure 6.3. There is no theoretical justification for the extrapolation but the extrapolated molar volumes at 25°C and 101 kPa are in good agreement with literature data, Table 6.6.

Effective densities determined from the extrapolated molar volumes are shown in Figure 6.4. The extrapolated densities were fit in a similar manner as for the higher carbon number components with Eq. 6.4a but the parameters were considered as temperature dependent and altered as follows:

$$\rho_0 = a_0 + b_0 T + c_0 T^2 \tag{6.5a}$$

$$\alpha_1 = a_1 + b_1 T \tag{6.5b}$$

$$\alpha_2 = a_2 + b_2 T + c_2 T^2 \qquad (6.5c)$$

The fit parameters for the light hydrocarbons are given in Table 6.7. Note, the density at 101 kPa is higher than predicted by Eq. 6.4 and the fits are only valid for pressures at or above 10 MPa.

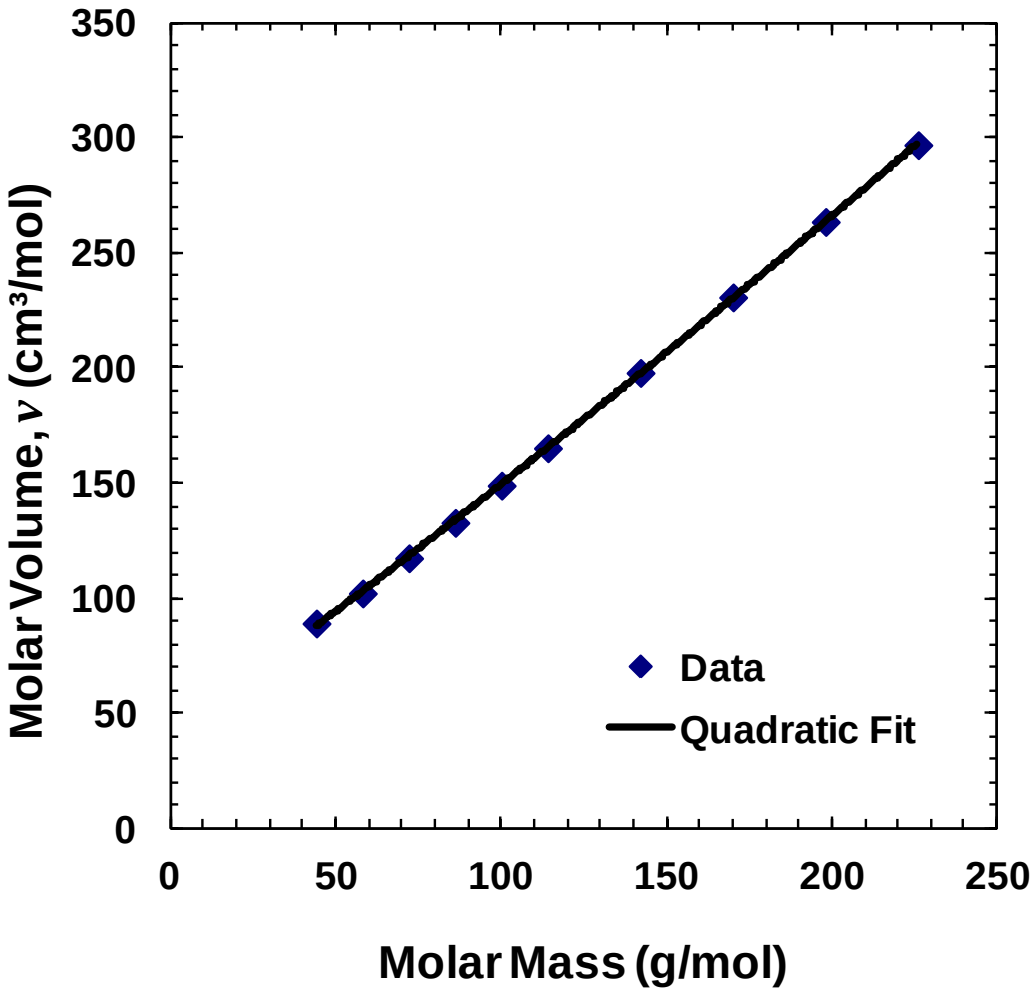

Figure 6.3: Molar volumes of *n*-alkanes at 60°C and 20 MPa. Molar volumes were obtained from fitted NIST data.

Table 6.6: Comparison of extrapolated molar volumes of methane and ethane at 20°C and 101 kPa with partial molar volumes in benzene at 25°C and 101 kPa.

Component	**Extrapolated Molar Volume at 20°C** **(cm^3/mol)**	**Partial Molar Volume in Benzene at 25°C (Hildebrand and Scott, 1950)** **(cm^3/mol)**
methane	52.5	52
ethane	68.0	67

Table 6.7: Parameters for fitting light component effective densities.

Component	a_0 **(kg/m^3)**	b_0 **(kg/m^3K)**	c_0 **(kg/m^3K^2)**	a_1 **($kPa^{-1},\times10^7$)**	b_1 **($1/kPaK,\times10^9$)**	a_2	b_2 **($K^{-1},\times10^3$)**	c_2 **($K^{-2},\times10^6$)**	β **($kPa^{-1},\times10^5$)**
methane	822	-2.713	2.854	-1.654	8.109	-0.6516	4.439	-5.561	4.8
ethane	1179	-3.801	4.082	0.243	5.472	-1.002	5.976	-7.54	4.8
propane	1051	-2.424	1.927	-1.056	4.684	-0.2943	1.557	-1.05	4.8
n-butane	817.8	-0.632	-0.736	-1.930	4.123	0.3015	-2.071	4.231	4.8

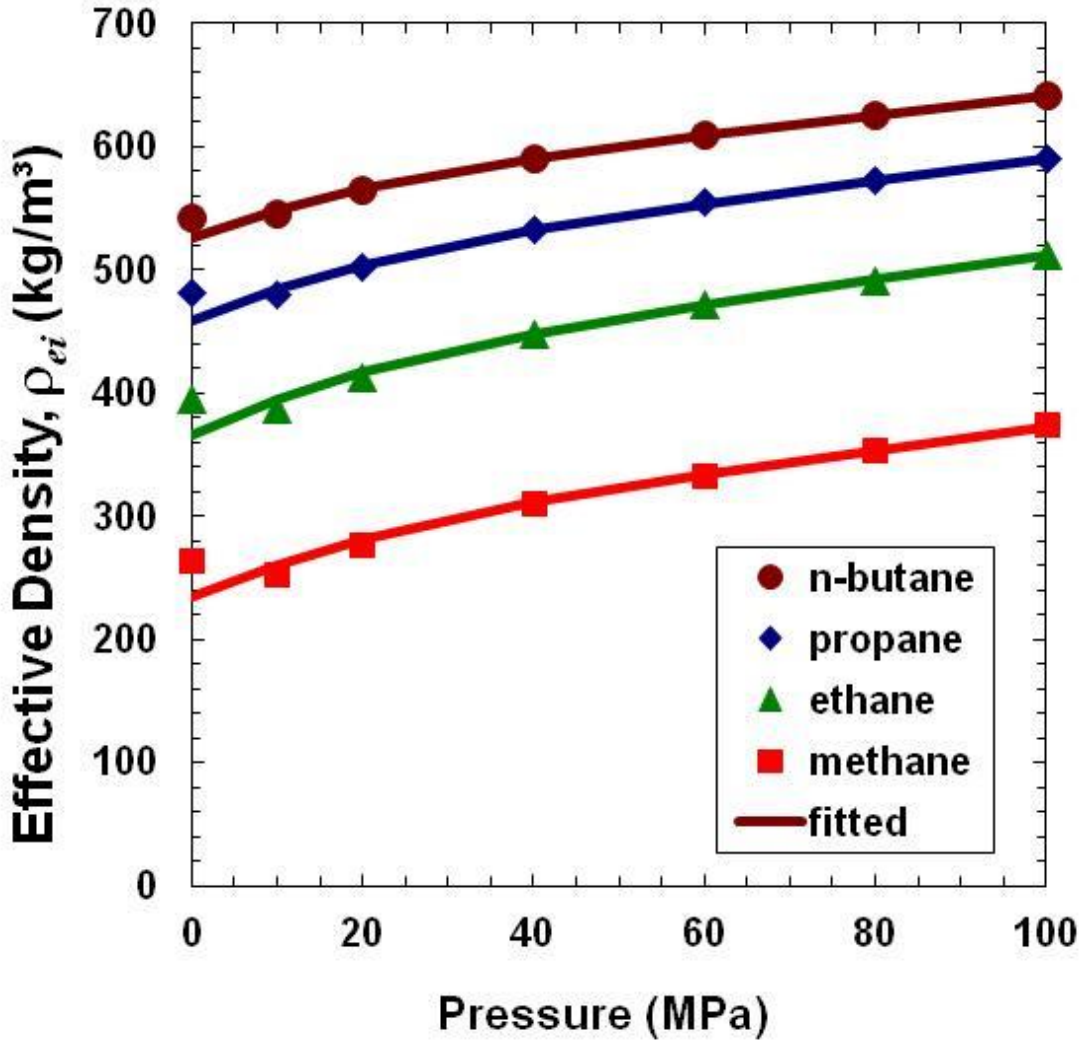

Figure 6.4: Estimated effective liquid densities of methane, ethane, propane, and *n*-butane at 60°C. Symbols are densities from extrapolation of *n*-alkane molar volumes. Lines are fits using Eq. 6.4a.

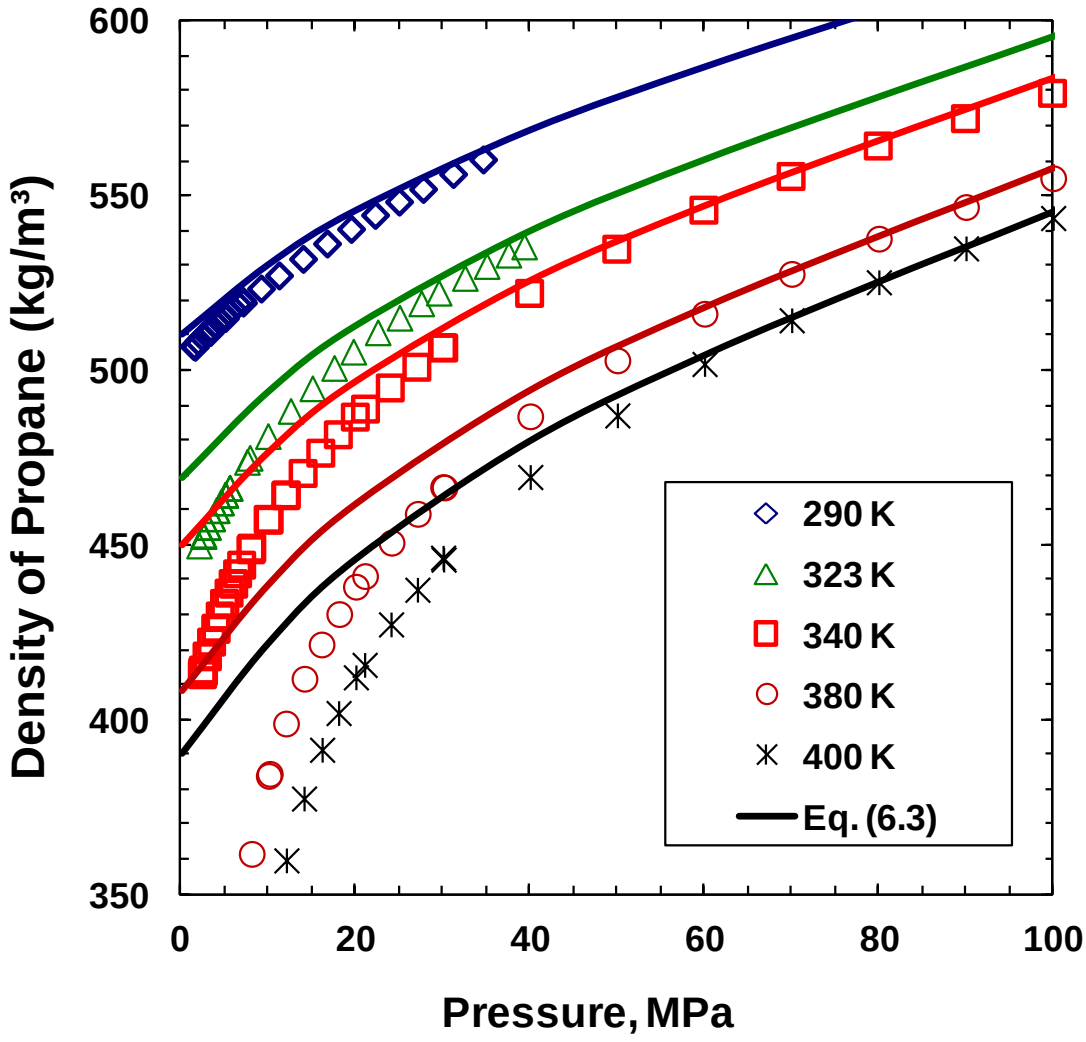

Figure 6.5: Comparison of effective and actual liquid density of propane. Symbols are data are from NIST. Solid lines are effective densities calculated using Eq. 6.3.

Figure 6.5 compares the effective densities calculated for propane versus actual densities. The effective densities are in good agreement with the measured densities at high pressure and low temperature (subcooled liquid). As expected, as propane approaches its critical point (370 K, 4.23 MPa), the deviation of the effective density from the actual density becomes increasingly significant.

Given the different structures, the extrapolated molar volumes for the *n*-alkanes could not be used for *i*-butane. Instead, the density of *i*-butane was scaled to that of *n*-butane. Based on the NIST data, the density of *i*-butane is approximately 97.5% that of *n*-butane.

6.3.2.3 Saturates, Aromatics, Resins, and Asphaltenes

A small set of density data at atmospheric pressure and temperatures from 15 to 55°C was available for saturate and aromatic fractions obtained from an Athabasca bitumen (Akbarzadeh et al., 2005). The saturate and aromatic data were fitted with expressions of the following form:

$$\rho_i = \rho_{0,i}(T)\exp\{\alpha_{1,i}(T)P\} \tag{6.6a}$$

A quadratic temperature dependence for $\rho_{0,i}$ was assumed based on the trends observed in the *n*-alkane data:

$$\rho_{0i} = a_0 + b_0 T + c_0 T^2 \tag{6.6b}$$

No data was available to determine the compressibility of the saturate and aromatic fractions. Instead, it was noted that at subcooled liquid conditions, the *n*-alkane compressibilities approached an asymptote at each temperature when plotted versus carbon number, molecular weight or density. The asymptotes followed a linear trend with temperature and therefore a linear trend was assumed for the temperature dependence of the saturate and aromatic compressibilities:

$$\alpha_{1,i} = a_1 + b_1 T \tag{6.6c}$$

The magnitude of the compressibility was scaled based on the ratio of methylcyclohexane to *n*-heptane compressibility for saturates and on the ratio of toluene to *n*-heptane for aromatics. The parameters for the saturate and aromatic densities are provided in Table 6.8.

Table 6.8: Parameters for saturates and aromatics density predictions.

Component	a_0 **(kg/m³)**	b_0 **(kg/m³K)**	c_0 **(kg/m³K²)**	a_1 **(kPa^{-1},×10^{7})**	b_1 **(1/kPaK,×10^{9})**
saturates	1065	-0.5457	-0.000150	-3.113	3.150
aromatics	1182	-0.5457	-0.000150	-2.681	2.659

The densities of the resins and asphaltenes were determined from a previously developed correlation (Alboudwarej et al., 2003):

$$\rho_A = 670\ M^{0.0639} \tag{6.7}$$

where ρ_A is the density of the asphaltene or resin in kg/m³ and M is the molar mass in g/mol. Both the temperature dependence of the density and the compressibility of the asphaltenes and resins were assumed to be negligible.

6.3.3 Solubility Parameter

6.3.3.1 Pure Components

Solubility parameters at 25°C were obtained from the literature (Barton, 1991) and the data are given in Table 6.9. Note the solubility parameters for the light hydrocarbons

(butanes and lower carbon number) had been estimated from gas solubility data. For convenience in programming and to interpolate for missing data, such as tridecane, the solubility parameters of the *n*-alkanes were correlated to molecular weight. Recall the definition of the solubility parameter:

$$\delta_{25°C} = \left(\frac{\Delta H^{vap*}_{25°C} - 298.15R}{v_{25°C}} \right)^{1/2} \tag{6.8}$$

where δ is the solubility parameter in $MPa^{0.5}$, ΔH^{vap*} is the molar heat of vaporization (J/mol), R is the universal gas constant in J/mol·K, v is the molar volume in cm^3/mol, and subscript 25°C indicates that the property is determined at 25°C. The value of the heat of vaporization that gave the correct solubility parameter at 25°C was calculated from Eq. 6.8 and the data were curve fit as follows:

Carbon Number ≤ 4: $$\Delta H^{vap*}_{25°C} = 3492.8 + 276.54M + 0.52400M^2 \tag{6.9a}$$

Carbon Number ≥ 5: $$\Delta H^{vap*}_{25°C} = 103.65 + 368.7M - 0.06030M^2 \tag{6.9b}$$

Note that ΔH^{vap*} is slightly different than the actual heat of vaporization but fits the solubility parameters to within 0.01 $MPa^{0.5}$ as shown in Table 6.9.

It was assumed that pressure only affected the molar volume and therefore the solubility parameter at any pressure is given by:

$$\delta_{25°C,P} = \delta_{25°C} \left(\frac{v_{25°C}}{v} \right)^{1/2} \tag{6.10}$$

The effect of temperature is accounted for using an expression developed for *n*-alkanes by Akbarzadeh et al. (2005):

$$\delta = \delta_{25°C}\left(\frac{v_{25°C}}{v}\right)^{1/2} - 0.0232(T - 298.15) \qquad (6.11)$$

Note, the slope of -0.0232 $MPa^{0.5}/K$ is consistent with the order of magnitude of the derivative of the solubility parameter ($d\delta/dT \approx$ -0.03 $MPa^{0.5}/K$) found for hydrocarbons in general (Barton, 1991).

6.3.3.2 Saturates, Aromatics, Resins, and Asphaltenes

The following correlations were developed by Akbarzadeh et al. (2005) to estimate the solubility parameters of saturates and aromatics:

$$\delta_{sat} = 22.381 - 0.0222\,T \qquad (6.12)$$

$$\delta_{aro} = 26.333 - 0.0204\,T \qquad (6.13)$$

where δ_{sat} and δ_{aro} are the solubility parameters of saturates and aromatics. The saturate and aromatic solubility parameters are assumed to be independent of pressure.

The solubility parameters of the resins and of each asphaltene pseudo-component were determined from the following correlation (Yarranton et al., 2007):

$$\delta_a = \left(\frac{1000A(T)\,M}{v}\right)^{1/2} \qquad (6.14)$$

where

$$A(T) = 0.579 - 0.00075T \qquad (6.15)$$

and δ_a is the solubility parameter ($MPa^{0.5}$) of resins or asphaltenes and A is approximately equal to the monomer heat of vaporization (kJ/g).

Table 6.9: Solubility parameters and heats of vaporization of pure components.

Component	**Data (Barton, 1991)** $\delta_{25°C}$ **(MPa$^{0.5}$)**	**Data (Perry and Green, 1997)** $\Delta H^{vap}_{25°C}$ **(J/mol)**	**Fitted** $\Delta H^{vap}_{25°C}$ **(J/mol)**	**Calculated** $\delta_{25°C}$ **(MPa$^{0.5}$)**
methane	9.6	-	8063	9.64
ethane	11.6	-	12282	11.56
propane	12.7	-	16704	12.70
n-butane	13.5	-	21335	13.53
n-pentane	14.3	26489	26391	14.35
n-hexane	14.8	32172	31430	14.83
n -heptane	15.2	35800	36446	15.18
n -octane	15.5	41467	41433	15.44
n-nonane	15.6	46172	46401	15.62
n-decane	15.8	50869	51339	15.79
n-undecane	-	55996	56262	15.91
n-dodecane	16.0	60469	61158	16.02
n-tridecane	-	65839	66031	16.11
n-tetradecane	16.2	70502	70877	16.20
n-pentadecane	-	75444	75702	16.24
n-hexadecane	16.3	79606	80504	16.28
i-butane	12.8	-	-	-
i-pentane	13.8	-	-	-
toluene	18.2	-	-	-

6.4 Results and Discussion

6.4.1 Density Prediction

The flashed oil density was calculated using Eq. 6.1 with effective densities for the merged and lumped analysis of Table 6.3. For the merged analysis, the densities for C11, C13, and C15 were taken to be the average of the next lower and higher carbon number *n*-alkane. The predicted densities at the flash conditions of 21°C and atmospheric pressure are within ±2 kg/m³ of the measured density as shown below:

Measured density	847.7 kg/m³
Predicted from merged analysis	849.9 kg/m³
Predicted from lumped analysis	846.5 kg/m³

Figure 6.6 shows the measured and predicted density of the live oil at 80, 100, and 120°C and pressures from 10 to 100 MPa. The predicted densities of live oil match the measured data to within the experimental error of ±2 kg/m^3 (approximately ±0.25% of reported value). The average absolute deviation of the predicted densities against the measured densities for 80, 100, and 120°C are 1.8, 7.1, and 1.2 kg/m^3, respectively. The deviation at 100°C is likely due to a systematic error as the 100°C data is shifted (about +5 kg/m^3) noticeably towards the 80°C data. The source of the error is suspected to be from operator reading the liquid height volume in the PVT cell at each pressure steps and from the dead volume calculation. Note, tests at each temperature were performed by a separate operator using separate charges to the PVT cell.

The accuracy of the predicted densities from pure component effective densities is remarkable considering that no tuning of the data was performed. The results suggest that for a crude oil above its bubble point, there is no significant volume change upon mixing if subcooled liquid densities are accounted for. This approach provides a method to rapidly calculate crude oil densities without resorting to an equation of state and volume

translation. Note, however, that this case study was performed well above the bubble point. It is not clear how well the predictions will stand up as the bubble point is approached. Also, a number of assumptions were required to estimate the saturate and aromatic densities. Density measurements of these fractions over a range of temperatures and pressures would strengthen the basis of the density predictions.

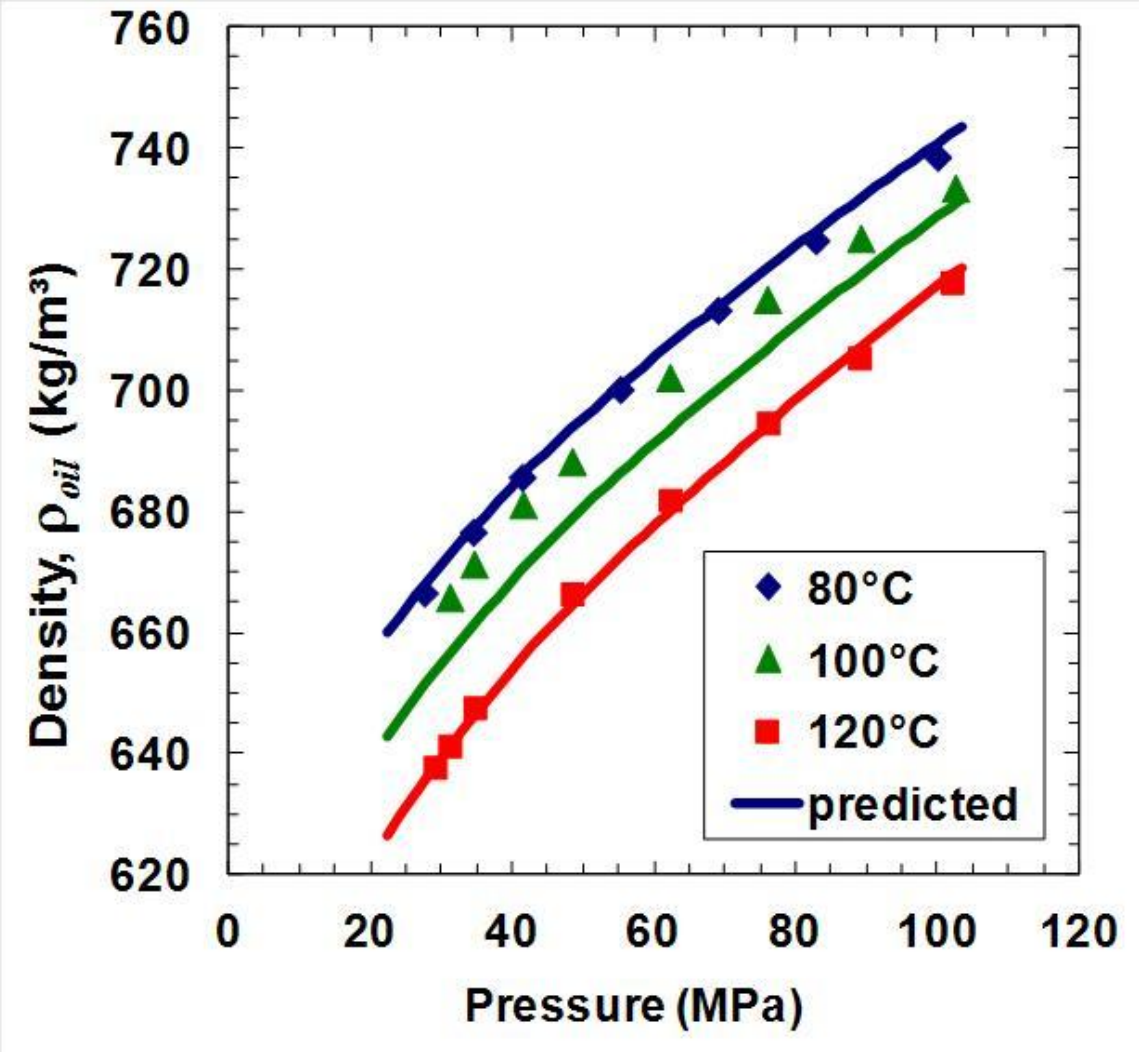

Figure 6.6: Comparison of predicted and actual density of live oil at 80, 100, and 120°C and pressures from 25 to 100 MPa.

6.4.2 Asphaltene Onset and Yield

6.4.2.1 Dead Oil

The asphaltene yields from the dead oil diluted with *n*-heptane are shown in Figure 6.7. As mentioned previously, there was a discrepancy in the asphaltene content of the dead oil (4.0 wt% asphaltene and 0.55 wt% solids) and the flashed oil (2.7 wt% asphaltenes and 0.14 wt% solids) which was attributed to the difference in washing temperature during the asphaltene content measurement procedures. The oil was characterized with the reported asphaltene content, as described previously, and the yield data was fitted to an AAD of 7.0% using an average nano-aggregate molar mass of 2930 g/mol, Figure 6.7. The average molar mass of nano-aggregate is consistent with the data found for Lloydminster heavy oil (3620 g/mol) presented in Section 4.3 of Chapter 4. Also, the nano-aggregate molar mass is consistent with reported average molar mass of nano-aggregates for many other crude oils from various geographical locations (Akbarzadeh et al., 2005).

6.4.2.2 Live Oil

The onset of precipitation was determined from high pressure microscope measurements. Figures 6.8, 6.9 and 6.10 show the still images of the live oil at selected pressures for test temperatures 80, 100 and 120°C, respectively. Even at the highest pressures, some water droplets and/or sand particles are observed. They are present at all pressures and temperatures and therefore the onset of asphaltene precipitation is the point where the particle concentration is observed to increase.

Since observations are only made at discrete pressure intervals, the exact pressure at the onset of precipitation may not be detected. Instead, the pressure at which the asphaltene particles first appear is defined as the minimum asphaltene precipitation onset pressure. The previous pressure step where no asphaltene precipitation was observed is defined as the maximum asphaltene onset pressure. The estimated onset pressure is the arithmetic average of the minimum onset pressure and the pressure of the previous observation,

Table 6.10 and Figure 6.11. Because the pressure increments were typically 3.4 MPa (500 psi), the onset pressure detected by HPM was only precise to ±1.7 MPa. Figure 6.11 shows that the bubble point ranges from 27 to 29 MPa from 80 to 120°C, respectively. Asphaltene yields were measured at pressures approximately 0.70 MPa above the bubble point at the given temperature. The yields are shown in Figure 6.12.

Table 6.10: Measured asphaltene onset pressures.

Temperature	Onset Pressure (MPa)		
(°C)	Minimum	Maximum	Estimated
80	72.4	75.9	74
100	67.2	69.0	68
120	62.1	65.5	64

The onset pressures were fitted by adjusting the average molar mass of the asphaltene nano-aggregates to 2900, 2720, and 2620 g/mol at 80, 100, and 120°C, respectively. The decreasing trend in molar mass with temperature is consistent with other data (Moschopedis et al., 1976; Yarranton et al., 2000).The nano-aggregate molar mass also compare reasonably well with the values determined for the dead oil, given the differences in the asphaltene content measurement for the samples. The model slightly over-predicted the yields near the bubble point. Note that the yield measurements were not repeated for the depressurization tests. Hence, the measurement error for the yield data was not reported.

The results indicate that a common characterization can be used to model both solvent- and pressure-induced precipitation. However, the modeling of the onset pressures was found to be very sensitive to the average molar mass of the nano-aggregates. A change of 100 g/mol in the molar mass causes a change in the onset pressure of approximately 5

MPa. This sensitivity to the nano-aggregate molar mass severely limits the predictive capability of the regular solution approach to pressure induced asphaltene precipitation. Also note that the modeling in this study only applies above the bubble point. Below the bubble point, the composition of the liquid phase changes with pressure and therefore vapour-liquid-liquid equilibrium model is required.

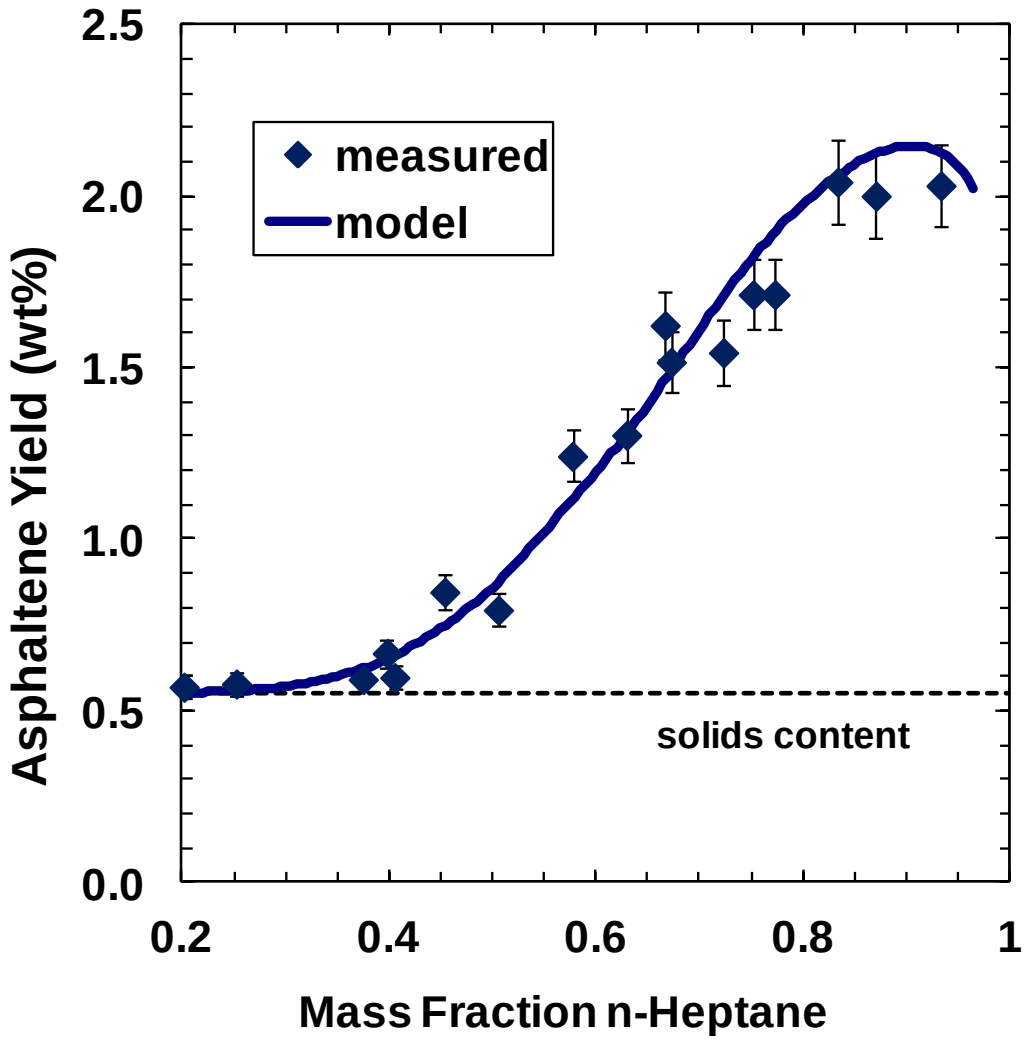

Figure 6.7: Asphaltene yields from dead Gulf of Mexico crude oil diluted with *n*-heptane at ambient conditions.

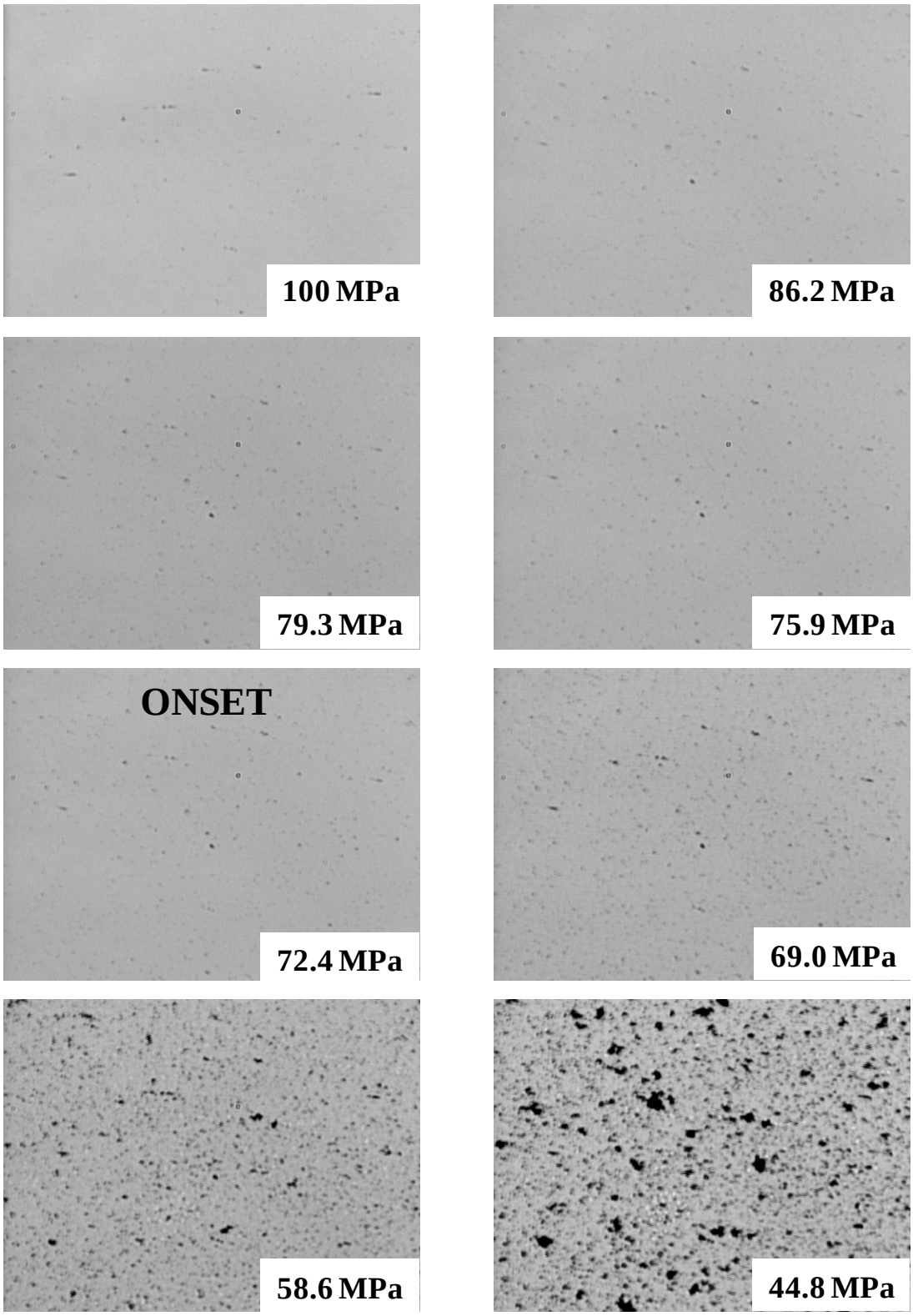

Figure 6.8: HPM still images of recombined live oil at 80°C.

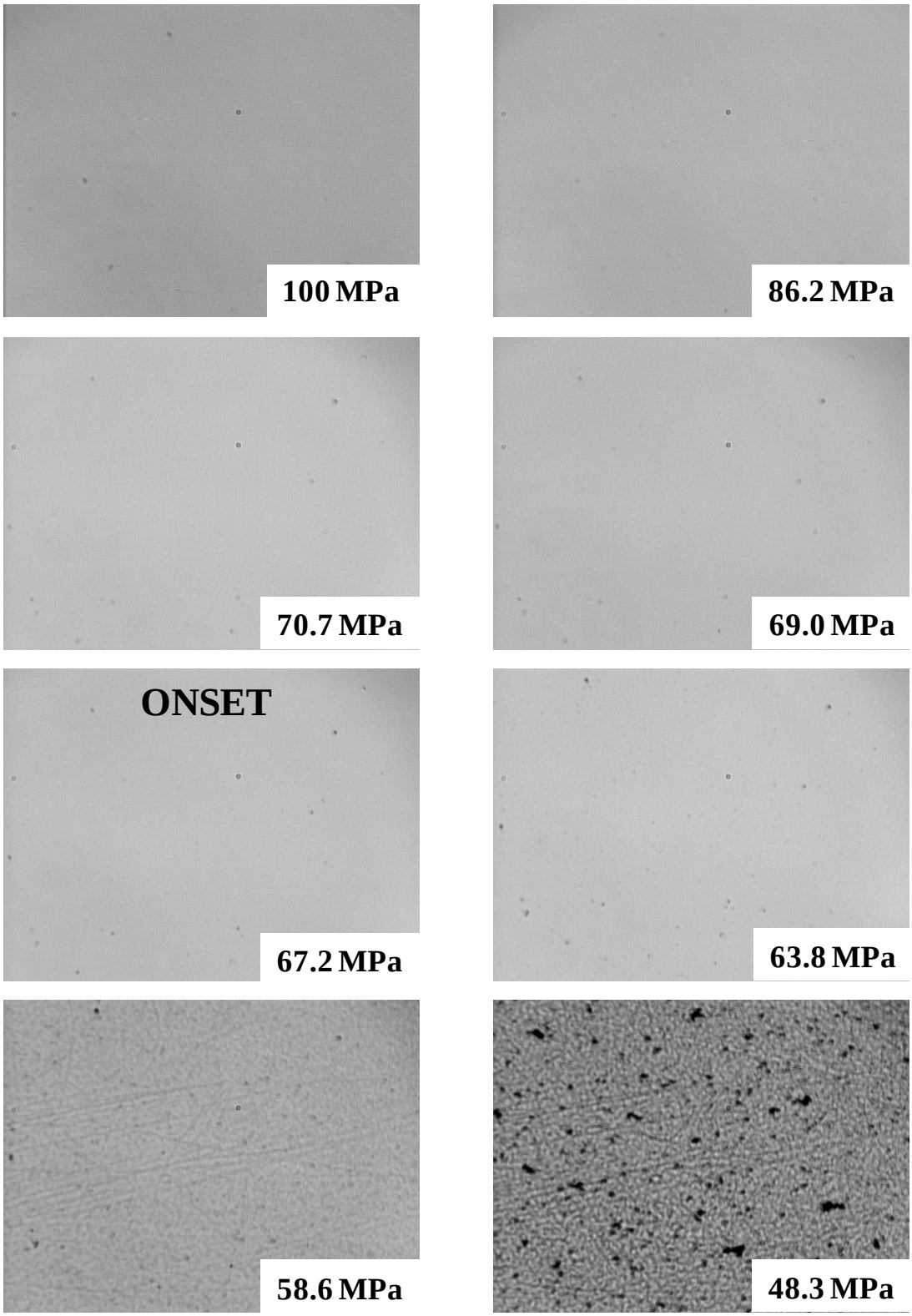

Figure 6.9: HPM still images of recombined live oil at 100°C.

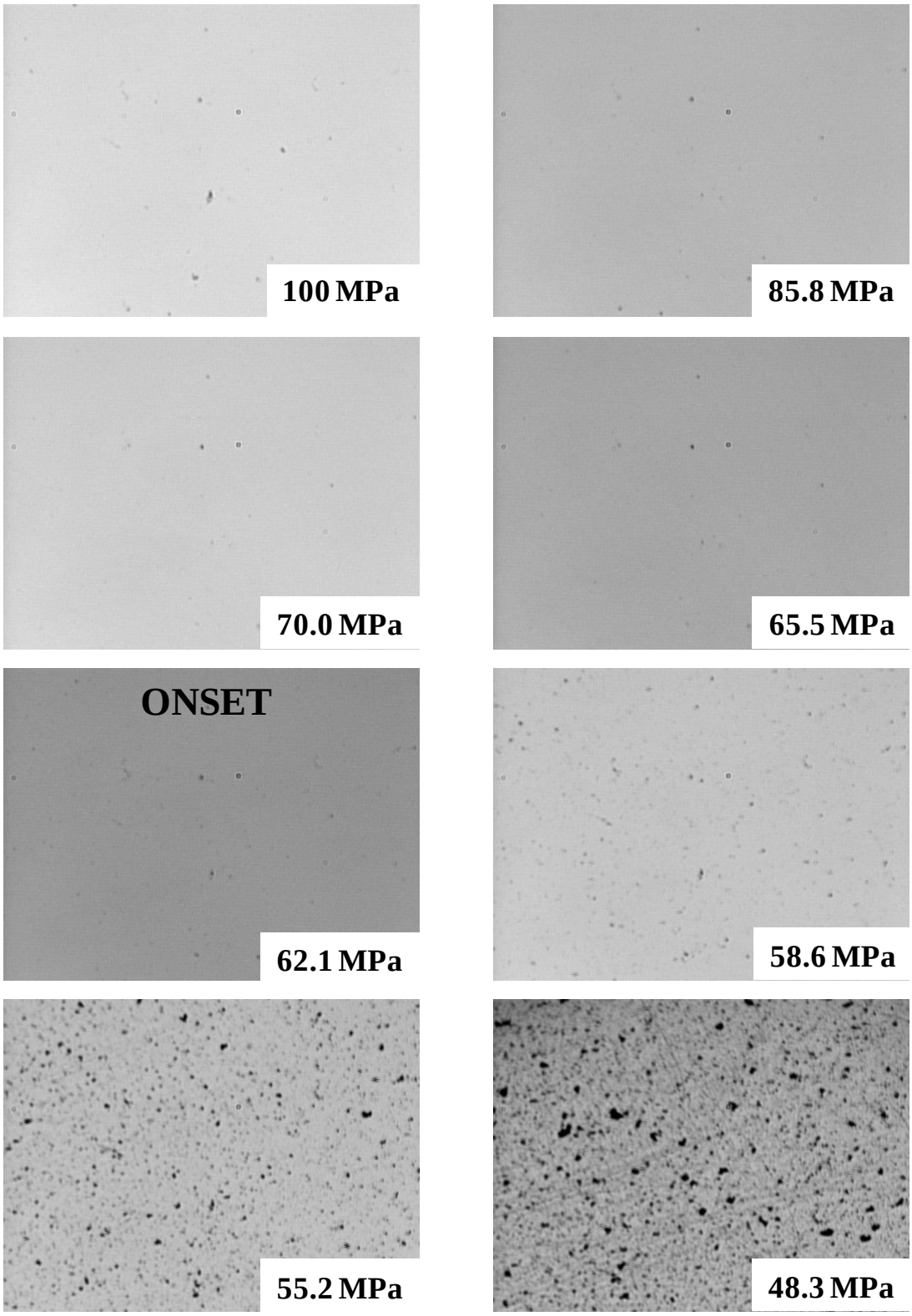

Figure 6.10: HPM still images of recombined live oil at 120°C.

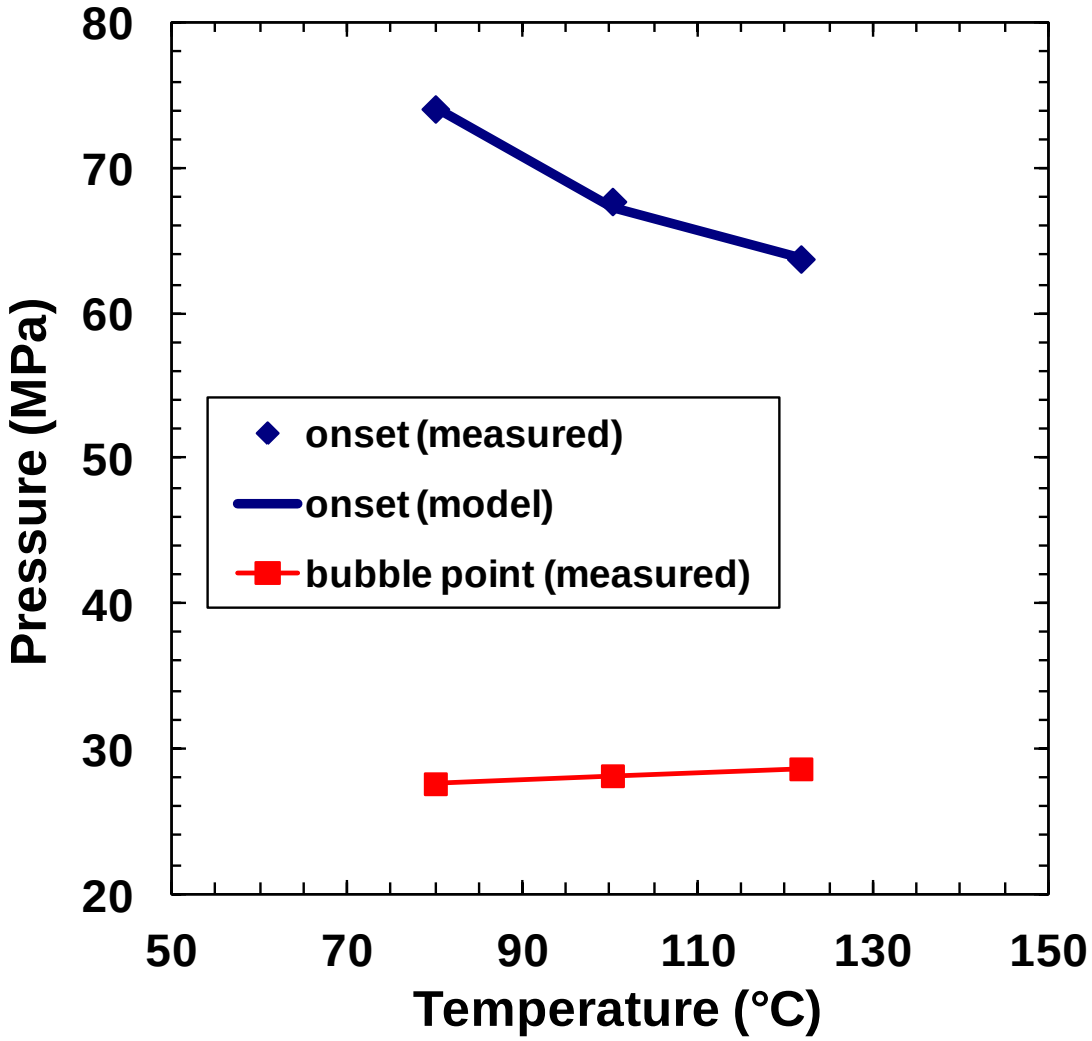

Figure 6.11: Bubble point and asphaltene precipitation onset pressures for live oil at 80, 100, and 120°C.

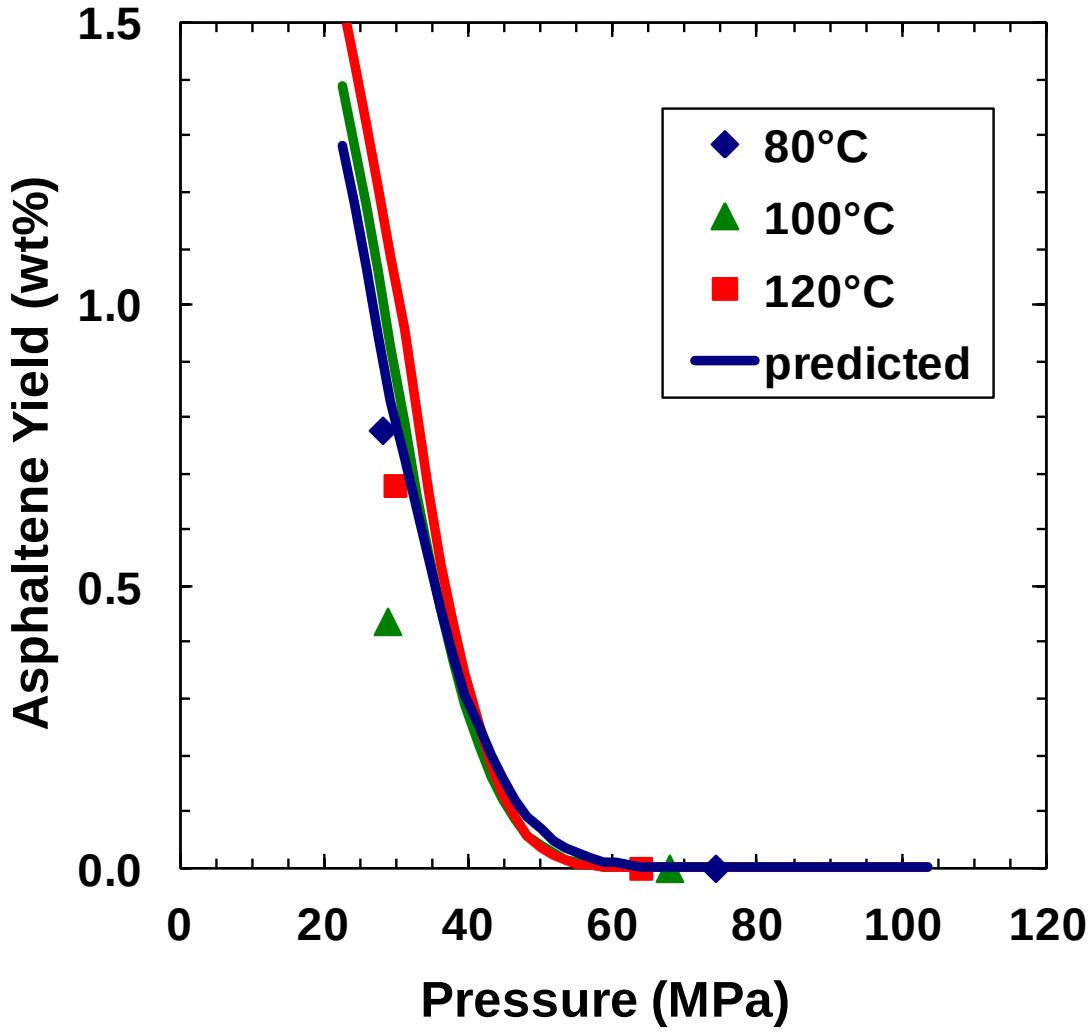

Figure 6.12: Asphaltene yield from live oil at 80, 100, and 120°C.

6.5 Summary

A regular solution approach developed to model asphaltene precipitation for heavy oils was successfully applied to asphaltene precipitation from a live oil undergoing depressurization. Inputs to the model are the mass fraction, density, molecular weight, and solubility parameter of each component. An oil characterization based on GC analysis up to C15 and SARA analysis for the C16+ fraction provided consistent results for asphaltene precipitation from both dead oil and live oil.

One challenge in adapting the model was to estimate the density of components which are gases in their native state but liquids in the oil. Effective liquid densities of light *n*-alkanes (<C5) were determined from extrapolations of higher carbon number *n*-alkane densities. For the C5+ components, liquid densities were obtained from the NIST Standard Reference Database. The density of the dead and live oil were predicted within the error of the measurement (±2 kg/m^3) for both dead and live oil using ideal mixing of the effective densities.

Solubility parameters were determined as a function of temperature and pressure. Pressure was assumed to have an effect on the molar volume contribution to the solubility parameter. Temperature was accounted for both through the molar volume and the enthalpy of vaporization. The only input parameter that was not fixed was the average molar mass of the asphaltene nano-aggregates which was used as a fitting parameter. The live oil onset conditions for asphaltene precipitation were very sensitive to this parameter limiting the predictive capability of the model. Nonetheless, once fitted to the onset condition, the model provided predictions of asphaltene yields. The model also has the advantage that it can easily be applied below the bubble point although the liquid phase composition would have to be determined from a separate flash; for example, using an equation of state.

CHAPTER 7

Asphaltene Precipitation from Crude Oils in the Presence of Emulsified Water

The primary objective of this chapter is to determine the effect of emulsified water on the onset and the amount of asphaltene precipitation from diluted crude oils. Asphaltene precipitation yields were measured from an Athabasca bitumen and a light Gulf of Mexico crude oil diluted with *n*-heptane. The experiments were performed with and without emulsified water added to the oils. Yields were compared to determine the effect of emulsified water.

The secondary objective of this chapter is to analyze the composition and structural differences between the asphaltenes precipitated at the onset condition, asphaltenes adsorbed onto the interface, and bulk asphaltenes. Elemental analysis was conducted to determine the compositional differences. Specifically, the analysis are used to determine if surface active asphaltenes are the type of asphaltene to aggregate most strongly, form the largest aggregates, and precipitate first.

7.1 Experimental

7.1.1 Oil Samples

Two different oil samples were used in this study. The first sample was Crude B (a coker-feed bitumen extracted from Athabasca oil sands). The bitumen was supplied to the University of Calgary after the treatment to remove water and sand. The second sample was topped Crude D (a light crude oil from Gulf of Mexico). Saturates, aromatics, resins and asphaltenes (SARA) content and non-asphaltenic solids content of

these oil samples can be found in Table 5.2 of Chapter 5. The water content of Crude B and topped Crude D before the analysis was found to be < 0.1 wt% and 0.4 wt%, respectively. These crude oils are denoted as water-free oil samples in this chapter.

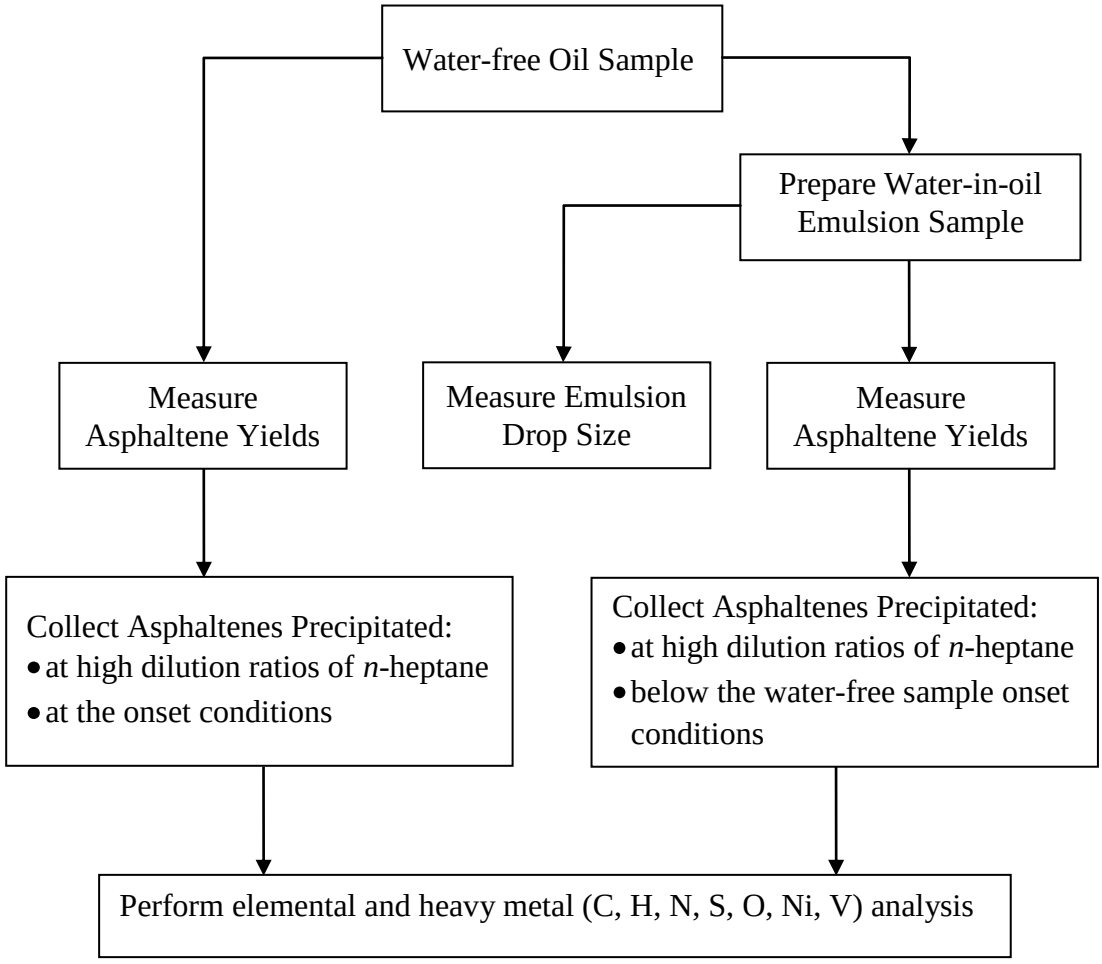

Figure 7.1: Workflow of the experiments to determine the effect of water on asphaltene precipitation.

7.1.2 Experimental Work Flow

A brief summary of experiments performed for this study is provided in Figure 7.1. For water-free samples, precipitation yields were measured, and elemental and heavy metal analysis were performed on precipitated asphaltenes. For water-in-oil emulsion samples, the experiments included emulsion preparation, emulsion drop size measurements, yield measurements, collection of precipitated asphaltenes, and elemental analysis on precipitated asphaltenes. The detailed experimental procedures are provided in Chapter 3 and the results are presented in the subsequent sections.

Specifically, asphaltene yields for water-free oil samples were determined by using the procedure described in Section 3.3.3. Water-in-oil emulsion samples were prepared and drop size measurements were conducted by following the procedure given in Section 3.3.4. A separate procedure was developed to determine the asphaltene yields for the water-in-oil emulsion samples, which is described in Section 3.3.5. The precipitated asphaltene samples were collected immediately after the yield experiments, stored in glass vials by purging with nitrogen gas and placed in a desiccator. The elemental analysis was then performed on selected asphaltene samples, Sections 3.2.5.

7.2 Results and Discussion

7.2.1 Solubility Effect

Asphaltene yields were measured for water-free samples of Crude B and topped Crude D at various dilution ratios of *n*-heptane. Yields were also measured for Crude B with 23 and 50 wt% water, and for topped Crude D with 25 wt% water. All the measured yield data were plotted against the mass fraction of *n*-heptane on a water-free basis for Crude B and topped Crude D in Figures 7.2 and 7.3, respectively. Note that, small amounts of water are solubilized in the bitumen in all of the experiments, as would exist in any naturally occurring sample. Hence, the experiments shown in Figures 7.2 and 7.3 only address the additional effect of emulsified water.

Figures 7.2 and 7.3 show that there is little to no difference in asphaltene yields for water-free oils and oils with emulsified water. Figure 7.2 also shows that varying the amount of emulsified water did not have any effect on asphaltene yields. Hence, the solubility of asphaltenes is not affected by the presence of emulsified water above the actual onset of precipitation, which implies that the presence of emulsified or free water is not a concern in asphaltene precipitation modeling.

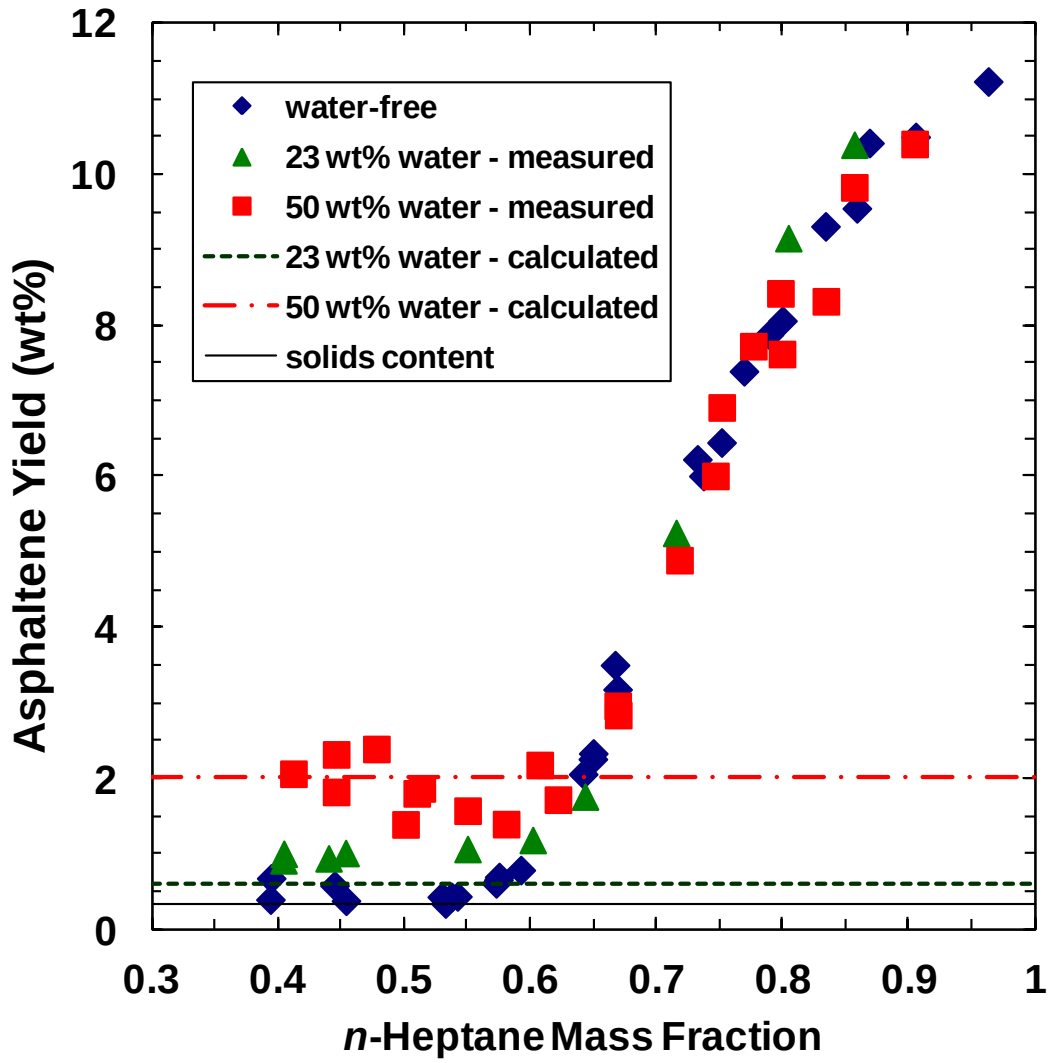

Figure 7.2: Asphaltene precipitation yields for Crude B diluted with *n*-heptane in the presence and absence of emulsified water at 23°C.

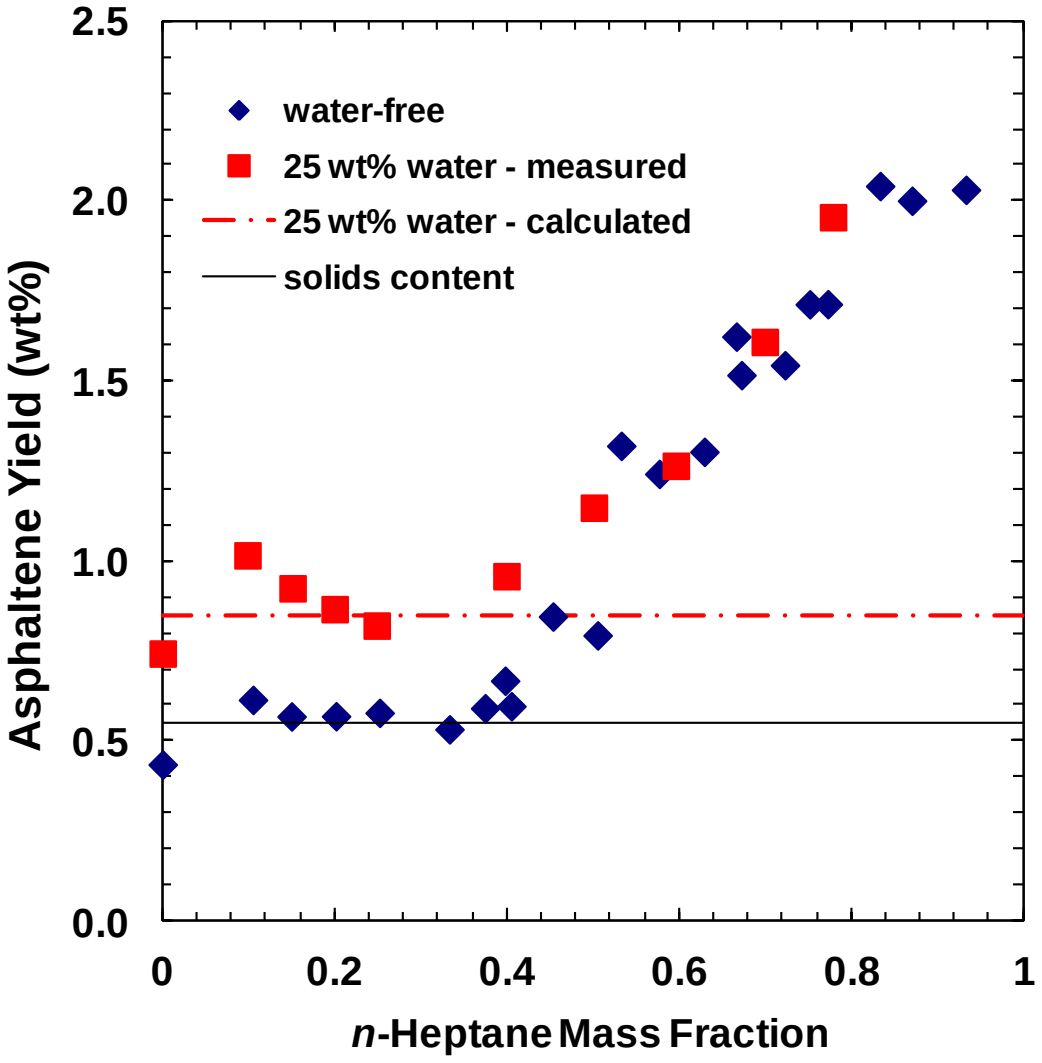

Figure 7.3: Asphaltene precipitation yields for topped Crude D diluted with *n*-heptane in the presence and absence of emulsified water at 23°C.

For dilution ratios below the onset of precipitation for water-free oils, apparent asphaltene yields for the samples with emulsified water were greater than the asphaltene yields for the water-free samples. Figure 7.2 also shows that, below the onset, the apparent yield increased as the water content increased from 23 wt% to 50 wt%. These

apparent yields are likely related to the asphaltenes adsorbed on to the surface of the water droplets. The water droplets are centrifuged out of the oil at any moderate dilution and the adsorbed asphaltenes are recovered and reported as a yield. For a water-in-oil emulsion, the amount of asphaltenes adsorbed on the water-oil (W/O) interface, $m_{A,I}$, is given by:

$$m_{A,I} = A\Gamma = \left(\frac{6V_w}{d_{32}}\right)\Gamma \tag{7.1}$$

where A is the surface area of emulsion; Γ is the asphaltene surface coverage; V_w is the volume of water; and d_{32} is the Sauter mean diameter of water drops. Γ was taken as 12 mg/m^2 (Gafonova and Yarranton, 2001). The measured Sauter mean diameters were 3.6 and 3.0 μm for water emulsified into the Crude B and topped Crude D oil samples, respectively.

The estimated masses of asphaltenes on the surface of the water droplets were compared with the apparent yields below the onset in Figures 7.2 and 7.3. The estimated interfacial asphaltene content matched the measured asphaltene yields to within the experimental error of ±10% for both oils. This good agreement strongly suggests that the apparent asphaltene yields below the onset were due to the adsorbed asphaltenes on to the water-oil interface. At higher dilution ratios, the recovered asphaltenes include both asphaltenes from the surface of the water droplets and asphaltenes precipitated from the bulk solution.

7.2.2 Asphaltene Characterization

The samples collected for the water effect experiments provided an opportunity to evaluate the relationship between surface active asphaltenes (those adsorbed on the water-oil interface), bulk asphaltenes, and the first asphaltenes to precipitate. A working

hypothesis is that the surface active asphaltenes have active functional groups that may also participate strongly in asphaltene association. If so, these species may aggregate more strongly than other asphaltene species and will be found in higher proportion in the largest aggregates. The largest aggregates are believed to be the first to precipitate and therefore a relatively high proportion of surface active asphaltenes is expected in the first asphaltenes to precipitate.

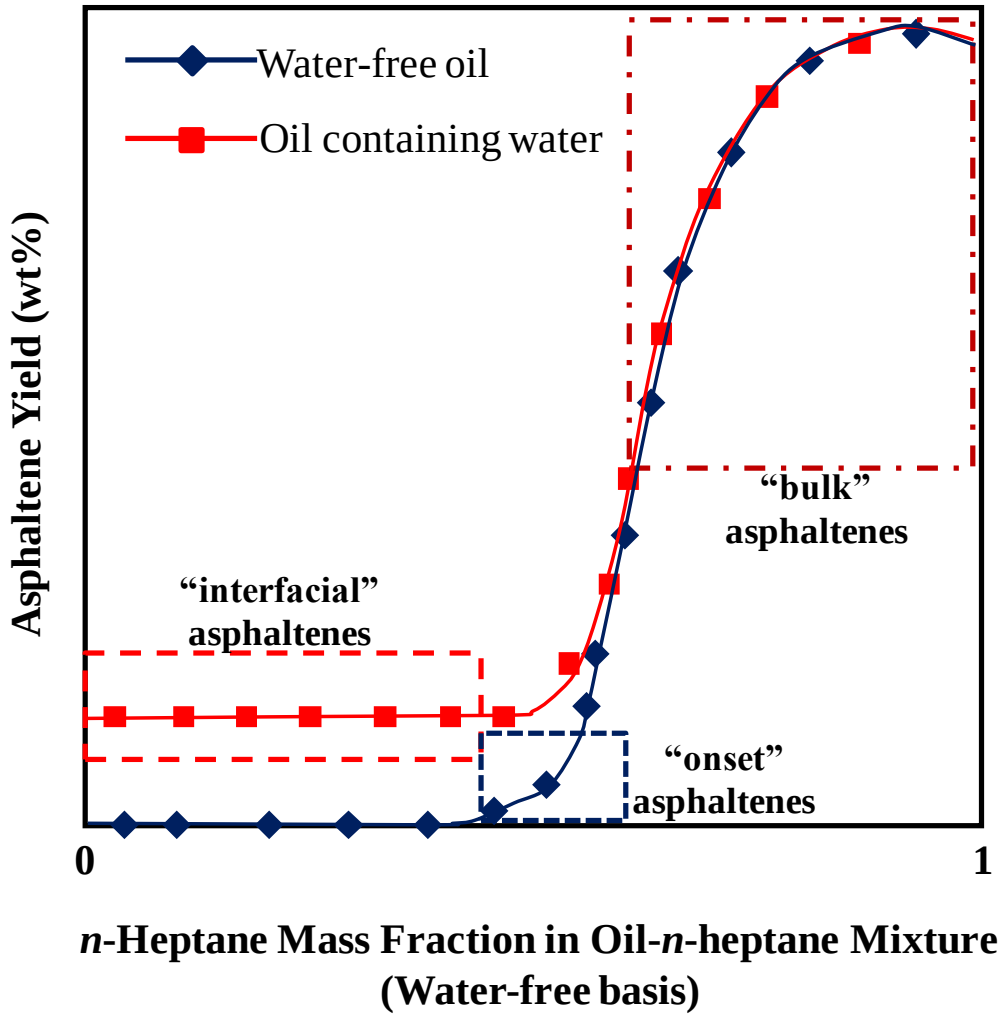

Figure 7.4: Schematic representation of yield curves and the sample collection location for asphaltene characterization.

In order to test this hypothesis, “bulk”, “interfacial”, and “onset” asphaltenes were isolated from both Crudes B and D and their compositional differences were assessed using elemental analysis. Figure 7.4 shows a schematic of the yield curves to indicate where on the yield curve the samples were collected. To confirm that the drying procedure removed all water from the asphaltenes, the “bulk” samples were collected from both water-free oils and oils containing emulsified water for comparison.

Table 7.1: Asphaltenes isolated from Crude B for composition analysis.

Asphaltene Type	***n*-Heptane Mass Fraction**	**Asphaltene Yield (wt%)**	**Amount of Water in Crude Oil (wt%)**
“bulk-dry”	> 0.7	> 6.5	~0.1
“bulk-wet”	>0.7	> 6.9	50
“onset”	0.65-0.67	2.3-3.2	~0.1
“interfacial”	0.51-0.55	1.6-1.9	50

Table 7.2: Asphaltenes isolated from topped Crude D for composition analysis.

Asphaltene Type	***n*-Heptane Mass Fraction**	**Asphaltene Yield (wt%)**	**Amount of Water in Crude Oil (wt%)**
“bulk-dry”	> 0.7	< 1.7	0.4
“bulk-wet”	> 0.7	< 1.6	25
“onset”	-	-	-
“interfacial”	< 0.4	< 1.0	25

The complete set of asphaltene samples collected in this study were: a) bulk asphaltenes precipitated from water-free oil samples at high dilution ratios of *n*-heptane (denoted as "bulk-dry"); b) bulk asphaltenes precipitated from oil samples with emulsified water at high dilution ratios of *n*-heptane (denoted as "bulk-wet"); c) asphaltenes precipitated from water-free oil samples diluted with *n*-heptane at the precipitation onset conditions, that is the asphaltenes that were first to precipitate (denoted as "onset"); and d) asphaltenes collected at the water-oil (W/O) interface or the asphaltenes precipitated from oil samples with emulsified water below the onset of precipitation (denoted as " interfacial"). Tables 7.1 and 7.2 show the mass fraction of *n*-heptane at which each asphaltene sample was precipitated from Crude B and topped Crude D, respectively. Note, the "onset" sample from topped Crude D was not considered in this work because the amount of precipitated material was too small. As well, the precipitated material from topped Crude D contained a relatively larger proportion of solids.

Elemental Analysis

Since the oil samples contain some amount of "solids" (see Table 5.2 in Chapter 5), precipitated asphaltenes at any dilution ratio of *n*-heptane always included these solids. The precipitated asphaltenes with "solids" were referred as "asphaltenes+solids". These solids were then removed by following the procedure described in Section 3.2.2 of Chapter 3 to obtain "solids-free asphaltenes". For Crude B, both elemental and heavy metal analysis was carried out for "asphaltenes+solids", while the elemental analysis alone was performed on "solids-free asphaltenes" precipitated from both oil samples.

Table 7.3 shows the elemental composition and atomic ratios of precipitated material ("asphaltenes+solids") isolated from Crude B at different dilution conditions. The analysis indicated the compositions of "bulk-dry" and "bulk-wet" asphaltenes are very similar, confirming that all of the water had been removed from the asphaltenes in the drying procedure.

The H/C ratio was approximately the same for the “bulk (-wet or -dry)” and “onset” asphaltenes. Based on the H/C ratio, the “interfacial” asphaltenes showed a lower degree of aromaticity when compared to the other asphaltene samples. There were no significant differences for nitrogen and sulphur contents in all the four asphaltene types. The amount of heavy metals in the asphaltene samples was similar. A notable variation was seen for oxygen content with the O/C ratios of “onset” and “interfacial” asphaltenes almost doubled the “bulk” asphaltenes. It is therefore tempting to conclude that the “onset” and the “interfacial” asphaltenes are very similar in composition when compared to the “bulk (-wet or –dry)” asphaltenes. However, one must consider how the solids contribute to this analysis.

Table 7.4 presents the elemental composition data for “solids-free asphaltenes” from Crude B. Although, Kotlyar et al. (1999) emphasized the importance of analyzing metal content of asphaltenes on a solids-free basis, no significant differences in the amount of both nickel and vanadium were observed in their work. Hence, the metal content analysis on the “solids-free asphaltene” samples was not performed.

The elemental compositions presented in Table 7.4 are similar to those of the “asphaltene+solids” in Table 7.3 except for the oxygen content. Hence, removing the solids significantly reduced the reported oxygen content of all the asphaltene types. This observation indicates that the solids associated materials are oxygen rich and can skew the asphaltene analysis.

Table 7.4 also shows that the oxygen content of interfacial asphaltenes is approximately twice the content in the “bulk” asphaltenes, while the oxygen content of first to precipitate or “onset” asphaltenes is just slightly higher than the “bulk” asphaltenes. Hence, for Crude B, the “onset” asphaltenes are more similar in composition to “bulk-dry” or “bulk-wet” asphaltenes than the “interfacial” asphaltenes.

Table 7.3: Composition analysis of precipitate ("asphaltenes+solids") from Crude B.

Asphaltene Type	Composition (wt%)					Atomic Ratios				Heavy Metals (μg/g)	
	C	H	N	S	O	H/C	N/C	S/C	O/C	Ni	V
"bulk-dry"	79.8	7.8	1.3	8.7	2.4	1.180	0.014	0.041	0.022	332	883
"bulk-wet"	79.5	7.8	1.3	8.6	2.8	1.172	0.015	0.041	0.026	338	878
"onset"	77.4	7.6	1.4	8.7	5.0	1.177	0.015	0.042	0.049	297	634
"interfacial"	76.5	7.7	1.5	9.1	5.3	1.209	0.016	0.044	0.051	299	744

Table 7.4: Elemental analysis of "solids-free asphaltenes" precipitated from Crude B.

Asphaltene Type	Composition (wt%)					Atomic Ratios			
	C	H	N	S	O	H/C	N/C	S/C	O/C
"bulk-dry"	80.5	7.9	1.4	8.4	1.7	1.182	0.015	0.039	0.016
"bulk-wet"	80.5	8.0	1.4	8.2	1.9	1.188	0.015	0.038	0.018
"onset"	80.1	8.0	1.4	8.4	2.2	1.192	0.015	0.039	0.020
"interfacial"	79.0	8.0	1.4	8.2	3.5	1.210	0.015	0.039	0.033

Table 7.5 shows the elemental analysis data for “solids-free asphaltenes” obtained from topped Crude D. Significant differences are noticed in carbon and sulphur content for “bulk-dry” asphaltenes from both crude oil samples. This is expected since light Gulf of Mexico oil (Crude D) should contain more carbon and less sulphur than the Canadian bitumen (Crude B). Both “bulk-dry” and “bulk-wet” asphaltenes exhibit similar composition except the oxygen content. This may be due to the presence of some solids because the solids removal methodology adapted in this study may not be able to remove all the fine solids from the small amount of precipitated material.

As observed with Crude B, the “interfacial” asphaltenes from topped Crude D contains less carbon and significantly more oxygen than the “bulk” asphaltenes. Based on the H/C ratio, the “interfacial” asphaltenes are less aromatic than the bulk asphaltenes. The elevated oxygen content of interfacial asphaltenes was observed in the literature as well (Stanford et al., 2007a, 2007b). Thus, the “interfacial” asphaltenes may be chemically distinct from the “bulk” asphaltenes. Based on the Crude B data, “onset” asphaltenes are not enriched with “interfacial” asphaltenes. In other words, the “interfacial” asphaltenes may be a part of “onset” asphaltenes, but no more so than in “bulk” asphaltenes.

Table 7.5: Elemental analysis of “solids-free asphaltenes” precipitated from topped Crude D.

Asphaltene Type	Composition (wt%)					Atomic ratios			
	C	H	N	S	O	H/C	N/C	S/C	O/C
“bulk-dry”	85.7	8.5	1.1	2.2	2.5	1.186	0.011	0.010	0.022
“bulk-wet”	84.2	8.7	0.9	2.0	4.2	1.239	0.010	0.009	0.037
“onset”	-	-	-	-	-	-	-	-	-
“interfacial”	81.3	9.2	1.0	1.9	6.8	1.351	0.010	0.009	0.062

7.3 Summary

Based on the light oil and bitumen tested, it appears that the presence of emulsified water has little to no effect on the solubility of asphaltenes in solvents or in a crude oil above the onset of precipitation. However, asphaltenes adsorbed on the surface of emulsified water droplets are removed with the water droplets and reported as yield below the precipitation onset.

Solids and associated materials are oxygen rich and can skew the analysis of the asphaltene composition, particularly at low asphaltene concentrations. Based on elemental analysis, there is no significant difference between first-to-precipitate, interfacial, and bulk asphaltenes except for elevated oxygen content in the interfacial asphaltenes. This result indicates that surface active asphaltenes are not concentrated in the largest asphaltene aggregates. Therefore, surface active asphaltenes do not appear to be involved in self-association any more than non-surface active asphaltenes.

CHAPTER 8

Conclusions, Recommendations, and Contributions

The primary objective of this thesis was to develop a generalized modeling approach to predict the onsets and amount of asphaltene precipitation from crude oil blends and depressurized live oils. The secondary objective was to investigate the effect of emulsified water on asphaltenes precipitation from crude oils. The major conclusions from this study, recommendations for future research and significant contributions from this thesis work are provided in this chapter.

8.1 Conclusions and Recommendations

Blend Study

1. Asphaltene precipitation onset and yield data were measured and successfully modeled for oil blends prepared from nine different crude oils from various geographical locations and a refinery gas oil. Overall, the mass fraction of *n*-alkane required to initiate precipitation was predicted with an average absolute deviation of 0.53% or less for a range of blends.
2. Oils and blends were characterized in terms of saturates, aromatics, resins and asphaltenes (SARA) fractions. The mass fraction of each SARA fraction in the blends was experimentally confirmed as the weight average of the respective fraction in the constituent oils.
3. The model was able to predict when blends are less stable than the constituent crude oils. The model was less successful at very high dilutions, for example, when toluene had been added to the crude oils prior to *n*-heptane addition. At these high

dilutions, asphaltenes tend to dissociate, and the assumption that the average asphaltenes aggregation number is constant breaks down.

4. The best regular solution model predictions for asphaltene precipitation were obtained when it was assumed that there was no interaction between the asphaltenes from each oil. The blended molar mass distribution of the asphaltenes was calculated as a mole based sum of the individual distributions. This result indicates that, over the time frame of the experiments, the asphaltenes from different crude oils did not interact with each other. Data should be collected for a longer time period to validate this assumption or to include kinetic effects in the model.
5. The proposed methodology has only been tested when the crude oil or blends are diluted with pure *n*-alkanes or a mixture of toluene and *n*-alkanes. In practice, the heavy oil or bitumen is usually diluted with multicomponent diluents such as condensates and naphtha which contain light components. It is recommended to test the live oil methodology on blends of diluents and heavy oils.

Live Oils

1. A methodology was developed to characterize live crude oils for the regular solution model. The dead oil fraction was characterized into pseudo-components corresponding to SARA fractions. The mass fractions of the lighter components were assigned on the basis of a gas chromatographic analysis. The only unknown in the model was the average molar mass of the asphaltene aggregates in the live oil which was determined by fitting the measured precipitation onset pressure data. The model successfully predicted asphaltenes yield data below the onset pressure for the live oil as well as yields for the dead oil diluted with *n*-heptane. Hence, a common oil characterization methodology can be used to model both solvent- and pressure-induced asphaltenes precipitation.

2. In developing the proposed characterization methodology, new correlations were created for the density and solubility parameters of the live oil components. For the C5+ components, liquid densities were obtained from the NIST standard reference database and correlations were developed for the pressure and temperature range tested in this work. For the *n*-alkane components that are gases in their native state but liquids in the oil (<C5), effective liquid density correlations were determined based on extrapolations of higher carbon number *n*-alkane densities. Assuming zero excess volumes, the correlations predicted the densities of the dead and live oil within the error of the measurement. Note, this approach is only valid in the liquid region and not near the critical point.
3. New correlations of the solubility parameter of each pure component were determined as a function of the pressure and temperature. The effect of pressure was introduced via the molar volume contribution to the solubility parameter. The temperature was accounted for through both the molar volume and enthalpy of vaporization.
4. The predictions of the live oil precipitation onset pressures were very sensitive to the fitted average molar mass of asphaltenes. A change of 100 g/mol in the molar mass caused a change in the onset pressure of approximately 5 MPa. This limits the predictive capability of the model.
5. The proposed model is limited to predict the precipitation onsets and yield above the bubble point or saturation pressure. The model should be extended below the bubble point or the two-phase region as well. One approach to applying the model below the bubble point is to determine the liquid-phase composition from a separate flash, for example, using an EoS. The major limitation would be collecting onset/precipitation data to validate the model. There is no published work on asphaltene resolubilization kinetics.
6. The model was tested only on a single light oil. Similar data should be collected from wide variety of oils with different compositions and properties to validate the predictive capability of the model.

Water Effect

1. The presence of emulsified water had no discernible effect on the solubility of asphaltenes in solvents or in a crude oil above the onset of precipitation. Asphaltenes adsorbed on water-oil interface appear as yield when the emulsion is separated from the oil below the precipitation onset.
2. Solids and associated materials in the crude oil are oxygen rich and can skew the analysis of asphaltene composition. Therefore, the non-asphaltenic materials should be removed prior to analyzing asphaltenes.
3. Based on the elemental analysis, there is no significant difference between first-to-precipitate, interfacial, and bulk asphaltenes except for elevated oxygen content in the interfacial asphaltenes. This result indicates that surface active asphaltenes are not concentrated in the largest asphaltene aggregates. Hence, the surface active asphaltenes are not involved in self-association any more than the non-surface active asphaltenes.
4. In the experiments, demineralised water was used for preparing the water-in-oil emulsion. Such an emulsion was tested to determine if there is any effect on asphaltene precipitation. However, the oilfield water (or brine) is always associated with ions and the presence of these ions may possibly interact with asphaltene molecules to alter the precipitation behavior. Therefore, the tests should be carried out by preparing the emulsion with an oilfield or a model brine solution.
5. Although this study suggests that emulsified water has no effect on asphaltene precipitation, tests should be conducted at high pressure and temperature to confirm the conclusion for live oil systems. For example, at high temperatures, an increase in water solubility in the oil may have an effect on asphaltene precipitation. If there is any effect, the precipitation models should be modified accordingly.
6. Based on the literature, water has been shown to have an effect on asphaltene aggregation. Hence, it is worthwhile to further investigate the effect of water on the kinetics of asphaltene precipitation and aggregation.

8.2 Significant Contributions

1. When two different crude oils are mixed, the composition of the blend is usually measured as a part of characterization. Through this study, it has been confirmed that the mass fraction of each SARA fraction in an oil blend can be calculated by weight averaging the respective fraction in constituent oils. In addition, it was proved that the molar mass distribution of asphaltenes in the blend can be calculated by summing up the distribution in the individual oils. Therefore, the regular solution approach was successfully applied to model crude oil blends diluted with *n*-alkanes or a mixture of toluene and *n*-alkanes.
2. A methodology was proposed by extrapolating the higher carbon number *n*-alkane densities to estimate the density of pure components that are gases in their native state but exist as liquid in the oil. As a result, correlations were developed for calculating densities of pure components (< C16) over a range of pressure and temperature. These correlations have been made available and can be used directly in any fluid phase behavior simulators.
3. Usually, the solubility parameters of pure components are available only at 25°C and 1 atm. The data at higher pressures or temperature are scarce and this limits the applicability of regular solution approach for modeling asphaltene precipitation in depressurized live oils. In this study, appropriate correlations were developed to calculate the solubility parameters of pure components (< C16) as a function of pressure and temperature.
4. Prior to this study, the regular solution approach was not completely applied to model asphaltene precipitation from live oils. One of the issues was the characterization of oils. In this study, a common characterization methodology was developed by combining both GC and SARA analysis. Specifically, GC analysis is used for components with carbon number less than C16 and SARA analysis is used for components with carbon number greater than C15. As a result, a fully compositional regular solution model has been developed for solvent- and pressure-induced asphaltene precipitation. The developed characterization

methodology can be readily used for all practical applications by implementing in phase behavior software.

5. Most of the published measurements for asphaltene precipitation were performed without or with very little water in the oil samples. Hence, the associated precipitation models do not account for any interactions between water and oil. In field operations, water is usually associated with oil. This study suggests that the presence of emulsified water has no effect on asphaltene precipitation. Below the onset of precipitation for water-free oils, however, asphaltenes adsorbed on to the water-oil interface and appear as a precipitation yield when the emulsion is separated.
6. While a negative result, the observation that interfacial asphaltenes do not contribute to self-association any more than other asphaltenes eliminates one of the interpretations for asphaltene self-association. The possibility of removing the least soluble asphaltenes from the oil by capturing them on water-oil interfaces is also eliminated.

References

Acevedo, S., Escobar, G., Gutierrez, L. B., Rivas, H., "Isolation and characterization of natural surfactants from extra heavy crude oils, asphaltenes, and maltenes. Interpretation of their interfacial tension-pH behavior in terms of ion pair formation", *Fuel*, **71**, 619-623, 1992.

Afghoul, A. C., Amaravadi, S., Boumali, A., Calmeto, J. C. N., Lima, J., Lovell, J., Tinkham, S., Zemlak, K. and Stall, T., "Coil tubing: the next generation", *Schlumberger Oilfield Review*, 38-57, Spring 2004.

Akbarzadeh, K., Alboudwarej, H., Svrcek, W. Y., Yarranton, H. W., "A generalized regular solution model for asphaltene precipitation from *n*-alkane diluted heavy oils and bitumens", *Fluid Phase Equilibria*, **232** (1-2), 159-170, 2005.

Akbarzadeh, K., Moshfeghian, M., Ayatollahi, S., Alboudwarej, H., Yarranton, H. W., "Estimation of SARA fraction properties with the SRK EOS", *J. Can. Pet. Tech.*, **43** (9), 31-39, 2004.

Alboudwarej, H., Beck, J., Svrcek, W. Y., Yarranton, H. W., "Sensitivity of asphaltene properties to separation techniques", *Energy* & *Fuels*, **16** (2), 462-469, 2002.

Alboudwarej, H., Akbarzadeh, K., Beck, J., Svrcek, W. Y., Yarranton, H. W., "Regular solution model for asphaltene precipitation from bitumens and solvents", *AIChE J.*, **49** (11), 2948-2956, 2003.

Alkafeef, S. F., "An investigation of the stability of colloidal asphaltene in petroleum reservoirs", Paper SPE 65018, SPE International Symposium on Oilfield Chemistry, Houston, TX, Feb 13-16, 2001.

Alkafeef, S. F., Al-Medhadi, F., Al-Shammari, A. D., "A simplified method to predict and prevent asphaltene deposition in oilwell tubings: field case", *SPE Production* & *Facilities*, 126-132, May 2005.

Al-Sahhaf, T. A., Fahim, M. A., Elkilani, A. S., "Retardation of asphaltene precipitation by addition of toluene, resins, deasphalted oil and surfactants", *Fluid Phase Equilibria*, **194-197**, 1047-1057, 2002.

Altgelt, K. H., Boduszynski, M. M., *Composition and Analysis of Heavy Petroleum Fractions*, Marcel Dekker, Inc. New York, 1994.

Ancheyta, J., Centeno, G., Trejo, F., Marroqun, G., Garca, J. A., Tenorio, E., Torres, A., "Extraction and characterization of asphaltenes from different crude oils and solvents", *Energy Fuels*, **16** (5), 1121-1127, 2002.

Andersen, S. I., Birdi, K. S., "Aggregation of asphaltenes as determined by calorimetry", *J. Coll. Int. Sci.*, **142** (2), 497-502, 1991.

Andersen, S. I., del Rio, J. M., Khvostitchenko, D., Shakir, S., Lira-Galeana, C., "Interaction and solubilization of water by petroleum asphaltenes in organic solution", *Langmuir*, **1** (2), 307-313, 2001.

Andersen, S. I., Speight, J. G., "Thermodynamic models for asphaltene solubility and precipitation", *J. Pet. Sci. & Eng.*, **22** (1-3), 53-66, 1999.

Andersen, S. I., "Flocculation onset titration of petroleum asphaltenes", *Energy Fuels*, **13** (2), 315-322, 1999.

Andersen, S. I., Keul, A., Stenby, E., "Variation in composition of subfractions of petroleum asphaltenes", *Pet. Sci. Technol.*, **15** (7&8), 611-645, 1997.

Anisimov, M. A., Yudin, I. K., Nikitin, V., Nikolaenko, G. L., Chernoutsan, A., Toulhoat, H., Frot, D., Briolant, Y., "Asphaltene aggregation in hydrocarbon solutions studied by photon correlation spectroscopy", *J. Phys. Chem.*, **99** (23), 9576-9580, 1995.

ASTM D2007, Standard Test Method for Characteristic Groups in Rubber Extender and Processing Oils and Other Petroleum-Derived Oils by the Clay-Gel Absorption Chromatographic Method, *Annual Book of ASTM Standards*, November 2002.

ASTM D2887, Standard test method for boiling range distribution of petroleum fractions by gas chromatography, *Annual Book of ASTM Standards*, January 2002.

ASTM D2892, Standard test method for distillation of crude petroleum, *Annual Book of ASTM Standards*, 2001.

ASTM D3279, Standard test method for *n*-heptane insolubles, *Annual Book of ASTM Standards*, August 1997.

ASTM D4006, Standard test method for water in crude oil by distillation, *Annual Book of ASTM Standards*, May 2005.

ASTM D4124, Standard test methods for separation of asphalt into four fractions, *Annual Book of ASTM Standards*, August 2001.

ASTM D6560 (IP 143/01), Standard test method for determination of asphaltenes (heptane insolubles) in crude petroleum and petroleum products, July 2000.

Badamchi-Zadeh, A., Yarranton, H. W., Maini, B. B., Satyro, M. A., "Phase behaviour and physical property measurements for VAPEX solvents: Part II. Propane, carbon dioxide and Athabasca bitumen", *J. Can. Pet. Technol*., 48 (3), 57-65, 2009.

Barton, A. F. M, *CRC Handbook of Solubility Parameters and Other Cohesion Parameters*, Second Edition, ISBN: 0849301769, CRC Press, Boca Raton, FL, 1991. Pages 84 and 303.

Beck, J., Svrcek, W. Y., Yarranton, H. W., "Hysteresis in asphaltene precipitation and re-dissolution", *Energy Fuels*, **19** (3), 944-947, 2005.

Betancourt, S. S., Todd Ventura, G., Pomerantz, A. E., Viloria, O., Dubost, F. X., Zuo, J., Monson, G., Bustamante, D., Purcell, J. M., Nelson, R. K., Rodgers, R. P., Reddy, C. M., Marshall, A. G., Mullins, O. C., " Nanoaggregates of asphaltenes in a reservoir crude oil and reservoir connectivity", *Energy Fuels*, **23**, 1178-1188, 2009.

Bouts, M. N., Wiersma, R. J., Muijs, H. M., Samuel, A. J., An evaluation of new asphaltene inhibitors. Laboratory and field testing, *SPE International Symposium on Oilfield Chemistry*, Paper SPE 28991, San Antonio, TX, Feb 14-17, 1995.

Buckley, J. S., Wang, J. X., "Crude oil and asphaltene characterization for prediction of wetting alteration", *J. Pet. Sci. Eng*., **33** (1-3), 195-202, 2002.

Buckley, J. S., "Microscopic investigation of the onset of asphaltene precipitation", *Fuel Sci. Technol*., **14** (1&2), 55-74, 1996.

Buckley, J. S., Wang, J., Creek, J. L., "Solubility of the Least-Soluble Asphaltenes", Chapter 16, *Asphaltenes, Heavy Oils*, and *Petroleomics*, Editors: Mullins, O. C., Sheu, E. Y., Hammami, A., Marshall, A. G., Springer Science + Business Media, LLC, New York, 2007.

Buckley, J. S., Hirasaki, G. J., Liu, Y., von Drasek, S., Wang, J-X., Gill, B. S., "Asphaltene precipitation and solvent properties of crude oils", *Pet. Sci. Technol.*, **16** (3&4), 251-285, 1998.

Buckley, J. S., "Predicting the onset of asphaltene precipitation from refractive index measurements", *Energy Fuels*, **13** (2), 328-332, 1999.

Buenrostro-Gonzalez, E., Lira-Galeana, C., Gil-Villegas, A., Wu, J., "Asphaltene precipitation in crude oils: theory and experiments", *AIChE J.*, **50** (10), 2552-2570, 2004.

Burya, Y. G., Yudin, I. K., Dechabo, V. A., Kosov, V. I., Anisimov, M. A., "Light-scattering study of petroleum asphaltene aggregation", *Applied Optics*, 40 (24), 4028-4035, 2001.

Cassani, F., Ortega, P., Davila, A., Rodriguez, W., Lagoven, S.A., Seranno, J., Evaluation of foam inhibitors a the Jusepin oil/gas separation plant, El Furrial Field, Eastern Venezuela, Paper SPE 23681, Second Latin American Petroleum Engineering Conference, II LAPEC, Caracus, Venezuela, March 8-11, 1992.

Castellanos Díaz, O., Modaresghazani, J., Satyro, M. A., Yarranton, H. W., "Modeling the phase behavior of heavy oil and solvent mixtures", *Fluid Phase Equilibria*, **304** (1-2), 74-85, 2011.

Chang, C. L., Fogler, H. S., "Peptization and coagulation of asphaltenes in apolar media using oil-soluble polymers", *Fuel Sci. Technol. Intl.*, **14** (1&2), 75-100, 1996.

Chapman, W. G., Gubbins, K. E., Jackson, G., Radosz, M., "New reference equation of state for associating liquids", *Ind. Eng. Chem. Res.*, **29** (8), 1709-1721, 1990.

Chung, T-H., "Thermodynamic modeling for organic solid precipitation", Paper SPE 24851, SPE Annual Technical conference and Exhibition, Washington DC, October 4-7, 1992.

Cimino, R., Correra, S., del Bianco, A., Lockhart, T. P., Solubility and phase behavior of asphaltenes in hydrocarbon media. In *Asphaltenes*: *Fundamentals and Applications*; Editors: Sheu, E. Y., Mullins, O. C.; Plenum Press, New York, Pages 97-130, 1995.

Correra, S., Merino-Garcia, D., "Simplifying the Thermodynamic Modeling of Asphaltenes in Upstream Operations", *Energy Fuels*, **21** (3), 1243-1247, 2007.

Creek, J. L., Buckley, J. S., Wang, J. X., "Asphaltene instability induced by light hydrocarbons", Paper OTC 19690, Offshore Technology Conference, Houston, TX, May 2008.

Creek, J. L., Wang, J. X., Buckley, J. S., "Verification of asphaltene-instability-trend (ASIST) predictions for low-molecular-weight alkanes", *SPE Production & Operations*, **24** (2), 360-367, 2009.

Dettman, H., Inman, A., Salmon, S., "Chemical characterization of GPC fractions of Athabasca bitumen asphaltenes isolated before and after thermal treatment", *Energy Fuels*, **19** (4), 1399-1404, 2005.

Dickie, J. P., Yen, T. F., "Macrostructures of the asphaltic fractions by various instrumental methods", *Analytical Chemistry*, **39** (14), 1847-1852, 1967.

Du, J. L., Zhang, D., "A Thermodynamic model for the prediction of asphaltene precipitation", *Pet. Sci. Technol.*, **22** (7 & 8), 1023-1033, 2004.

Edmonds, B., Moorwood, R. A. S., Szczepanski, R., Zhang, X., Heyward, M., Hurle, R., "Measurement and prediction of asphaltene precipitation from live oils", Proceedings of the Third International Symposium on Colloid Chemistry in Oil Production, Asphaltene and Wax Deposition Session, Huatulco, Mexico, 14-17 November 1999.

Eskin, D., Ratulowski, J., Akbarzadeh, K., Pan, S., "Modelling asphaltene deposition in turbulent pipeline flows", *Can. J. Chem. Eng.*, **89** (3), 421-441, 2011.

Fahim, M. A., Dang, T., Verdier, S., Andersen, S. I., "Measurements of precipitation of asphaltenes from live oil systems using a filtration technique", Presented at the 5th International Conference on Petroleum Phase Behaviour and Fouling, Banff, June 14-17, 2004.

Ferworn, K. A., Svrcek, W. Y., Mehrotra, A. K., "Measurement of asphaltene particle size distributions in crude oils diluted with *n*-heptane", *Ind. Eng. Chem. Res.*, **32** (5), 955-959, 1993.

Flory, P. J. "Thermodynamics of high polymer solutions", *J. Chemical Physics*, **9**, 660-661, 1941.

Frenier, W. W., Ziauddin, M., Venkatesan, R. and Creek, J. L. *Organic Deposits in Oil and Gas Production*, Society of Petroleum Engineers, Richardson, Texas, 2010.

Gafonova, O. V., Yarranton, H. W., "The stabilization of water-in-hydrocarbon emulsions by asphaltenes and resins", *J. Coll. Int. Sci*., **241** (2), 469-478, 2001.

Gelin, F., Grutters, M., Cornelisse, P., Taylor, S. D, "Asphaltene precipitation from live oil containing emulsified water", Presented at the 5th International Conference on Petroleum Phase Behavior and Fouling, Banff, Alberta, Canada, June 14-17, 2004.

George, S., *Asphaltene-Rich Phase Composition*, M.Sc. Thesis, Department of Chemical and Petroleum Engineering, University of Calgary, Calgary, Alberta, Canada, 2009.

Gonzalez, D. L., Ting, P. D., Hirasaki, G. J., Chapman, W. G., "Prediction of asphaltene instability under gas injection with the PC-SAFT equation of state", *Energy Fuels*, **19** (4), 1230-1234, 2005.

Gray, M. R., "Consistency of asphaltene chemical structures with pyrolysis and coking behavior", *Energy Fuels*, **17** (6), 1566-1569, 2003.

Gray, M. R., *Upgrading Petroleum Residues and Heavy Oils*, Marcel Decker Inc., New York, 1994.

Gross, J., Sadowski, G., "Perturbed-chain SAFT: an equation of state based on a perturbation theory for chain molecules", *Ind. Eng. Chem. Res*., **40** (5), 1244-1260, 2001.

Groenzin, H., Mullins, O.C., Asphaltene Molecular Size and Weight by time-Resolved Fluorescence Depolarization. Chapter 2, In *Asphaltenes*, *Heavy Oils*, and *Petroleomics*, Editors: Mullins, O. C., Sheu, E. Y., Hammami, A., Marshall, A. G., Springer Science + Business Media, LLC, New York, 2007.

Gupta, A. K., *A Model for Asphaltene Flocculation*, M.Sc. Thesis, Department of Chemical and Petroleum Engineering, University of Calgary, Calgary, Alberta, Canada, 1986.

Hammami, A., Ratulowski, J., Precipitation and Deposition of Asphaltenes in Production Systems: A Flow Assurance Overview, Chapter 23, *Asphaltenes*, *Heavy Oils*, and *Petroleomics*, Editors: Mullins, O. C., Sheu, E. Y., Hammami, A., Marshall, A. G., Springer Science + Business Media, LLC, New York, 2007.

Hammami, A., Phelps, C. H., Monger-McClure, T., Little, T. M., "Asphaltene precipitation from live oils: an experimental investigation of onset conditions and reversibility", *Energy Fuels*, **14** (1), 14-18, 2000.

Hansen, C. M., *Hansen's Solubility Parameters: A User's Handbook*, ISBN: 0849372488, CRC Press, Boca Raton, FL, 2007.

Haskett, C. E., Tartera, M., "Practical solution to problem of asphaltenes deposits – Hassi Messaoud field, Algeria", *J. Pet. Technol*., **17** (4), 387-391, 1965.

Hildebrand, J. H., "A critique of the theory of solubility of non-electrolytes", *Chem. Rev*., **44** (1), 37-45, 1949.

Hildebrand, J. H., Scott, R. L., *Solubility of Nonelectrolytes*, Third Edition, Reinhold, New York, 1950, Page 247.

Hirschberg, A., deJong, L. N. J., Schipper, B. A., Meijer, J. G., "Influence of temperature and pressure on asphaltene flocculation", *Soc. Pet. Eng. J*., **24**, 283-291, 1984.

Hong, E., Watkinson, P., "A study of asphaltene solubility and precipitation", *Fuel*, **83** (14-15), 1881-1887, 2004.

Huggins, M. L., "Solutions of long chain compounds", *J. Chemical Physics*, **9**, 440, 1941.

Idem, R. O., Ibrahim, H. H., "Kinetics of CO2-induced asphaltene precipitation from various Saskatchewan crude oils during CO2 miscible flooding", *J. Pet. Sci. Eng*., **35** (3-4), 233-246, 2002.

Jamaluddin, A. K. M., Nighswander, J., Joshi, N., A systematic approach in deepwater flow assurance fluid characterization, Paper SPE 71546, SPE Annual Technical Conference and Exhibition, New Orleans, Louisiana, September-October, 2001.

Kawanaka, S., Park, S.J., Mansoori, G.A., "Organic deposition from reservoir fluids: a thermodynamic predictive technique", *SPE Reservoir Eng*., 185-192, May 1991.

Kharrat, A. M., Zacharia, J., John Cherian, V., Anyatonwu, A., "Issues with comparing SARA methodologies", *Energy Fuels*, **21** (6), 3618-3621, 2007.

Kharrat, A. M., "Characterization of Canadian heavy oils using sequential extraction approach", *Energy Fuels*, **23** (2), 828-834, 2009.

Kharrat, A. M., DBR Technology Center, Schlumberger, Edmonton, Canada, Personal Communication, 2010.

Khristov, Khr., Taylor, S. D., Masliyah, J., "Thin liquid film technique – application to water-oil-water bitumen emulsion films", *Colloids Surfaces A: Physicochemical Engineering Aspects*, **174** (1-2), 183-196, 2000.

Khvostichenko, D. S., Andersen, S. I., "Interactions between asphaltenes and water in solutions in toluene", *Energy Fuels*, **22** (5), 3096-3103, 2008.

Khvostitchenko, D. S., Andersen, S. I., Viktorov, A. I., "Solubility and binding of water in toluene solutions of asphaltenes", *Russian J. Applied Chemistry*, **77** (6), 1013-1018, 2004.

Kokal, S. L., Najman, J., Sayegh, S. G., George, A. E., "Measurement and correlation of asphaltene precipitation from heavy oils by gas injection", *J. Can. Pet. Technol*., **31** (4), 24-30, 1992.

Kotlyar, L. S., Sparks, B. D., Woods, J. R., Chung, K. H., "Solids associated with the asphaltenes fraction of oil sands bitumen", *Energy Fuels*, **13** (2), 346-350, 1999.

Kraiwattanawong, K., Fogler, H. S., Gharfeh, S. G., Singh, P., Thomason, W.H., Chavadej, S., "Thermodynamic solubility models to predict asphaltene instability in live crude oils", *Energy Fuels*, **21** (3), 1248-1255, 2007.

Kumar, P. S., van Gisberger, S., Harris, J., Ferdiansyah, E., Brady, M., Harthy, S. A., Pandey, A., "Eliminating multiple interventions using a single rig-up coiled-tubing solution", *SPE Production Operations*, **23** (2), 119-124, 2008.

Laštovka, V., Fulem, M., Becerra, M., Shaw, J. M., "A similarity variable for estimating the heat capacity of solid organic compounds part II. Application: Heat capacity calculation for ill-defined organic solids", *Fluid Phase Equilibria*, **268** (1-2), 134-141, 2008.

Leόn, O., Rogel, E., Espidel, J., Torres, G., "Asphaltenes: structural characterization, self-association, and stability behavior", *Energy Fuels*, **14** (1), 6-10, 2000.

Leontaritis, K. J., Amaefule, J. O., Charles, R. E., "A systematic approach for the prevention of formation damage caused by asphaltene precipitation", *SPE Production & Facilities*, **9**, 157-164, August 1994.

Leontaritis, K. J., Mansoori, G. A., "Asphaltene deposition: a survey of field experiences and research approaches", *J. Pet. Sci. Eng.*, **1** (3), 229-239, 1988.

Leontaritis, K. J., Mansoori, G. A., Asphaltene flocculation during oil production and processing: a thermodynamic colloidal model, Paper SPE 16258, SPE International Symposium on Oilfield Chemistry, San Antonio, TX, 1987.

Li, Z., Firoozabadi, A., "Modeling asphaltene precipitation by *n*-alkanes from heavy oils and bitumens using cubic-plus-association equation of state", *Energy Fuels*, **24** (2), 1106-1113, 2010a.

Li, Z., Firoozabadi, A., "Cubic-plus-association equation of state for asphaltene precipitation in live oils", *Energy Fuels*, **24** (5), 2956-2963, 2010b.

Lian, H., Lin, J-R., Yen, T. F., "Peptization studies of asphaltene and solubility parameter spectra", *Fuel*, **73** (3), 423-428, 1994.

Liao, Z., Zhao, J., Creux, P., Yang, C., "Discussion on the structural features of asphaltene molecules", *Energy Fuels*, **23** (12), 6272-6274, 2009.

Lindemuth, P. M., Lessard, R.B., Lozynski, M., Kremer, M. "Improve desalter operations", *Hydrocarbon Processing*, 67-70, September 2001.

Luo, P., Wang, X., Gu, Y., Zhang, H., Moghadam, S., Asphaltene precipitation and its effects on the vapour extraction (VAPEX) heavy oil recovery process, Paper SPE/PS/CHOA 117527, SPE International Thermal Operations and Heavy Oil Symposium, Calgary, Alberta, 20-23 October, 2008.

Maqbool, T., Balgoa, A. T., Fogler, H. S., "Revisiting asphaltene precipitation from crude oils: a case neglected kinetic effects", *Energy Fuels*, **23** (7), 3681-3686, 2009.

Maruska, H. P., Rao, B. M. L., "The role of polar species in the aggregation of asphaltenes", *Fuel Sci. Technol. Intl.*, **5** (2), 119, 1987.

McKenna, A. M., Rodgers, R. P., Hendrickson, C. L., Blakney, G. T., Savory, J. T., Kaiser, N. T., Mapolelo, M. M., Marshall, A. G., Robbins, W. K., Ehrmann, B. M., Hsu,

C. S., The compositional continuum of petroleum: detailed molecular characterization of heavy crude oils and asphaltenes by ultrahigh resolution FT-ICR mass spectrometry, AIChE Annual Meeting, Salt Lake City, UT, 2010.

McLean, J. D., Kilpatrick, P. K., "Effects of asphaltene solvency on stability of water-in-crude-oil emulsions", *J. Coll. Int. Sci*., **189** (2), 242-253, 1997.

Mohammed, R. A., Bailey, A. I., Luckham, P. F., Taylor, S. E., "Dewatering of crude oil emulsions: 1. Rheological behaviour of the crude oil-water interface", *Colloids Surfaces, A: Physicochemical Engineering Aspects*, **80** (2-3), 223-235, 1993.

Moschopedis, S. E., Fryer, J. F., Speight, J. G., "Investigation of asphaltene molecular weights", *Fuel*, **55** (3), 227-223, 1976.

Mullins, O. C., "The modified Yen model", *Energy Fuels*, **24** (4), 2179-2207, 2010.

Murgich, J., Merino-Garcia, D., Andersen, S. I., del Rio, J. M., Galeana, C. L., "Molecular mechanics and microcalorimetric investigations of the effects of molecular water on the aggregation of asphaltenes in solutions", *Langmuir*, **18** (23), 9080-9086, 2002.

Murgich, J., "Intermolecular forces in aggregates of asphaltenes and resins", *Pet. Sci. Technol*., **20** (9&10), 983-997, 2002.

Nalwaya, V., Tangtayakom, V., Piumsomboon, P., Fogler, S., "Studies of asphaltenes through analysis of polar fractions", *Ind. Eng. Chem. Res*., **38** (3), 964-972, 1999.

National Institute of Standards and Technology (NIST) Standard Reference Database; NIST/TRC Source Database; WinSource, Version 2008.

Negahban, S., Bahamaish, J. N. M., Joshi, N., Nighswander, J., Jamaluddin, A. K. M., "An experimental study at an Abu Dhabi reservoir of asphaltene precipitation caused by gas injection", *SPE Production & Facilities*, **20**, 115-125, May 2005.

Nghiem, L. X., Coombe, D. A., "Modeling asphaltene precipitation during primary depletion", Paper SPE 36106, SPE Fourth Latin American and Caribbean Petroleum Engineering Conference, Trinidad, Tobago, 1996.

Nielsen, B. B., Svrcek, W. Y., Mehrotra, A. K., "Effect of temperature and pressure on asphaltene particle size distribution in crude oils diluted with *n*-pentane", *Ind. Eng. Chem. Res.*, **33** (5), 1324-1330, 1994.

Pan, H., Firoozabadi, A., "Thermodynamic micellization model for asphaltene aggregation and in petroleum fluids", *SPE Production & Facilities*, 118-127, May 1998.

Pedersen, C., *Asphaltene Characterization: Permittivity Measurements and Modelling*, PhD Thesis, IVC-SEP, Department of Chemical Engineering, Technical University of Denmark, Lyngby, Denmark, 2000.

Pedersen, K. S., Christensen, P. L., *Phase Behavior of Petroleum Reservoir Fluids*, CRC Press, Taylor & Francis Group, Boca Raton, FL, 2007.

Peramanu, S., Pruden, B. B., Rahimi, P., "Molecular weight and specific gravity distributions for Athabasca and Cold Lake bitumens and their saturate, aromatic, resin, and asphaltene fractions", *Ind. Eng. Chem. Res.*, **38** (8), 3121-3130, 1999.

Perry, R. H., Green, D. W., *Perry's Chemical Engineers' Handbook*, 7th Edition, Mc Graw-Hill, 1997.

Pomerantz, A. E., Hammond, M. R., Morrow, A. L., Mullins, O. C., Zare, R. N., "Asphaltene molecular-mass distribution determined by two-step laser mass spectrometry", *Energy Fuels*, **23** (3), 1162-1168, 2009.

Qin, X., Wang, P., Sepehrnoori, K., Pope, G. A., "Modeling asphaltene precipitation in reservoir simulation", *Ind. Eng. Chem. Res.*, **39** (8), 2644-2654, 2000.

Rastegari, K., Svrcek, W. Y., Yarranton, H. W., "Kinetics of asphaltene flocculation", *Ind. Eng. Chem. Res.*, **43** (21), 6861-6870, 2004.

Reid, R. C., Prausnitz, J. M., Poling, B. E., *The Properties of Gases and Liquids*, 4th edition, McGraw-Hill, New York, 1989.

Rijkers, M. P. W., Heidemann, R. A., Convergence Behavior of Single-Stage Flash Calculations, Article in *Equations of State, Theories and Applications*, Editors: K. C. Choa and R. L. Robinson, Jr, ACS Symposium Series 300, Washington, DC, 476-493, 1986.

Rodgers, R. P., Marshall, A. G., Petroleomics: Advanced Characterization of Petroleum-Derived Materials by Fourier Transform Ion Cyclotron Resonance Mass Spectrometry (FT-ICR MS), Chapter 3, *Asphaltenes, Heavy Oils*, and *Petroleomics*, Editors: Mullins, O. C., Sheu, E. Y., Hammami, A., Marshall, A. G., Springer Science + Business Media, LLC, New York, 2007.

Rogel, E., Carbognani, L., "Density estimation of asphaltenes using molecular dynamic simulations", *Energy Fuels*, **17** (2), 378-386, 2003.

Rogel, E., "Simulation of interaction in asphaltene aggregates", *Energy Fuels*, **14** (3), 566-574, 2000.

Sabbagh, O., Akbarzadeh, K., Badamchi-Zadeh, A., Svrcek, W. Y., Yarranton, H. W., "Applying the PR-EoS to asphaltene precipitation from *n*-alkane diluted heavy oils and bitumens", *Energy Fuels*, **20** (2), 625-634, 2006.

Saniere, A., Hénaut, I., Argiller, J. F., "Pipeline transportation of heavy oils, a strategic, economic and technological challenge", *Oil & Gas Sci. Technol. – Rev. IFP*, **59** (5), 455-466, 2004.

Sarma, H. K., "Can we ignore asphaltene in a gas injection project for light-oils?", Paper SPE 84877, Proceedings of SPE International Improved Oil Recovery Conference in Asia Pacific, Kuala Lumpur, Malaysia, 20-21 October 2003.

Scatchard, G., "Equilibrium in non-electrolyte mixtures". *Chem. Rev.*, **44** (1), 7-35, 1949.

Schermer, W. E. M., Melein, P. M. J., van den Berg, F. G. A., "Simple Techniques for Evaluation of Crude Oil Compatibility", *Pet. Sci. Technol.*, **22** (7-8), 1045–1054, 2004.

Sheu, E. Y., Storm, D. A., Shields, M. B., "Adsorption kinetics of asphaltenes at toluene/acid solution interface", *Fuel*, **74** (10), 1475-1479, 1995.

Sheu, E.Y., de Tar, M.M., Strom, D. A., "Dielectric properties of asphaltene solutions", *Fuel*, **73 (1)**, 45-50, 1994.

SMS 1600, Determination of state of peptization of asphaltenes in heavy oil streams, *Shell Method Series*, 2001.

Speight, J. G., *The Chemistry and Technology of Petroleum*, 3rd edition, Marcel Dekker, Inc., New York, 1999.

Spiecker, P. M., Gawrys, K. L., Kilpatrick, P. K., "Aggregation and solubility behaviour of asphaltenes and their subfractions", *J. Coll. Int. Sci.*, **267** (1), 178-193, 2003.

Stanford, L. A., Rodgers, R. P., Marshall, A. G., Czarnecki, J., Wu, X. A., "Compositional characterization of bitumen/water emulsion films by negative- and positive-ion electrospray ionization and field desorption/ionization Fourier transform ion cyclotron resonance mass spectrometry", *Energy Fuels*, **21** (2), 963-972, 2007a.

Stanford, L. A., Rodgers, R. P., Marshall, A. G., Czarnecki, J., Wu, X. A., Taylor, S. D., "Detailed elemental compositions of emulsion interfacial material versus parent oil for nine geographically distinct light, medium, and heavy crude oils, detected by negative- and positive-ion electrospray ionization Fourier transform ion cyclotron resonance mass spectrometry", *Energy Fuels*, **21** (2), 973-981, 2007b.

Stephenson, W. K., "Producing asphaltenic crude oils: problems and solutions, *Pet. Engr. Intl.*, 24-31, June 1990.

Strausz, O. P., Mojelsky, T. W., Faraji, F., Lown, E. M., "Additional structural details on Athabasca asphaltene and their ramifications", *Energy Fuels*, **13** (2), 207-227, 1999.

Strausz, O. P., Mojelsky, T. W., Lown, E. M., "The molecular structure of asphaltene: an unfolding story", *Fuel*, **71** (12), 1355-1363, December 1992.

Taylor, S. D., Czarnecki, J., Masliyah, J., Disjoining pressure isotherms of water-in-bitumen emulsion films, *J. Coll. Int. Sci.*, **252** (1), 149-160, 2002.

Tharanivasan, A., Svrcek, W. Y., Yarranton, H. W., Taylor, S. D., Merino-Garcia, D., Rahimi, P., "Measurement and modeling of asphaltene precipitation from crude oil blends", *Energy Fuels*, **23** (8), 3971-3980, 2009.

Tharanivasan, A., Yarranton, H. W., Taylor, S. D., "Application of regular solution based models to asphaltene precipitation from live oils", *Energy Fuels*, **25** (2), 528-538, 2011.

Thawer. R., Nicoll, D. C. A., Dick, G., "Asphaltene Deposition in Production Facilities", *SPE Production Engineering*, November 1990.

Ting, P. D., Hirasaki, G. J., Chapman, W. G., "Modeling of asphaltene phase behavior with the SAFT equation of state", *Pet. Sci. Technol.*, **21** (3-4), 647-661, 2003.

Vargas, F. M., Gonzalez, D. L., Creek, J. L., Wang, J., Buckley, J. S., Hirasaki, G. J., Chapman, W. G., "Development of a general method for modeling asphaltene stability", *Energy Fuels*, **23** (3), 1147-1154, 2009.

Verdier, S., Andersen, S. I., "Internal pressure and solubility parameter as a function of pressure", *Fluid Phase Equilibria*, **231** (2), 125-137, 2005.

Verdier, S., *Experimental Study and Modelling of Asphaltene Precipitation Caused by Gas Injection*, PhD Thesis, Technical University of Denmark, Lyngby, Denmark, 2006.

Wang, J. X., Buckley, J. S., "A two-component solubility model of the onset of asphaltene flocculation in crude oils", *Energy Fuels*, **15** (5), 1004-1012, 2001.

Wang, J. X., Buckley, J. S., Burke, N. E., Creek, J. L., "A practical method for anticipating asphaltene problems", *SPE Production & Facilities*, **19**, 152-160, August 2004.

Wauquier, J.–P., *Crude Oil Petroleum Products Process Flowsheets*, Editions Technip, Paris, 1995.

Whitson, C. H., "Characterizing hydrocarbon plus fractions", *Soc. Pet. Eng. J.*, **23** (4), 683-694, 1983.

Wiehe, I. A, Kennedy, R. J., Dickakian, G., "Fouling of nearly incompatible oils", **15** (5), 1057-1058, 2001.

Wiehe, I. A., Kennedy, R. J., "The oil compatibility model and crude oil incompatibility", *Energy Fuels*, **14** (1), 56-59, 2000.

Wu, J., Prausnitz, J. H., Firoozabadi, A., "Molecular-thermodynamic framework for asphaltene-oil equilibria", *AIChE J.*, **44** (5), 1188-1199, 1998.

Wu, X., "Investigating the stability mechanism of water-in-diluted bitumen emulsions through isolation and characterization of the stabilizing materials at the interface", *Energy Fuels*, **17** (1), 179-190, 2003.

Xu, Y., Dabros, T., Hamza, H., Shefantook, W., "Destabilization of water in bitumen emulsion by washing with water", *Pet. Sci. Techol.*, **17** (9 & 10), 1051-1070, 1999.

Xu, Y., Koga, Y., Strausz, O. P., "Characterization of Athabasca asphaltenes by small-angle X-ray scattering technique", *Ind. Eng. Chem. Res.*, **18** (1), 60, 1995.

Yan, J., Plancher, H., "Wettability changes induced by adsorption of asphaltenes", *SPE Production & Facilities*, **12** (4), 239-266, 1997.

Yang, Z., Ma, G.–F., Lin, X.-S., Yang, J.-T., Guo, T.-M., "Experimental and modeling studies on the asphaltene precipitation in degassed and gas-injected reservoir oils", *Fluid Phase Equilibria*, **157** (1), 143-158, 1999.

Yang, X., Hamza, H., Czarnecki, J., "Investigation of subfractions of Athabasca asphaltenes and their role in emulsion stability", *Energy Fuels*, **18** (3), 770-777, 2004.

Yarranton, H. W., Alboudwarej. H., Jakher, R., "Investigation of asphaltene association with vapor pressure osmometry and interfacial tension measurements", *Ind. Eng. Chem. Res.*, **39** (8), 2916-2924, 2000.

Yarranton, H. W., Masliyah, J. H., "Molar mass distribution and solubility modeling of asphaltenes" *AIChE J.*, **42** (12), 3533-3543, 1996.

Yarranton, H. W., "Asphaltene self-association", *J. Disp. Sci. Tech.*, **26** (1), 5-8, 2005.

Yarranton, H. W., Fox, W. A., Svrcek, W. Y., "Effect of resins on asphaltene self-association and solubility", *Can. J. Chem. Eng.*, **85** (5), 635-642, 2007.

Yen, T. F., "Structure of petroleum asphaltenes and its significance", *Energy Sources*, **1** (4), 447-463, 1974.

Yonebayashi, H., Masuzawa, T., Dabbouk, C., Urasaki, D., "Ready for gas injection: asphaltene risk evaluation by mathematical modeling of asphaltene-precipitation envelope (APE) with integration of all laboratory deliverables", *SPE Projects, Facilities & Construction*, June 2011.

Yudin, I. K., Nikolaenko, G. L., Gorodetskii, E. E., Kosov, V. I., Melikyan, V. R., Markhashov, E. L., Frot, D., Briolant, Y., "Mechanisms of asphaltene aggregation in toluene-heptane mixtures", *J. Pet. Sci. Eng.*, **20**, 297-301, 1998.

Zhao, B., Shaw, J. M., "Composition and size distribution of coherent nanostructures in Athabasca bitumen and Maya crude oil", *Energy Fuels*, **21** (5), 2795-2804, 2007.

Zhou, H., Thomas, F. B., Moore, R. G., “Modelling of solid precipitation from reservoir fluid”, *J*. *Can*. *Pet*. *Technol*., **35** (10), 37-45, 1996.

Zuo, J. Y., Mullins, O. C., Freed, D., Zhang, D., “A simple relation between solubility parameters and densities for live reservoir fluids”, *J*. *Chem*. *Eng*. *Data*, **55** (9), 2964-2969, 2010.

Appendix A: Average Absolute Deviation

The Average Absolute Deviation (AAD) of the fitted or predicted curve to the experimental data are assessed with the following equation:

$$AAD = \frac{\sum_{q=1}^{q} \left| \upsilon_{fit} - \upsilon_{exp} \right|}{q} \tag{G.1}$$

where υ_{fit} is the fitted or predicted model measurement, υ_{exp} is the experimental measurement, q is the number of measurements. AAD is also given in percent by multiplying the R.H.S of the Eq. (G.6) by 100.

Appendix B: Composition Data for Synthetic Solvent Mixture

Synthetic solvent (or solution gas) mixture is used to create the recombined oil sample. In order to prepare the synthetic solvent mixture, various known pure components (primarily gases) are added in a pre-evacuated high pressure vessel. The amount each component added to the vessel, and the final mixture composition determined by GC is provided in Table B.1.

Table B.1: Composition of synthetic solvent mixture.

Component	Molar Mass (g/mol)	Amount Taken (g)	Amount Taken (wt %)	No. of Moles (mole)	Estimated (mole %)	GC analysis (mole %)
CO2	44.01	0.0	0.0	0.0000	0.0	0.0
N2	28.01	0.8	0.5	0.0286	0.5	0.5
C1	16.04	75.4	50.7	4.7007	76.2	75.9
C2	30.07	12.8	8.6	0.4257	6.9	6.9
C3	44.10	18.8	12.6	0.4263	6.9	6.9
i-C4	58.12	4.4	3.0	0.0757	1.2	1.2
n-C4	58.12	11.7	7.9	0.2013	3.3	3.2
i-C5	72.15	5.3	3.6	0.0735	1.2	1.3
n-C5	72.15	7.6	5.1	0.1053	1.7	1.8
C6	84.00	5.5	3.7	0.0655	1.1	1.1
mcyclo-C5	84.16	1.1	0.7	0.0131	0.2	0.2
benzene	78.11	0.0	0.0	0.0000	0.0	0.0
cyclo-C6	84.16	0.5	0.3	0.0059	0.1	0.1
C7	96.00	2.7	1.8	0.0281	0.5	0.5
mcyclo-C6	98.19	0.6	0.4	0.0061	0.1	0.1
toluene	92.14	0.3	0.2	0.0033	0.1	0.1
C8	107.00	0.8	0.5	0.0075	0.1	0.1
C2-benzene	106.17	0.0	0.0	0.0000	0.0	0.0
m&*p*-xylene	106.17	0.0	0.0	0.0000	0.0	0.0
o-xylene	106.17	0.0	0.0	0.0000	0.0	0.0
C9	121.00	0.4	0.3	0.0033	0.1	0.1
Total		148.7	100.0	6.1699	100.0	100.0

Appendix C: Composition Data for Flashed Gas, Flashed Oil, and Recombined Live Oil

The prepared recombined live oil is flashed using the GOR apparatus at atmospheric conditions to isolate the flashed gas and flashed oil. The composition analysis of flashed gas and flashed oil is carried out using GC. The measured density of flashed oil and flashed gas at standard conditions (1 atm, 288.6 K) were 847.7 kg/m^3 and 0.95 kg/m^3, respectively. The measured GOR of the recombined live oil was 195 m^3/m^3. This translates to 82.2 wt% of flashed oil and 17.8 wt% of flashed gas in the live oil. Accordingly, the composition of live oil is determined from the compositions of flashed gas and flashed oil. Table C.1 provides the composition of flashed gas, flashed oil and the recombined live oil.

Table C.1: Composition of flashed gas, flashed oil, and recombined live oil.

Component	Molar Mass (g/mol)	Flashed Gas (wt %)	Flashed Oil (wt %)	Recombined Oil (wt %)
CO2	44.01	0.019	0.000	0.003
N2	28.01	0.694	0.000	0.124
C1	16.04	50.867	0.000	9.079
C2	30.07	8.603	0.000	1.536
C3	44.10	12.762	0.161	2.410
i-C4	58.12	3.227	0.090	0.650
n-C4	58.12	8.442	0.396	1.832
i-C5	72.15	3.846	0.508	1.104
n-C5	72.15	5.009	0.956	1.680
C6	84.00	3.379	2.274	2.471
mcyclo-C5	84.16	0.515	0.557	0.550
benzene	78.11	0.061	0.059	0.060
cyclo-C6	84.16	0.317	0.373	0.363
C7	96.00	1.184	2.862	2.562
mcyclo-C6	98.19	0.321	0.904	0.800

Table C.1 continued on next page…

Component	Molar Mass (g/mol)	Flashed Gas (wt %)	Flashed Oil (wt %)	Recombined Oil (wt %)
toluene	92.14	0.101	0.248	0.222
C8	107.00	0.378	3.728	3.130
C2-benzene	106.17	0.008	0.109	0.091
m&*p*-xylene	106.17	0.012	0.351	0.290
o-xylene	106.17	0.012	0.221	0.183
C9	121.00	0.181	3.853	3.198
C10	134.00	0.053	4.670	3.846
C11	147.00	0.009	4.146	3.408
C12	161.00	0.000	3.704	3.043
C13	175.00	0.000	3.826	3.143
C14	190.00	0.000	3.506	2.880
C15	206.00	0.000	3.765	3.093
C16	222.00	0.000	3.272	2.688
C17	237.00	0.000	3.146	2.585
C18	251.00	0.000	3.137	2.577
C19	263.00	0.000	3.054	2.509
C20	275.00	0.000	2.646	2.174
C21	291.00	0.000	2.683	2.204
C22	300.00	0.000	2.391	1.964
C23	312.00	0.000	2.264	1.860
C24	324.00	0.000	2.127	1.747
C25	337.00	0.000	2.037	1.673
C26	349.00	0.000	1.903	1.563
C27	360.00	0.000	1.911	1.570
C28	372.00	0.000	1.810	1.487
C29	382.00	0.000	1.847	1.517
C30+	750.00	0.000	24.506	20.132

Appendix D: Data for Bubble Point Pressure and Liquid Density Measurements

Bubble point measurements were carried out at Schlumberger's DBR Technology Center, Edmonton. The experiment was conducted by gradually expanding the recombined live oil in several pressure steps at constant test temperature. After allowing the fluid to equilibrate at each pressure step, the "fluid+piston" height and cell pressure were measured. The piston height was then used to calculate the total fluid volume (V_{tot}) in the PVT cell by using the following equation:

$$V_{tot} = [(h_{fp} - h_p) \times \text{Tube constant}] + \text{Dead volume} \qquad \text{(D.1)}$$

where, h_{fp} and h_p are the measured "fluid + piston" height and piston height, respectively. The piston height was determined prior to the experiment. Tube constant is the volume per length of tube inside the cell and it was found to be 7.93 cm³/cm. Dead volume is the trapped fluid volume in the tubing and connections. The piston height, tube constant and dead volume for the experimental setup at the test temperatures are given in Table D.1.

Table D.1: Pre-experimental conditions to bubble point and liquid density measurements.

Test Temperature (°C)	Piston Height, h_p (cm)	Dead Volume (cm³)	Mass of Oil, m_{oil} (g)
80	2.886	0.954	17.85
100	2.872	1.260	18.81
121	2.886	0.954	17.85

The total fluid volume and the corresponding PVT cell pressure at each equilibration step were then used to determine the bubble point of the fluid at the test temperature (see Section 3.4.5 in Chapter 3). The data collected during bubble point pressure measurements at 80, 100 and 121°C, are provided in Tables D.2, D.3 and D.4, respectively.

Table D.2: Measured data for bubble point pressure and liquid density measurements at 80°C.

Pressure P **(MPa)**	**"Fluid + Piston" Height** h_{fp} **(cm)**	**Total Fluid Volume** V_{tot} **(cm^3)**	**Liquid Density** ρ_{liq} **(kg/m^3)**	**Y-function**
100.01	5.814	24.173	738.6	
82.83	5.872	24.633	724.8	
69.00	5.922	25.029	713.3	
55.21	5.981	25.497	700.2	
41.36	6.049	26.037	685.7	
34.45	6.093	26.386	676.7	
27.62†		26.754‡		
27.54†	6.143	26.782		
26.85	6.162	26.933		
26.15	6.183	27.099		4.36
25.49	6.206	27.282		4.38
24.10	6.261	27.718		4.24
22.03	6.358	28.487		4.06
18.53	6.604	30.438		3.92
15.04	7.018	33.721		3.56

† Calculated bubble point (P_{sat*})

‡ Calculated fluid volume at bubble point pressure (V_{sat*})

† Visually observed bubble point pressure

Table D.3: Measured data for bubble point pressure and liquid density measurements at 100°C.

Pressure P **(MPa)**	**"Fluid + Piston" Height** h_{fp} **(cm)**	**Total Fluid Volume** V_{tot} **(cm^3)**	**Liquid Density** ρ_{liq} **(kg/m^3)**	**Y-function**
102.51	5.947	25.64	733.5	
89.15	5.984	25.94	725.2	
75.98	6.030	26.30	715.1	
62.20	6.091	26.79	702.2	
48.41	6.159	27.33	688.4	
41.48	6.195	27.61	681.2	
34.58	6.246	28.02	671.4	
31.14	6.275	28.25	665.9	
29.41	6.291	28.37	663.0	
28.38	6.300	28.44	661.3	
27.68	6.306	28.49	660.2	
28.18†		28.38‡		
27.33⁋	6.319	28.59		
27.23	6.322	28.62		
27.00	6.330	28.68		
26.63	6.343	28.79		4.04
25.96	6.367	28.98		4.06
25.27	6.394	29.19		4.02
24.24	6.443	29.58		3.84
22.51	6.536	30.32		3.69
20.80	6.648	31.20		3.56
17.33	6.976	33.80		3.27
13.89	7.525	38.16		2.98

† Calculated bubble point (P_{sat*})

‡ Calculated fluid volume at bubble point pressure (V_{sat*})

⁋ Visually observed bubble point pressure

Table D.4: Measured data for bubble point pressure and liquid density measurements at 121°C.

Pressure P **(MPa)**	**"Fluid + Piston" Height** h_{fp} **(cm)**	**Total Fluid Volume** V_{tot} **(cm^3)**	**Liquid Density** ρ_{liq} **(kg/m^3)**	**Y-function**
102.03	5.938	25.57	717.9	
88.99	5.995	26.03	705.5	
76.04	6.046	26.43	694.7	
62.26	6.108	26.92	682.0	
48.43	6.187	27.55	666.5	
34.67	6.288	28.35	647.6	
31.14	6.323	28.63	641.4	
29.07	6.343	28.79	637.8	
28.65†		28.76‡		
28.00†	6.363	28.94		3.68
27.65	6.376	29.05		3.67
26.63	6.414	29.35		3.73
25.60	6.462	29.73		3.55
23.89	6.554	30.46		3.38
20.47	6.802	32.42		3.14
13.60	7.818	40.48		2.72
8.45	9.939	57.30		2.41

† Calculated bubble point (P_{sat*})

‡ Calculated fluid volume at bubble point pressure (V_{sat*})

† Visually observed bubble point pressure

Tables D.2, D.3 and D.4 also include the calculated liquid density and Y-function at each equilibration pressure step. The liquid density is calculated by using the equation:

$$\rho_{liq} = \frac{m_{oil}}{V_{tot}} \tag{D.2}$$

where, m_o is the mass of live oil taken for the measurement, Table D.1. The Y-function is calculated from the Eq. (3.5) in Chapter 3. P_{sat*} and V_{sat*} are denoted in Tables D.2, D.3 and D.4 for the three test temperatures.

Appendix E: Asphaltene Precipitation Yield Calculation for Live Oil

Asphaltene yield is calculated from the precipitated material in the toluene rinse and on the filter (filter cake). Table E.1 provides the data collected from the depressurization experiments at the test temperatures. Note that the *italicized* data in the Table E.1 are calculated and all the other data are measured.

The *italicized* data in the Table E.1 are calculated from the measured data (all in grams) by using the following equations:

Maltenes in trapped oil = Sample collected – (C7-asphaltenes in the sample) (E.1)

$$\textit{Asphaltenes in trapped oil} = \textit{Maltenes in trapped oil} \times \frac{\text{Wt\% of asphaltenes in flashed oil}}{\text{Wt\% of maltenes in flashed oil}} \quad \text{(E.2)}$$

Precipitated asphaltenes = (C7-asphaltene in the sample) – *Asphaltenes in trapped oil* (E.3)

$$\textit{Asphaltene Yield} = 100 \times \frac{\left(\begin{array}{l}\textit{Precipitated asphaltenes in toleuene rinse} \\ +\textit{Precipitated asphaltenes in filter cake}\end{array}\right)}{\text{Live oil sample}} \quad \text{(E.4)}$$

Table E.1: Data collected from the depressurization experiments for calculating asphaltene yield from live oil.

Data Collected/Calculated	**80°C**	**100°C**	**120°C**
Live Oil Sample (g)	37.1940	37.4730	37.0620
Wt% of asphaltenes in flashed oil	1.38	1.38	1.38
Wt% of maltenes in flashed oil	98.62	98.62	98.62
Toluene Rinse (toluene + precipitated asphaltenes + trapped oil)			
Sample collected (g)	185.6010	312.9300	344.2090
Precipitated asphaltenes and trapped oil (g)	3.0567	3.3882	3.2252
C7-asphaltenes in the sample (g)	0.3272	0.2086	0.2855
Maltenes in trapped oil (g)	2.7295	3.1796	2.9398
Asphaltenes in trapped oil (g)	0.0383	0.0446	0.0413
Precipitated asphaltenes in toluene rinse (g)	0.2889	0.1640	0.2442
Filter Cake (precipitated asphaltenes + trapped oil)			
Sample collected (g)	0.0045	0.0218	0.0343
C7-asphaltenes in the sample (g)	0.0004	0.0007	0.0082
Maltenes in trapped oil (g)	0.0041	0.0211	0.0261
Asphaltenes in trapped oil (g)	0.0001	0.0003	0.0004
Precipitated asphaltenes in filter cake (g)	0.0003	0.0004	0.0078
***Asphaltene Yield* (wt%)**	0.778	0.439	0.680

Appendix F: Component Lumping for Characterizing Live Oil in Table 6.2

Recombined live oil composition is obtained from GC analysis, whereas the dead oil composition is measured using SARA analysis. In this thesis, a generalized characterization methodology is developed for both live and dead oils. The generalized characterization methodology combines both the GC composition analysis and the SARA analysis. Table 6.2 provides measured composition data in Columns B and C for live and dead oils, respectively. The merged composition in Column D of Table 6.2 is calculated according to Table F.1. The lumped composition in Column E of Table 6.2 is calculated according to Table F.2. Note that, the calculation is performed only for the components mentioned in the Tables F.1 and F.2.

Table F.1: Merged composition calculation details for Column D of Table 6.2.

Component (Column A)	**Merged (wt%) (Column D)**
saturates	saturates (Column C) × [(C11+C12+…+C29+C30+)/100](Column B)
aromatics	aromatics (Column C) × [(C11+C12+…+C29+C30+)/100](Column B)
resins	resins (Column C) × [(C11+C12+…+C29+C30+)/100](Column B)
asphaltenes	asphaltenes (Column C) × [(C11+C12+…+C29+C30+)/100](Column B)

Table F.2: Lumped composition calculation details for Column E of Table 6.2.

Component (Column A)	**Lumped for C16+ SARA (wt%) (Column E)**
C1	(CO2+N2+C1)(Column B)
C2	C2 (Column B)
C3	C3 (Column B)
i-C4	*i*-C4 (Column B)
n-C4	*n*-C4 (Column B)
i-C5	*i*-C5 (Column B)
n-C5	*n*-C5 (Column B)
C6	(C6 + mcyclo-C5)(Column B)
C7	(benzene+cyclo-C6+C7)(Column B)
C8	(mcyclo-C6+toluene+C8+C2-benzene+*m*&*p*-xylene+o-xylene)(Column B)
C10	(C9+C10+(C11/2))(Column B)
C12	((C11/2)+C12+(C13/2))(Column B)
C14	((C13/2)+C14+C15)(Column B)
saturates	saturates(Column D) – [(C11+C12+C13+C14+C15)×0.76](Column B)
aromatics	aromatics(Column D) – [(C11+C12+C13+C14+C15)×0.24](Column B)
resins	resins(Column D)
asphaltenes	asphaltenes(Column D)

Appendix G: Component Lumping for Characterizing Flashed Oil in Table 6.3

A procedure similar to characterization of live oil was used to obtain the composition of flashed oil. Both GC and SARA analyses were carried out for flashed oil. GC analysis of flashed oil is given in Column G of Table 6.3, whereas SARA analysis for flashed oil is provided in Column C of table 6.2. Therefore, the merged composition in Column I of Table 6.3 is calculated according to the Table G.1. Then the lumped composition in Column J of Table 6.3 is calculated based on Table F.2. Note that, the calculation is performed only for the components mentioned in the Tables G.1 and G.2.

Table G.1: Merged composition calculation details for Column I of Table 6.3.

Component (Column F)	**Merged for C16+ SARA (wt%) (Column I)**
toluene	(toluene+C2-benzene+*m*&*P*-xylene+*o*-xylene)(Column G)
saturates	{saturates (Column C of Table 6.2) × [(C11+C12+…+C29+C30+)/100](Column G)} – {[(C11+C12+C13+C14+C15)×0.76](Column G)}
aromatics	{aromatics (Column C of Table 6.2) × [(C11+C12+…+C29+C30+)/100](Column G)} – {[(C11+C12+C13+C14+C15)×0.24](Column G)}
resins	resins (Column C of Table 6.2) × [(C11+C12+…+C29+C30+)/100](Column G)
asphaltenes	asphaltenes (Column C of Table 6.2) × [(C11+C12+…+C29+C30+)/100](Column G)

Table G.2: Lumped composition calculation details for Column J of Table 6.3.

Component (Column F)	**Lumped for C16+ SARA (wt%) (Column J)**
C3	C3 (Column G)
i-C4	*i*-C4 (Column G)
n-C4	*n*-C4 (Column G)
i-C5	*i*-C5 (Column G)
n-C5	*n*-C5 (Column G)
C6	(C6 + mcyclo-C5)(Column G)
C7	(benzene+cyclo-C6+C7)(Column G)
C8	(mcyclo-C6+toluene+C8)(Column G)
C10	(C9+C10+(C11/2))(Column G)
C12	((C11/2)+C12+(C13/2))(Column G)
C14	((C13/2)+C14+C15)(Column G)
saturates	saturates(Column I)
aromatics	aromatics(Column I)
resins	resins(Column I)
asphaltenes	asphaltenes(Column I)